THE EFFECTS OF SMALL-SCALE HETROGENEITY ON THE LARGE-SCALE DYNAMICS OF WEST SIBERIAN WETLAND CARBON FLUXES

Theodore J. Bohn

A dissertation

submitted in partial fulfillment of the

requirements for the degree of

Doctor of Philosophy

University of Washington

2013

Reading Committee:

Dennis P. Lettenmaier, Chair

Michael T. Brett

Rebecca Neumann

Program Authorized to Offer Degree:

Civil and Environmental Engineering

University of Washington

Abstract

THE EFFECTS OF SMALL-SCALE HETROGENEITY ON THE LARGE SCALE DYNAMICS OF WEST SIBERIAN WETLAND CARBON FLUXES

Theodore J. Bohn

Chair of the Supervisory Committee:

Professor Dennis P. Lettenmaier

Department of Civil and Environmental Engineering

Wetlands are the world's largest natural source of methane and an historically large sink of atmospheric carbon. High-latitude wetlands have received increasing scrutiny recently, due to the temperature sensitivity of their carbon emissions, and the implications of ongoing and predicted warming – including implications of permafrost thawing. The centerpiece of this dissertation is a new large-scale wetland modeling scheme that accounts for the heterogeneous effects of microtopography on water table depth and carbon fluxes. I incorporated this new scheme into the Variable Infiltration Capacity (VIC) land surface model, extended it to include carbon cycle processes, and linked it to an existing wetland methane emissions model. Using this modeling framework, I simulated wetland hydrology

and biogeochemistry in the West Siberian Lowland (WSL) over the period 1948-2010. Changes in temperature and precipitation influenced both water table depth and methane emissions. I found that simpler schemes used in previous studies were subject to errors of +/- 30% in their predictions of end-of-century boreal wetland methane emissions due to the nature of their simplifying assumptions. While calibrating to intensive methane flux observations in the WSL, I found a strong north-south gradient in observed methane emissions, which could only be reproduced a) accounting for sub-grid heterogeneity in water table depth and b) using spatially-varying methane emissions parameters. Because most previous studies neglected at least one of these two controls, the majority of methane emissions from the WSL have, apparently incorrectly, been attributed to permafrost wetlands in the northern half of the domain. Finally, I used the outputs of the CMIP5 global climate model projections to force simulations over the WSL for the 21st century and explored the possible responses of the soil microbial communities to climate change. End-of-century methane emissions from the WSL ranged from 6 to 120% more than historical levels, with the range primarily determined by the nature of the response of soil microbes to climate change. Crucially, under one potential scenario, the majority of methane emissions will shift from the south of the WSL to the north, where permafrost thaw is a concern. These results suggest a need to both a) account for sub-grid heterogeneity in wetland soil moisture conditions and b) constrain the response of soil microbial communities to future changes in climate and vegetation.

TABLE OF CONTENTS

List of Figures

List of Tables

ACKNOWLEDGMENTS

We are not the sole owners of our accomplishments; nothing can be achieved in a vacuum. I could not have completed this dissertation without the support and help of many people. I am grateful to my parents, who have always believed in me, encouraged my curiosity, and taught me to not give up easily. My wife has been amazingly patient, supportive, and accommodating during this multi-year ordeal; I feel very fortunate to have her in my life. My advisor, Dennis Lettenmaier, has given me both guidance and the freedom to make most of the decisions (and mistakes) in this effort; as a result I feel I have learned an immense amount about how to design research projects. He has also provided me with a multitude of opportunities to collaborate with other researchers around the world, which have enriched my work and expanded my future career options enormously. I am grateful to my current and former committee members (Michael Brett, Jeff Richey, Kyle McDonald, Laura Bowling, Rebecca Neumann, Martin Heimann, Gerard Roe, and Cecilia Bitz) for their generous advice, insights, and time invested into my PhD. I would also like to thank Xiaodong Chen and Sasha Richey for their assistance in the tedious work of preparing model parameters; Bart Nijssen for his advice; and my other colleagues in the UW CEE department for their insights, support, and friendship. I also thank my colleagues and collaborators outside the University of Washington. In particular, Jed Kaplan and Pasha Groisman have brought me together with many other researchers (e.g., Shamil Maksyutov and Mikhail Glagolev), without whose contributions my work would not have been possible. Finally, I would like to thank the National Oceanographic and Atmospheric Administration (NOAA) and the National Aeronautics and Space Administration (NASA), who funded my efforts over the last 8 years.

I. INTRODUCTION

As the world's largest natural source of methane (CH_4), wetlands are an important component of the global carbon cycle (Fung et al., 1991). Northern wetlands have been a large net sink of carbon dioxide (CO_2) since the last Ice Age (Smith et al., 2004). Because the fluxes of both of these greenhouse gases are highly sensitive to soil moisture and temperature, there is concern that wetland CH_4 and CO_2 emissions could provide a positive feedback to climate change (Melton et al., 2013; Tang et al., 2008; Eliseev et al., 2008; Gedney et al., 2004). Boreal and arctic wetlands are of particular concern, due to their large extent (Lehner and Döll, 2004), pronounced ongoing and projected warming at high latitudes (Serreze et al., 2000; Diffenbaugh and Giorgi, 2012) and the possibility of previously-frozen soil carbon decomposing as permafrost thaws (Koven et al., 2011; Schaefer et al., 2011; Walter et al., 2006; Zimov et al., 2006). Despite the importance of these ecosystems to the global carbon cycle, large-scale estimates of wetland carbon fluxes have been hampered by crude representations of wetland hydrology and soil biogeochemistry in land surface models, and the neglect of spatial variation in processes at scales ranging from meters to hundreds of kilometers.

I focus in this dissertation on improving the prediction of boreal wetland carbon fluxes (primarily methane) in large-scale models, with an emphasis on accurately representing the hydrologic and biogeochemical processes that give rise to spatial variability in methane emissions. The key hydrologic feature on which I focus is spatial variation in water table depth. Because of the anoxic conditions below the water table, the water table position partitions the decomposition of soil carbon between CO_2 and CH_4

(Walter and Heimann, 2000; Frolking et al., 2002), whose greenhouse warming strength is approximately 25 times that of CO_2 over the course of a century (IPCC, 2007). In situ observations have shown that high-latitude wetland CH_4 emissions are highly and non-linearly sensitive to the local water table depth (e.g., Dise et al., 1993; Saarnio et al., 1997), which can vary spatially on the scale of meters (Saarnio et al., 1997; Eppinga et al., 2008). Thus, using the average water table depth over a large (e.g., 10- to 100-km) grid cell to compute average CH_4 emissions, as has been the practice in many large-scale models (e.g., Meng et al., 2012; Riley et al., 2011; Zhuang et al., 2006; Zhuang et al., 2004) will yield large errors (Baird et al., 2009). In addition, because climate controls the hydrologic fluxes that determine water table depth, a model's water table formulation should have an effect on the simulated sensitivity of wetland CH_4 emissions to climate change. Thus, the first objective of my research was to implement a scheme that accounts for small-scale (sub-grid cell) variability in water table depth in a process-based way, and to compare the response of its simulated methane emissions to climate with that of other schemes that neglect spatial variation in water table depth. This work was carried out using the Variable Infiltration Capacity (VIC) large-scale hydrology model (Liang et al., 1994), with extensions to account for carbon cycling and wetland-specific processes, and coupled to the wetland methane emissions model of Walter and Heimann (2000).

Another issue that has contributed to uncertainty in understanding the role of northern wetlands as related to the global carbon cycle is the lack of observational constraints on large-scale spatial variability. Due to a scarcity of in situ methane and water table observations, most previous large-scale studies have applied a single methane emissions parameter set, calibrated to match a handful of isolated sites, across the entire

globe or large portions of it (e.g., Riley et al., 2011; ; Ringeval et al., 2010; Zhuang et al., 2004). One advantage of a spatially distributed water table scheme is that it predicts a time-varying area fraction of saturated soil, which can be compared with, and calibrated to match, passive and active microwave remote sensing observations (e.g., Schroeder et al., 2010). In addition, it allows easier comparison between whole-grid-cell simulations and in situ observations of CH_4 fluxes and water table depths at discrete points on the land surface. Recent intensive field campaigns (e.g., Peregon et al., 2009; Glagolev et al., 2011) have yielded large numbers of in situ observations along a 1000-km transect across the West Siberian Lowland (WSL), making it possible for the first time to examine large-scale spatial patterns in water table depths and methane emissions. These observations reveal a strong South-North gradient in CH_4 emissions within the WSL, with much lower emissions over the permafrost portion of the region, where the release of carbon from thawing permafrost is a concern (Schaefer et al., 2011; Koven et al., 2011). This stands in stark contrast to the spatial patterns predicted by most models. Thus, the second objective of this research effort was to understand these patterns in the WSL, to reproduce them in model simulations, and to evaluate the key model features that are necessary to reproduce them.

In addition to the thawing of permafrost, future changes in high-latitude climate will be accompanied by northward shifts in the distribution of vegetation (e.g., Kaplan and New, 2006). The potential responses of soil microbial communities (which are the primary agents of decomposition) to these changes are poorly understood (Conant et al., 2011). One potential response is acclimatization, in which the initial increase in CH_4 emissions due to elevated temperatures fades over time (Allison et al., 2010). Another response is the shifting of species abundances (Pickles et al., 2012), which could result in northern

microbial communities having similar species abundances (and CH_4 emissions response) to those in the south. The strong South-North gradient in CH_4 emissions observed in the WSL implies distinct differences between the microbial communities in the South and North. Population shifts could therefore result in a dramatic increase in microbial methane production rates in the North. Thus, the third objective of this research effort was to estimate the potential range of end-of-century CH_4 emissions in the WSL and to identify the relative contributions of climate, vegetation, and soil microbes to these changes. This was accomplished by forcing the VIC model with the outputs from the Climate Model Intercomparison Project, phase 5 (CMIP5; Taylor et al., 2012).

1.1 Science questions

I develop in this dissertation a new representation of sub-grid heterogeneity in wetland soil moisture dynamics for use in large-scale models, and examine the role of small- to large-scale spatial heterogeneity in wetland carbon fluxes over large-scales. The science questions that motivated this model development and implementation effort are:

1. What are the dominant mechanisms controlling the behavior of a heterogeneous water table in boreal wetlands, and how do they influence the response of high-latitude wetland carbon fluxes to future climate change?
2. Can a model that represents these mechanisms be used to characterize the errors inherent in previous global estimates of wetland carbon fluxes?
3. How does small-scale heterogeneity in water table depths and large-scale variability in methane productivity affect the large-scale behavior of high-latitude wetland carbon fluxes?

4. What are the dominant factors affecting future carbon fluxes from high-latitude wetlands?

The following four chapters address these questions. Chapter II (published as Bohn et al., 2007), describes the structure of a modeling framework, consisting of the Variable Infiltration Capacity (VIC) model (Liang et al., 1994), extended to include a distributed water table scheme and a representation of net primary productivity, and linked to the wetland methane emissions model of Walter and Heimann (2000). Application of this new modeling structure to the WSL addresses question 1 above. Chapter III (published as Bohn and Lettenmaier, 2010), addresses question 2 by replacing the distributed water table scheme with two other popular (but simpler) schemes and comparing their responses to climate change. Chapter IV (in review as Bohn et al., 2013b) addresses question 3 above by describing the further development of this modeling framework to include soil respiration, the calibration of this framework against intensive observations of CH_4 and water table depth across West Siberia, the resulting large-scale spatial and temporal patterns in carbon fluxes, and their consequences for understanding the response of boreal wetlands to climate change. Chapter V (submitted as Bohn and Lettenmaier, 2013) addresses question 4 by driving this modeling framework with the land surface climate outputs of 32 CMIP5 climate models over the 21st century and comparing the effects of changes in climate and LAI, as well as several potential responses of soil microbes to these changes, on the large-scale carbon fluxes from the WSL.

II. METHANE EMISSIONS FROM WESTERN SIBERIAN WETLANDS: HETEROGENEITY AND SENSITIVITY TO CLIMATE CHANGE

This chapter has been published in its current form in *Environmental Research Letters* (Bohn et al., 2007).

2.1 Introduction

Wetlands play an important dual role in the global carbon cycle as both the largest natural methane source (115 Tg CH_4 y^{-1}; Matthews and Fung, 1987) and a large net carbon sink (76 Tg C y^{-1} for high-latitude peatlands alone; Gorham, 1991). Both the extent of wetlands and the balance between their methane emissions and carbon sequestration depend on climatological and hydrological factors, leading to potentially significant feedbacks to the global climate system. This is especially true in the northern high latitudes, where ongoing and projected climate change is most pronounced (Serreze et al., 2000; IPCC, 2007), and particularly so in northern Eurasia, where roughly 30% of global wetlands are found (Matthews and Fung, 1987; Gorham, 1991). Despite the importance of these systems to the global carbon cycle, substantial uncertainties remain in estimates of their extents, carbon fluxes, and responses to climate change. This is due in large part to the sparseness of in situ observations in northern Eurasia.

Field studies have shown that wetland methane emissions depend on a number of environmental factors, among the most important of which are soil temperature, water table

depth, and substrate (organic carbon) quality (e.g. Dise et al., 1993; Shannon and White, 1994; Valentine et al., 1994; Panikov and Dedysh, 2000). In a review of field studies, Christensen et al. (2003) found that the dependence of methane emissions on water table depth is highly non-linear. When the water table is within roughly 10 cm of the surface, soil temperature becomes the limiting factor on methane production and sensitivity to the water table becomes small. Below a depth of 10 cm, water table depth quickly becomes the limiting factor. In addition, while temperature drives methane emissions through its control on metabolic rates, it also influences the water table depth indirectly through snow melt and evapotranspiration.

Simulations of future climate suggest that western Siberia may become wetter and warmer (IPCC, 2007) over the next century. The resulting water table depths, and, in turn, wetland methane emissions, could rise or fall depending on the balance between increasing precipitation and higher temperatures. In addition, soil moisture storage can be highly heterogeneous, due mostly to microtopographic effects (e.g. Famiglietti et al.,1998; Famiglietti et al., 1999). This raises the question of whether water tables at sites where methane emissions have been measured are representative of the wetlands in the surrounding region, especially in the case of large wetland complexes such as those found in western Siberia, where measurements from only a handful of sites have been published. Indeed, wetland methane emissions have been found to vary considerably along transects of only a few hundred metres (e.g. Panikov and Dedysh, 2000; Saarnio et al., 1997), often as a result of variations in water table depth associated with local topographic features. Thus, it is reasonable to suppose that the areal extent of methane-emitting regions across

the landscape, and therefore total methane emissions, are a function of the spatial distribution of water table depths.

Large-scale modeling offers a means of understanding these interactions across the landscape in the face of sparse observations. To predict the response of global wetland methane emissions to future climate, several large-scale modeling studies have been performed (e.g. Zhuang et al., 2006; Gedney et al., 2004; Shindell et al., 2004), the consensus of which is that northern wetland methane emissions will at least double by the end of the 21st century. Of these, only Gedney et al. considered the sub-grid heterogeneity of the water table. They found that wetland extent did not increase substantially under future predicted climate, and that the primary driver of increased methane emissions was increased temperature. However, they applied their model globally over a coarse (2.5° × 3.75°) grid, and calibrated it against global interannual variability in atmospheric methane concentrations. On the other hand, Shindell et al. found that increases in wetland extent played a major role in increasing emissions; however, they only considered average water table depths over a coarse (1° × 1°) grid.

In this study, we investigate the response of northern wetlands to changes in climate by applying a macroscale hydrological and biogeochemical model with a parameterization of sub-grid heterogeneity of the water table depth over a 100 km × 100 km region of western Siberia. After calibrating with local observations of water table depth and methane emissions, we examine the effects of increased temperature and increased precipitation, both separately and in conjunction, on the spatial distribution of water table depths and the resulting distribution of methane emissions over the region.

2.2 Methods

Our study region consists of a single 100 km × 100 km grid cell (from the EASE grid equal area projection; Brodzik and Knowles, 2002) centered at 56° 29’ N, 83° 09’ E, near the town of Plotnikovo in western Siberia (Figure 2.1a). This grid cell contains the Bakchar Bog, a roughly 15 km×30 km portion of the large Vasyugan wetlands complex, where several research teams (e.g. Panikov and Dedysh, 2000, Panikov et al., 2001, Friborg et al., 2003) sampled methane emissions throughout the 1990s. The sample site (56° 51’ N, 82° 50’ E) is located near the edge of the bog, just outside a network of drainage canals.

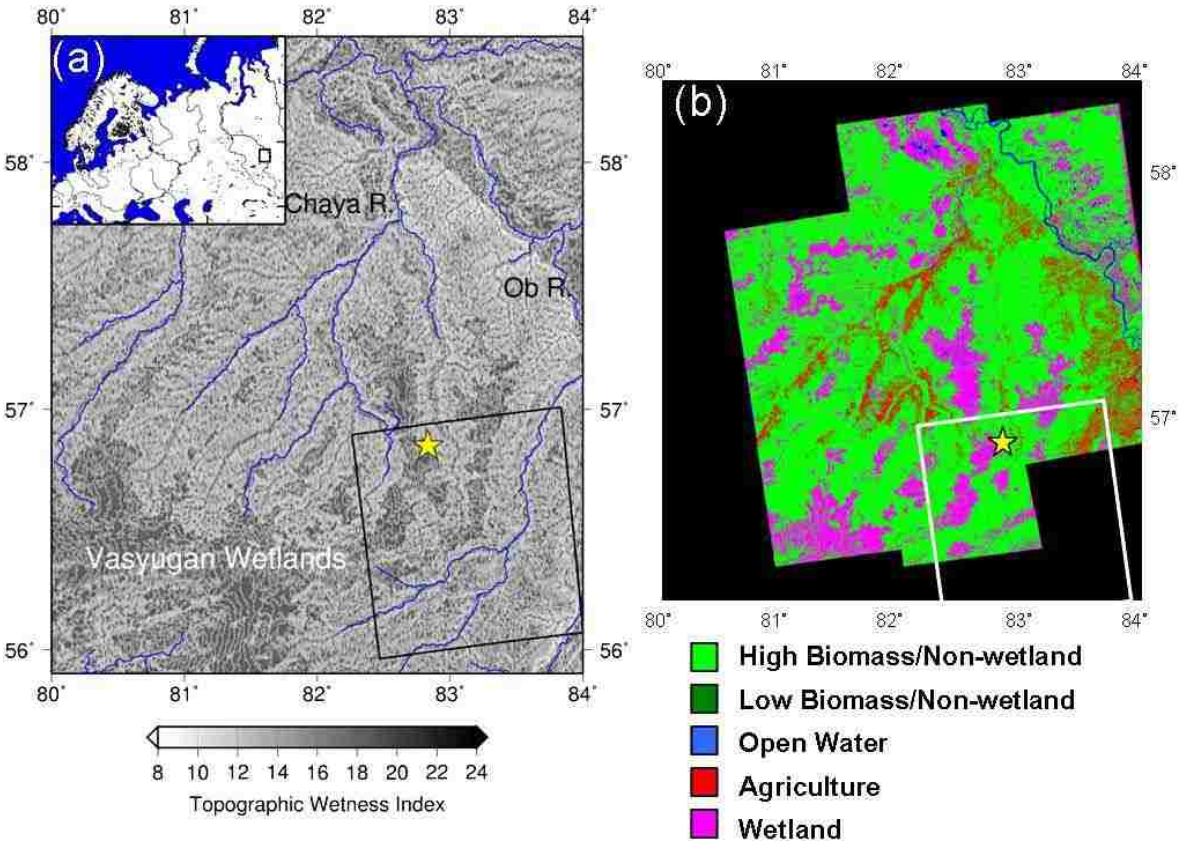

Figure 2.1: Location of study region. (a) Map of the topographic wetness index, derived from SRTM30 DEM (Farr and Kobrick, 2000), over the region. (b) Landcover of the region, derived from random forest (Chen et al., 2004) classification of ALOS/PALSAR imagery (courtesy of JAXA). In panels (a) and (b), the Bakchar Bog observation site is marked with the yellow star, and the 100 km × 100 km EASE-grid cell centered at (56° 51' N, 82° 50' E) is outlined in black (a) and white (b). Note the close correspondence between areas of high topographic wetness index (>14) in panel (a) and areas of wetland in panel (b).

Our modeling framework couples the variable infiltration capacity macroscale hydrology model (VIC; Liang et al., 1994) with the biosphere–energy-transfer–hydrology terrestrial ecosystem model (BETHY; Knorr, 2000) and the wetland methane emissions model of Walter and Heimann (2000). Following the standard VIC protocol, each grid cell in the domain (a single cell in this case) consists of a horizontally uniform, multi-layer soil column overlain by a mosaic of landcover 'tiles'. For each tile, given meteorological observations as input, VIC solves the moisture and energy balances for the land surface at an hourly time step, tracking soil moisture and temperature profiles, snow water equivalent,

transpiration, and soil freezing depth. Since the study region lies outside the southernmost extent of Eurasian permafrost, permafrost dynamics are not simulated. Similarly, the BETHY component computes hourly net primary productivity (NPP) via a Farquhar formulation (Farquhar et al.; 1980), given meteorological fluxes and VIC's soil moisture and temperature. Stomatal conductances are computed using a resistance-factor approach (Dickinson et al.; 1991) that takes into account evapotranspiration limitations due to temperature, light, vapor pressure deficit, and soil moisture. Nutrient availability is not simulated. Fluxes and storages from the individual tiles are then aggregated to produce grid-cell-average values. Daily average soil temperatures, the distribution of water table depth (see below), and NPP (as a proxy for carbon substrate availability) are provided to the methane model, which simulates methane production below the water table; transport of methane through the soil via diffusion, ebullition, and plant-aided transport; and oxidation above the water table to arrive at an estimate of daily methane emissions.

Among the extensions we have made to the VIC model is a simple scheme to convert the grid-cell-average soil moisture profile into a grid-cell-average water table depth. Our method follows Letts et al. (2000), with one exception. For each modeled soil layer, we compute the fractional volume of saturated soil Θ_v as

$$\Theta_v = (\theta_i - \theta_r)/(\theta_p - \theta_r) \quad (2.1)$$

where θ_i is the volumetric moisture of the i^{th} soil layer, θ_p is the porosity of the i^{th} soil layer and θ_r is the residual moisture of the i^{th} soil layer.

Next, the total water table depth z_{wt} is computed as the sum of the moisture deficits of all of the model soil layers:

$$z_{WT} = \sum_{i=1}^{3} dz_i(1 - \Theta_{vi}) \quad (2.2)$$

where dz_i is the thickness of the i^{th} soil layer.

In Letts et al. (2000), θ_r in equation (2.1) represented the specific retention of the i^{th} soil layer, essentially equivalent to the layer's field capacity. Since the hydraulics of the VIC model follow Brooks and Corey (1964), and drainage can continue well beyond field capacity, we were unable to produce results using the Letts et al. (2000) parameterization for which the soil moisture was greater than specific retention in any layer for more than a short period of time. Therefore, we replaced specific retention with residual moisture in equation (2.1).

To account for spatial heterogeneity of the water table depth within each grid cell, we employ a relationship between sub-grid topography and local water table depth taken from TOPMODEL (Beven and Kirkby, 1979), and incorporate the bias correction of Saulnier and Datin (2004). Sub-grid topography in this case is supplied by the 30-Arc-Second Shuttle Radar Topography Mission (SRTM30) digital elevation model (DEM) (Farr and Kobrick, 2000), which has a spatial resolution of 900 m. Under the assumptions that the surface infiltration rate and soil properties are uniform across a basin, and that subsurface transmissivity has an exponential profile with water table depth, the local water table depth $z_{wt,i}$ in pixel i of the DEM at time t can be expressed as a function of the average grid cell water table at time t and grid cell topography as

$$z_{wt,i}(t) = \overline{z_{wt}}(t) - m(\kappa_i - \lambda) \qquad (2.3)$$

where m is the scaling parameter, κ_i is the topographic wetness index = $ln(a_i / tan\ \beta_i)$, a_i is the upslope contributing area above location i, $tan\beta_i$ is the local surface slope and λ is the average of κ_i over the unsaturated area of the grid cell.

The distribution of the topographic wetness index κ_i across the basin depends only on basin topography and is constant in time. Thus, across the basin, the distribution of water table depths over time has the same shape as the distribution of κ_i, but with a time-dependent grid-cell-average value given by the VIC model. While this is strictly true only for the distribution over an entire basin, rather than a grid cell, the 100 km × 100 km grid cells we are considering here are sufficiently large that the relationship is still approximately true, i.e. pixels for which a significant fraction of their upslope contributing area lies outside the cell boundaries make up only a small fraction of the grid cell. Figure 2.1a shows the spatial distribution of the topographic wetness index for the study region. Comparison with a map of the region's landcover derived from ALOS/PALSAR imagery (Figure 2.1b) reveals a close correspondence between high topographic wetness index values (>14) and the occurrence of bogs.

For each day, the resulting distribution of water table depths is discretized, and methane emissions are estimated for each water table value in the discretized distribution. The total methane emission of the grid cell, then, is the area-weighted sum of the methane emissions from all of the discrete values of the water table depth.

Soil properties were based on typical peat characteristics as outlined in Letts et al. (2000). Although peat soils only occupy about 37% of the grid cell (based on Sheng et al., 2004), we nonetheless assume uniform soil properties across the grid cell. Because the sample site is underlain by peat soil, we found it necessary to use peat soil properties to simulate the observed water table drawdown with sufficient accuracy. Since, due to its high porosity, peat soil can accommodate a given change in moisture storage with a smaller change in water table depth than mineral soil, we expect that our estimates of water table

variability will be biased downward somewhat for areas of mineral soil. However, the mineral soils in this area are highly correlated with low topographic index values, yielding water table depths that are too deep for substantial methane production. Therefore, this choice should not have much effect on our methane prediction results.

For the VIC and BETHY elements of our model, the plant functional types and area fractions of the grid cell's vegetation tiles were derived from the landcover classification of Hansen et al. (2000). Vegetation parameters typical of a mix of non-vascular and vascular plants, with a maximum rooting depth of 30 cm, were used for the methane emissions model uniformly throughout the grid cell. The inputs to the models were gridded monthly meteorological forcings based on Adam and Lettenmaier (2007) with daily variability taken from the Sheffield et al. (2006) data set.

Additional parameters, including the VIC bottom-layer drainage parameters (Ds, Dsmax, and Ws), the TOPMODEL scaling factor *m*, and the methane emission parameters *vmax* and *r0*, were calibrated by comparing model results to water table depths and methane fluxes measured at the Bakchar Bog site in 1999 as reported by Friborg et al. (2003). Gaps in the observed temperature and precipitation records at the site prompted us to use the regional gridded meteorological forcings described above to drive our models for the calibration. Soil column layer thicknesses were set to 0.1 m, 0.4 m, and 2.0 m for the top, middle, and bottom layers, respectively. The resulting simulated and observed 3 cm soil temperatures, water table depths, and methane emissions (Figures 2.2a, b, and c, respectively) matched closely, with the exception of undersimulation of soil temperature in May and undersimulation of methane emissions in September. The undersimulation of soil temperature in May is likely due to differences between the gridded meteorological

forcings and local observations for that summer reported by Friborg et al. (2003) and Shimoyama et al. (2003). The underprediction of methane emissions in September may indicate that the model's sensitivity to water table depth is somewhat too high, although the model performance is generally better for other months.

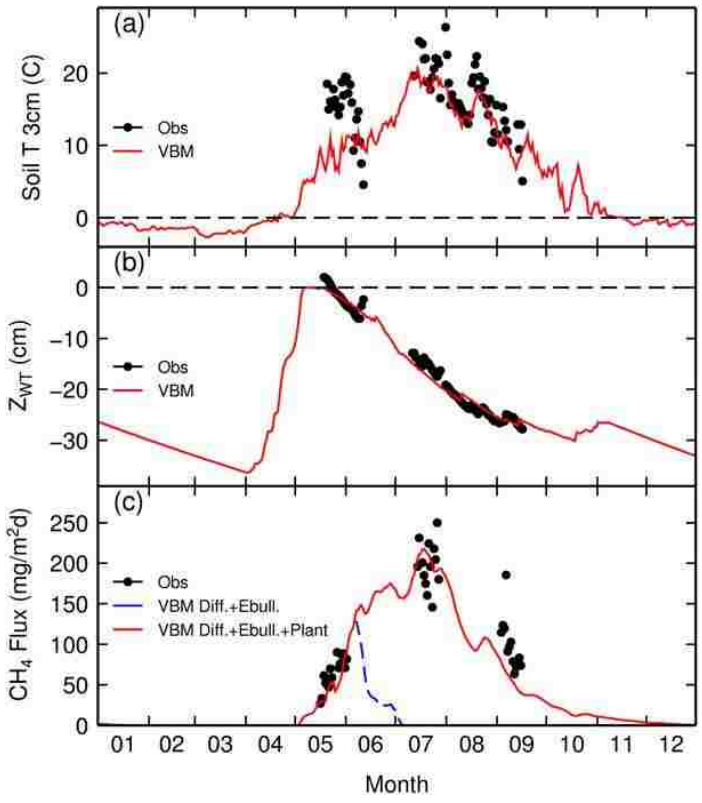

Figure 2.2: Simulated (labeled as 'VBM' for VIC/BETHY/methane modeling framework) and observed 3 cm soil temperature (a), water table (b), and methane flux (c) at the Bakchar Bog site, 1999. In panel (c), the contribution of diffusion and ebullition pathways to the simulated flux is plotted in the blue dashed line, while the total simulated flux is plotted in the solid red line.

2.3 Results

To evaluate the ability of our modeling framework to capture interannual variability in methane emissions, we compare simulated and observed soil temperatures, water table depths, and methane emissions for the summers of 1993–1997 at the Bakchar Bog site

(Figure 2.3). While the simulated July methane emissions (Figure 2.3c) approximate the values of the observed emissions in 1994, 1996, and 1997, large discrepancies exist in July 1993 and 1995, in which observed methane emissions were much higher than in the other years. It is possible that the simulated water table depth (Figure 2.3b) in those years is too low. We examined this possibility by prescribing observed soil temperatures and water table depths of 0 cm for the years 1993 and 1995. While this reduced errors somewhat, large discrepancies still remained. Unfortunately observations of the water table depth from most of these years were not available.

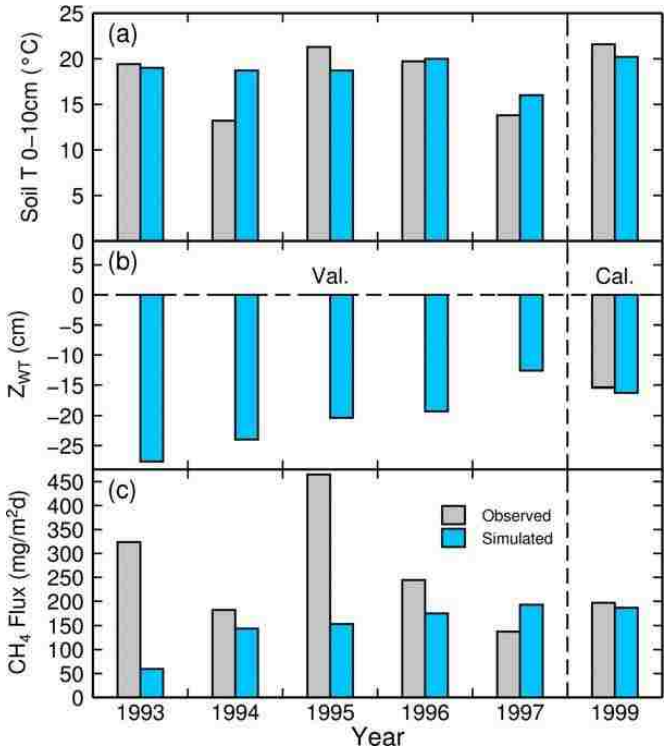

Figure 2.3: July average simulated and observed (a) soil temperature in the top 10 cm, (b) water table depth, and (c) methane fluxes for the Bakchar Bog site, for the validation years 1993–1997, and calibration year 1999. Observations for years 1993–1997 from Panikov and Dedysh (2000), for an unspecified number of days in July (and August, in the case of 1997). Observations for 1999 from Friborg et al. (2003) for 14–27 July.

It should also be noted that, except for 1999, the observed fluxes are the averages over an unspecified number of days, while the model results shown are the average over the entire month of July, which complicates comparisons. However, our landscape-scale

estimates of methane emissions over the 100 km×100 km region compare favorably to estimates made by remote sensing and aircraft flyovers. Takeuchi et al. (2003) extrapolated field observations taken in July 1993 and 1994 to the region bounded by 56°–60° N and 78°–86° E, using landcover classifications derived from AVHRR and SPOT/HRV images, yielding a regional average July flux of 59.3 mg CH_4 m^{-2} d^{-1} for 1993 and 1994. Meanwhile, estimates of methane fluxes based on vertical profiles from aircraft flyovers in the region in 1994 range from 34 to 126 mg CH_4 m^{-2} d^{-1} (Tohjima et al., 1994). In comparison, our modeling framework predicts average methane emissions of 43.0 mg CH_4 m^{-2} d^{-1} for the same time intervals. Figure 2.4 shows a map of simulated average annual methane emissions for the 100 km×100 km region for the period 1980–1999. The spatial pattern of emissions exhibits a high correlation with the topographic wetness index (Figure 2.1a) and wetland vegetation (Figure 2.1b). Note that much of the landscape (primarily outside the bogs) actually has a negative methane flux, due to oxidation in the soil; this behavior is typical of non-wetland soils (Nakano et al., 2004; Crill, 1991).

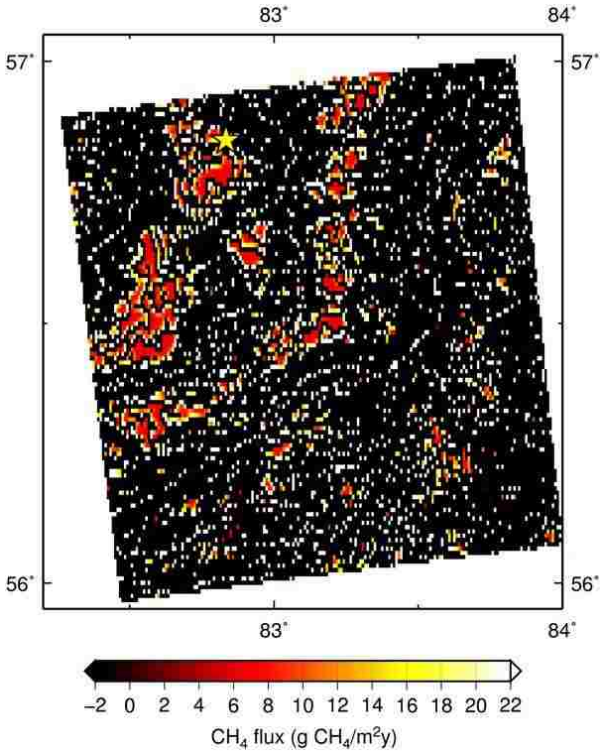

Figure 2.4: Simulated annual average methane emissions for the 100 km × 100 km grid cell, for the period 1980–1999. The yellow star denotes the Bakchar Bog site.

Climate models suggest that northern Eurasia will experience increases in temperature and precipitation by the end of the 21st century (IPCC, 2007). In particular, summer temperatures are likely to increase by 2.0–5.6 °C and summer precipitation is likely to change by −1 to +16%, with median values of +3 °C and +9%, or roughly 5–7 mm per month (temperature and precipitation in other seasons may increase even more than this). To investigate the response of wetland water tables and methane emissions to the predicted range of changes in climate, we constructed 24 climate scenarios consisting of the 'baseline' meteorological forcings from 1980–1999 and all 24 combinations of six uniform (year-round) increases in air temperature (0 (1) 5 °C) and four uniform (year-round) increases in precipitation (0 (5) 15%).

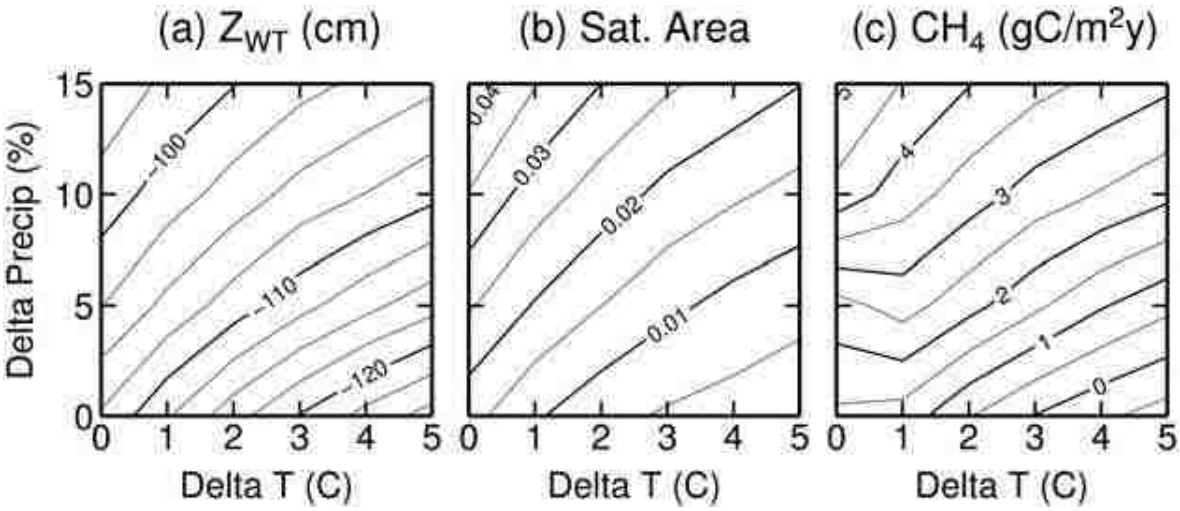

Figure 2.5: Sensitivity of simulated water table depth (a), saturated area fraction (b), and annual total methane emissions (c), for the 100 km × 100 km grid cell, to changes in temperature and precipitation relative to the 1980–1999 baseline scenario.

Contour plots of the resulting mean annual water table depths, saturated area fractions, and methane emissions, averaged over the 100 km × 100 km grid cell, are shown in Figure 2.5. Some general relationships are evident: increasing temperature and constant precipitation tends to lower the water table (Figure 2.5a), reducing the fraction of the grid cell for which soil moisture is at saturation (Figure 2.5b), and reducing methane emissions (Figure 2.5c), while increasing precipitation, while holding temperature constant, tends to raise the water table, increase the saturated area, and increase methane emissions. One exception to these relationships is for small increases in temperature (1 °C) and precipitation (5%), for which the temperature increase can cause a slight increase in methane emissions.

Results for selected scenarios are given in Table 2.1. For the baseline simulation, average annual methane emissions and water table depth were 1.4 g CH_4 m^{-2} y^{-1} and 108 cm, respectively. For the extreme case of an increase in air temperature of 5 °C methane emissions decreased by 2.1 g CH_4 m^{-2} y^{-1} relative to the baseline, to −0.7 g CH_4 m^{-2} y^{-1}. In

this case, methane production in the bogs was less than methane oxidation elsewhere, leading to net consumption of methane in the grid cell. This reduction was accompanied by a lowering of the water table to 126 cm below the surface. In contrast, increasing precipitation by 15% raised the water table to 96 cm below the surface, which in turn raised methane emissions to 5.1 g CH_4 m^{-2} y^{-1}, a 264% increase relative to the baseline. Combining the increase in temperature and the increase in precipitation ('T + 5 & P + 15%') resulted in intermediate effects: the water table depth (104 cm) remained similar to that of the baseline, and methane emissions rose to 3.1 g CH_4 m^{-2} y^{-1} (or 121% above the baseline). For the median case of an increase in air temperature of 3 °C and an increase in precipitation of 10%, methane emissions increased by 2.8 g CH_4 m^{-2} y^{-1} (or 100% above the baseline) and the water table depth (106 cm) remained similar to that of the baseline.

Table 2.1: Simulated average annual methane emissions, water table depths, and saturated areas for baseline and various future climate scenarios.

Scenario	Annual CH_4 emission (g m^{-2} y^{-1})	Average water table (cm below surface)	Average saturated area fraction
Baseline	1.4	108	0.017
T + 5[a]	-0.7	126	0.002
P + 15% [a]	5.1	96	0.014
T + 5 & P + 15% [a]	3.1	104	0.020
T + 3 & P + 10% [a]	2.8	106	0.019

[a]'T + 5' indicates a uniform 5 ◦C increase over 1980–1999 temperatures. 'P + 15%' indicates a uniform 15% increase over 1980–1999 precipitation.

The mechanisms underlying these results are illustrated in Figure 2.6, which shows the seasonal cycles of relevant variables for the following four scenarios: (1) the current climate baseline, (2) an increase in temperature of 5 °C ('T+5'), (3) an increase in precipitation of 15% ('P + 15'), and (4) increases of 5 °C in temperature and 15% in precipitation ('T + 5 & P+15'). While soil temperature (Figure 2.6a) exerts the primary

influence on the seasonal evolution of methane emissions (Figure 2.6f) within a single year, differences in the annual mean water table depth (Figure 2.6e) exert a considerable influence on emissions when comparing different years or climate scenarios. Both air temperature and precipitation determine the seasonal shape and annual mean of the water table depth. The higher air temperatures of the 'T + 5' and 'T + 5 & P + 15%' scenarios result in smaller snow packs (Figure 2.6b) that start and finish melting earlier than the baseline (Figure 2.6c), as well as greater evapotranspiration in late spring and early summer (Figure 2.6d), leading to lower annual mean water table depths (Figure 2.6e). The resulting methane emissions (Figure 2.6f) for these scenarios are lower throughout the year than their lower-temperature counterparts (baseline and 'P + 15%', respectively) with the exception of the month of May, when water table depths are at their shallowest and soil temperatures are the limiting factor. On the other hand, the greater precipitation of the 'P + 15%' and 'T + 5 & P + 15%' scenarios results in a larger snow pack (Figure 2.6b) and larger peak in snow melt flux (Figure 2.6c) but modest change in the timing of melt in comparison with the baseline and 'T+5' scenarios, respectively. Evapotranspiration (Figure 2.6d) is also higher in these scenarios, due to greater upper-layer soil moisture. The larger snowmelt pulses and rainfall infiltration lead to higher annual mean water tables (Figure 2.6e) and greater methane emissions throughout the year (Figure 2.6f). Thus, the balance between temperature- and precipitation-induced effects on the water table plays a major role in the response of these wetlands to climate change.

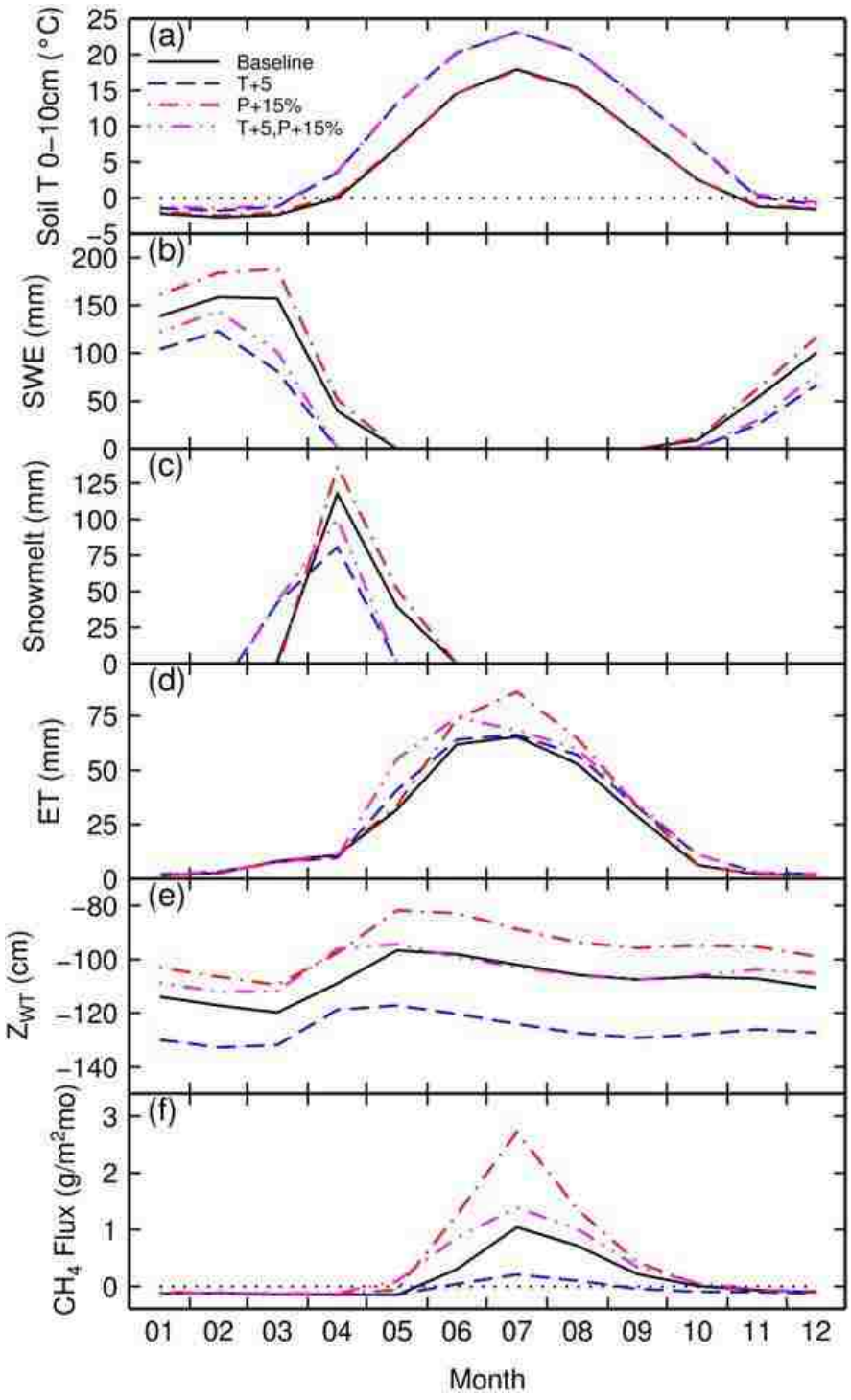

Figure 2.6: Panels (a) to (f) show monthly average values of soil temperature, snow water equivalent, snow melt flux, evapotranspiration, grid cell-average water table level, and grid cell-average methane emission, respectively, for the 100 km × 100 km grid cell, for the 1980–1999 baseline and for the 'T + 5', 'P + 15%', and 'T + 5 & P + 15%' scenarios for 2080–2099.

These interactions between temperature and precipitation are not uniform across the landscape, as illustrated in Figure 2.7. For reference, Figure 2.7a shows the distribution of topographic wetness index as a function of cumulative area fraction within the 100 km × 100 km grid cell. Present-day bogs, indicated on the plot, fall in pixels with wetness index values above 14, with a high concentration above 18. Owing to their higher topographic wetness index values, these pixels tend to have much shallower water table depths than the rest of the grid cell. In the baseline scenario, many of the present-day bog areas (5% of the grid cell) have mean annual water table depths (Figure 2.7b) no deeper than 20 cm, and a small portion of these areas are completely saturated (i.e. the water table is at the surface) year round. Accordingly, those bog areas with mean annual water table depths less than 20 cm emit from 20 to 48 g CH_4 m^{-2} y^{-1} (Figure 2.7c). Meanwhile, approximately 80% of the grid cell (including some of the bog areas) has water table depths greater than 50 cm, and has a net emission of −2 g CH_4 m^{-2} y^{-1} due to the oxidation of methane in the soil.

In the three future climate scenarios described above, the responses of the water table (Figure 2.7b) and methane emissions (Figure 2.7c) to changes in climate vary spatially, and in some cases the responses of different regions cancel each other out. In the 'T + 5' scenario, the drop in the grid-cell average water table causes (a) a reduction in the area of the grid cell that is saturated year round, and (b) a lowering of the local water table in all non-saturated areas. While methane emissions increase up to 75 g CH_4 m^{-2} y^{-1} in the saturated areas due to temperature-driven increases in metabolic activity, emissions decrease elsewhere in response to the deeper water table depths, resulting in a net reduction in methane emissions over the whole grid cell. In contrast, the 'P + 15%' scenario raises

the water table in all areas of the grid cell that are not completely saturated in the baseline scenario, increasing emissions throughout the areas with a topographic index >18.

In particular, the rise in the water table causes the saturated and near-saturated areas (water table depth shallower than 20 cm), which emit methane at 20 g CH_4 m^{-2} y^{-1} or more, to expand from 5% to 10% of the grid cell area. Finally, in the 'T + 5 & P + 15%' scenario, the higher precipitation approximately cancels the effect of higher temperature on the water table depth, causing water table depths across the grid cell to remain similar to the baseline. While higher temperatures lead to higher peak methane production rates (75 g CH_4 m^{-2} y^{-1}), the increase in methane production rates occurs primarily in the saturated areas of the grid cell, due to the shallower water table depths, and thus when summed over the entire grid cell, amounts to a smaller increase in emissions than in the 'P + 15%' scenario. In general, because the distribution of water table depths depends on the shape of the distribution of topographic wetness index, we can expect the net change in methane emissions to vary from region to region as a function of topography.

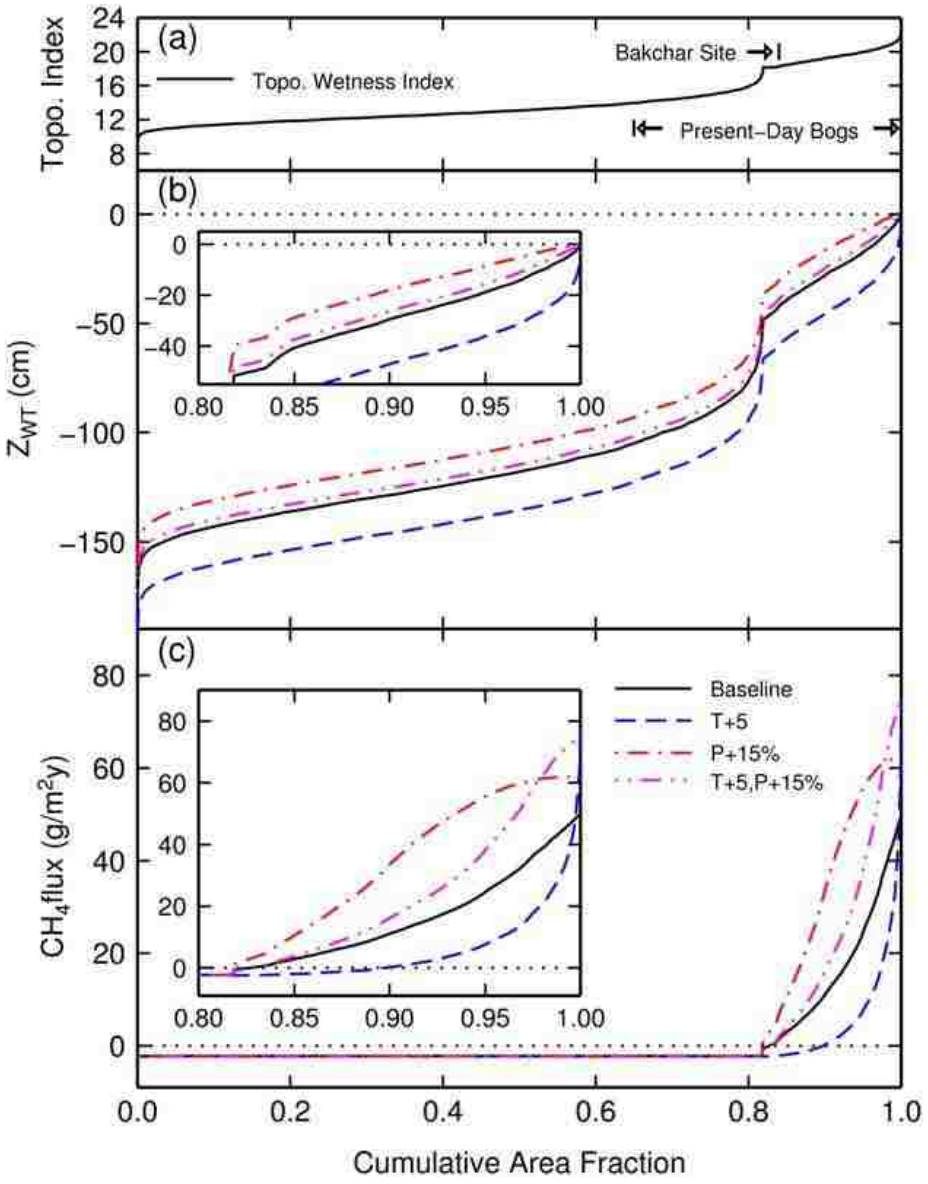

Figure 2.7: (a) Cumulative distribution of topographic wetness index for the 100 km×100 km grid cell. The range of wetness index values containing present-day bogs is indicated. Panels (b) and (c) show cumulative distributions of simulated annual average water table level and simulated annual average methane emission, respectively, for the grid cell, for the 1980–1999 baseline and for the 'T + 5', 'P + 15%', and 'T +5 & P + 15%' scenarios for 2080–2099.

2.4 Discussion

From Figure 2.5, we can see that increases in temperature and precipitation can balance each other to some extent, causing some climate scenarios (for example, 'T + 3 &

P + 10%' and 'T + 5 & P + 15%') to have similar impacts on regional methane emissions. The most extreme impacts occur for those scenarios involving substantial changes in either temperature alone or precipitation alone. However, these less-balanced scenarios tend to fall on the outskirts of the range of climate predictions (IPCC, 2007). Under scenarios closer to mid-range of the IPCC (2007) estimates, regional water table depths would experience modest changes, while methane emissions would increase between 50 and 125% according to our model results.

Our prediction of a 100% increase in annual average methane emissions for the median end-of-century climate scenario ('T +3 & P + 10%') is consistent with other modeling studies (e.g., Zhuang et al., 2006; Gedney et al., 2004; Shindell et al., 2004) that have predicted substantial increases in methane emissions from northern wetlands under various climate scenarios for the 21st century. Like Shindell et al., we find that changes in the extent of saturated and near-saturated area (annual average water table depth shallower than 20 cm) play a large role in the response of wetlands to climate change. Despite using a similar approach to Gedney et al., we find the change in wetland extent to be more important to methane emissions than they did. One reason for this may be that our methane emissions are more sensitive to water table depth than theirs. Another reason may be that we calibrated our models to match local observations, while Gedney et al. calibrated their model to reflect global atmospheric methane concentrations.

More simultaneous observations of water table depth, soil temperature, and methane emissions, over more points across the landscape, would help constrain our models. Our results also depend in part on the accuracy of our simulated water table depths, which in turn are particularly sensitive to the soil porosity. A higher-porosity soil can

accommodate a given change in soil moisture (e.g. due to infiltration or evaporative demand) with a smaller change in water table depth than a lower-porosity soil. In order to preserve the assumptions of the TOPMODEL framework, we have assumed spatially uniform soil properties. In reality, the mineral soils outside present-day bogs tend to have lower peat content, and thus lower porosity than the values we used in our simulations. Therefore, we might expect that the water table will exhibit more variability outside the bogs than we have predicted. On the other hand, these areas also tend to have lower topographic index values, and therefore deeper water table depths and much lower methane production rates, than the bogs, and thus have very little influence on total methane emissions across the landscape. Zhuang et al. (2006) avoided this problem by prescribing the wetland fraction of each grid cell, and only modeling a uniform water table in the wetland fraction. However, this approach does not consider the non-linear response of methane emissions to heterogeneity in the water table depth and therefore neglects the changes in methane emissions due to changes in the extent of the saturated region. Some combination of these approaches, in which the water table distribution is modulated by local soil properties, could prove useful in this regard.

While we have only considered uniform increases in temperature and precipitation throughout the year, climate models in fact suggest that winter temperature and precipitation will likely increase more than in summer (IPCC, 2007). The resulting size and melt dates of the snow pack under these conditions may lead to earlier and larger rises in the water table, which, coupled with higher spring temperatures, could lengthen the duration of substantial methane emissions. It also should be noted that our modeling framework predicts very low methane emissions during the winter. Some field studies have

found that winter methane emissions can account for up to 22% of the annual total (e.g., Aurela et al., 2002; Panikov and Dedysh, 2000; Alm et al., 1999). On the other hand, given that soil temperatures during the winter do not change appreciably among scenarios due to the insulation of the snow pack, and that the snow pack effectively decouples soil moisture from winter precipitation until snow melt, we do not expect winter emissions to be nearly as sensitive to climate change as summer emissions.

Other factors we have not considered include increased atmospheric CO_2 concentrations and changes in nutrient availability. Increased atmospheric CO_2 would likely reduce transpiration somewhat, reducing the summertime drop in the water table and increasing methane emissions during late summer. Increased temperatures and drying of soils could lead to the mineralization and subsequent loss of nutrients from the soil, which could reduce methane emissions. Although we believe that these secondary effects would likely be smaller in magnitude than the primary effects of water table changes that we have modeled, these mechanisms should nonetheless be the focus of future research.

2.5 Conclusions

We have created a modeling framework for the prediction of regional wetland methane emissions by coupling of the VIC macroscale hydrology model with the BETHY terrestrial carbon model and the wetland methane emissions model of Walter and Heimann (2000), incorporating an implementation of the TOPMODEL concept of sub-grid heterogeneity of the water table. This framework reasonably captures seasonal changes in methane emissions as a function of climate, and makes plausible estimates of methane emissions over large areas. Results from a sensitivity analysis indicate that, for the

Vasyugan wetlands in western Siberia, methane emissions may increase by 100% over current values under likely climate conditions at the end of this century. In addition, we have found that the interaction of temperature and precipitation, through their effects on the water table depth, play an important role in determining methane emissions from these wetlands. The balance between these effects varies spatially, and their net effect depends in part on sub-grid topographic heterogeneity.

Increases in temperature alone tend to reduce emissions because the lowering of the water table (and reduction of the methane-producing area) in response to smaller snow packs and higher evaporative demand more than compensates for the temperature-driven increase in methane production in those areas that remain relatively wet. Meanwhile, increases in precipitation alone tend to increase methane emissions through the expansion of saturated and near-saturated areas across the landscape. Under conditions of both increased temperature and increased precipitation, the net result depends on the relative strengths of the increases, in addition to the local topography.

Acknowledgments

ALOS/PALSAR imagery of the region was provided courtesy of JAXA.

III. SYSTEMATIC BIASES IN LARGE-SCALE ESTIMATES OF WETLAND METHANE EMISSIONS ARISING FROM WATER TABLE FORMULATIONS

This chapter has been published in its current form in *Geophysical Research Letters* (Bohn and Lettenmaier, 2010).

3.1 Introduction

Wetland methane emissions depend strongly on climate and have the potential to exert a positive feedback to climate change (Intergovernmental Panel on Climate Change (IPCC), 2007). This is of particular concern in boreal and arctic regions, where much of the world's wetlands reside (Lehner and Döll, 2004) and where climate change has been and is predicted to be most pronounced (IPCC, 2007). Among other factors, wetland methane emissions depend non-linearly on water table depth, which controls the transition from aerobic to anaerobic decomposition (Walter and Heimann, 2000), and which varies considerably over small distances in boreal wetlands (Eppinga et al., 2008; Saarnio et al., 1997).

Several recent modeling studies have estimated the response of wetland methane emissions across the high latitudes to predicted changes in climate over the next century. Most earth system models that simulate wetland methane emissions use variants of the methane emissions model of Walter and Heimann (2000), applied to simplified representations of water table depth over the wetland portions of large (typically 0.5–2.5

degree) grid cells. Due to the lack of water table measurements over most of the Earth's surface, these simplifications either assume a) a spatially uniform but temporally-varying water table depth (uniform scheme) (e.g., Zhuang et al., 2004; 2006; Shindell et al., 2004; Walter et al., 2001a, 2001b) or b) a temporally-varying mix of wet (perpetually saturated) and dry (non-emitting) fractions (wet-dry scheme) (Ringeval et al., 2010; Gedney et al., 2004). Both of these schemes constitute major simplifications. The uniform scheme neglects the effects of spatial heterogeneity in water table depth (and therefore in methane emissions). The wet-dry scheme neglects emissions from the non-saturated portion of the wetland, which depend on water table depth. A scheme that takes spatial variation of the water table depth into account (a distributed scheme) (e.g., Bohn et al., 2007) should not be subject to such biases if it represents the water table distribution accurately.

Here we investigate the question: how do end-of-century methane emissions projections resulting from the aforementioned simplified water table schemes compare with those of a distributed water table scheme, as a function of the spatial variation in the wetland's water table depth? To ensure a fair comparison, we require all schemes to use the same methane model parameter set and: a) same saturated area (for the wet-dry scheme), or b) same current-day spatial average methane emissions (for the uniform scheme).

3.2 Methods

Because the uniform and wet-dry schemes are special cases of the distributed scheme, we first ran the distributed scheme and then used those results to derive the emissions of the other schemes. To generate hydrologic inputs, we used the Variable

Infiltration Capacity (VIC; Liang et al., 1994) large-scale hydrologic model, with modifications for carbon cycling taken from Knorr (2000) and the spatially distributed water table parameterization described by Bohn et al. (2007). The resulting simulated soil temperatures, net primary production (NPP), and spatially-distributed water table depths were then provided to the methane emissions model of Walter and Heimann (2000), which generated a time series of spatially-distributed methane emissions. We ran this modeling framework for the period 1948–2007 over a single 100 × 100 km grid cell centered at (56° 29′N, 83° 09′E) in West Siberia, using meteorological drivers and soil and vegetation parameters described by Bohn et al. (2007) and the methane model parameter sets described below. While the methane model parameters we are using here differ from those of Bohn et al. (2007), it is worth noting that simulations in that study compared favorably to in situ measurements of soil temperature, water table depth, and methane emissions, and to aircraft measurements of areal methane fluxes.

As described by Bohn et al. (2007), the distributed water table depth within the wetland portion of the domain was generated as a post-processing step using the topographic wetness index concept from TOPMODEL (Beven and Kirkby, 1979). First, the topographic wetness index was computed at approximately 90 m resolution for each pixel of the Shuttle Radar Topography Mission (SRTM) DEM (Farr and Kobrick, 2000) falling within the 100 × 100 km grid cell; non-wetland pixels (43% of the grid cell) were then masked out using the peatland map of Sheng et al. (2004). Then, for each day of the simulation, each wetland pixel's water table position $z_{wt,i}$ (negative values indicate that the water table is below the

soil surface) was assumed to be a function of the wetland's spatially-averaged water table position $\overline{z_{wt}}$ and the pixel's wetness index κ_i:

$$z_{wt,i}(t) = \overline{z_{wt}}(t) - m(\kappa_i - \lambda) \quad (3.1)$$

where λ is the wetland's spatially-averaged wetness index, and m is a parameter that controls the spatial variance of water table depths across the wetland.

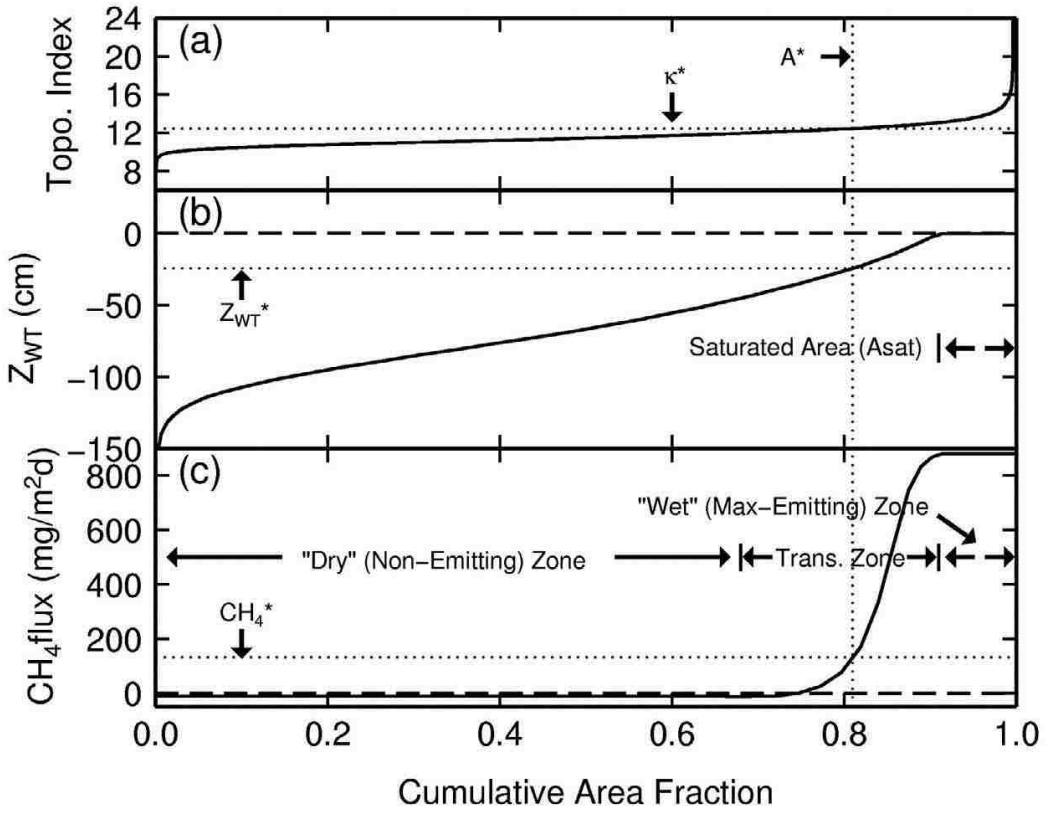

Figure 3.1: Example spatial distributions of (a) topographic wetness index, (b) water table position z_{wt}, and (c) net CH_4 emissions across the grid cell's wetland fraction. Quantities ending in an asterisk correspond to the pixel selected to represent the uniform scheme.

An example wetness index distribution and the corresponding water table depth and methane emissions distributions are shown in Figures 3.1a–c. The area of saturated soil (where the local water table is at the surface), expressed as a fraction of total wetland area, is denoted in Figures 3.1 and 3.2 as A_{sat}. A wetland's emissions come from three distinct

spatial zones (denoted in Figure 3.1c): a "wet" zone (corresponding to A_{sat} in Figure 3.1b), in which all of the pixels are saturated and have nearly identical, maximum emissions; a "dry" zone, in which the water table depth varies spatially but is deep enough everywhere that methane emissions are negligible; and a "transition" zone, in which emissions fall between these minimum and maximum values. Only in the transition zone are individual pixels' emissions sensitive to water table depth. Temporary, shallow standing water was treated as completely saturated soil in this study; whenever $z_{wt,i}$ was greater than 0 (above the soil surface), it was set to 0 (Figure 3.1b). The methane emissions model used here (Walter and Heimann, 2000) assumes that ebullition and plant-mediated pathways transport methane very quickly from the soil surface to the surface of any overlying shallow water; thus this approximation should not affect the results. As in previous studies that used the same emissions model (e.g., Gedney et al., 2004; Zhuang et al., 2004, 2006), emissions from permanent lakes were ignored (lakes were not simulated), allowing us to focus on biases arising from water table formulations.

As noted above, our goal was to examine the impact of spatial variability of the water table on the relative performance of the various schemes described above, for a given observed A_{sat}. To this end, we repeated the simulations using m values of 2.6, 5.3, 10.5, 20.9, and 41.8 cm. The resulting spatial standard deviation σ_{zwt} of water table depth ranged from 2.4 cm (almost uniform), to 38 cm (a large value, more typical of uplands). Typical σ_{zwt} values for boreal wetlands likely fall near the middle of this range (e.g., Eppinga et al., 2008; Saarnio et al., 1997). Estimates of fractional inundation over the wetland derived from combined passive (AMSR-E) and active (QuikSCAT) microwave satellite observations (Schroeder et al., 2010) indicated a seasonal fluctuation of A_{sat} between 0.04

and 0.12. The simulations in which m = 41.8 cm yielded A_{sat} values that compared most favorably to these observations. Therefore, as we varied m (and σ_{zwt}), we bias-corrected all pixels' water table depths by the appropriate spatially uniform offset to yield the same A_{sat} values as the m = 41.8 cm (σ_{zwt} = 38 cm) case. To simulate the wet-dry scheme, we took the methane emissions from the distributed scheme's wettest pixel, which in all cases was perpetually saturated (i.e., z_{wt} = 0 at all times). We multiplied these emissions by the (time-varying) saturated fraction, A_{sat}. To mimic a spatially uniform scheme, we extrapolated the behavior of one of the wetland's pixels to the entire wetland, as illustrated in Figure 3.1. To ensure a fair comparison, we chose a pixel whose average methane emissions over the warm season (May–October) equaled the grid cell's spatial average warm-season emissions over the baseline period 1980–1999. This pixel's location is denoted on the cumulative distribution functions in Figures 3.1a–c as A^*, and its topographic wetness index, water table level, and net methane emissions are denoted as κ^*, z_{wt}^*, and CH_4^*, in Figures 3.1a–c. Due to the non-linearity of the dependence of emissions on water table depth, this point was not in general the point whose water table depth matched the wetland's spatial average water table depth. The difference in CH_4 sensitivity between the two points was small, but choosing the pixel having the average water table depth would have created a positive bias in simulated CH_4, which we thought would be unfair.

To the extent possible, we used the same methane model parameter sets used in previous studies (see Table 3.1): the boreal wetland parameter set used in the uniform scheme of Zhuang et al. (2004, 2006); the "global" parameter set of the wet-dry scheme of Gedney et al. (2004); and the Abisko parameter set used in the wet-dry scheme of Ringeval et al. (2010). Because the wet-dry scheme neglects emissions from non-saturated areas, it

does not consider oxidation. Therefore, to approximate the responses of the distributed and uniform schemes for the parameter sets used by Gedney et al. (2004) and Ringeval et al. (2010), we supplied moderate values for the parameters *r0*, *xvmax*, *rkm*, and *oxq10*. In addition, we approximated the temperature dependent Q10 of Gedney et al. (2004) with a value of 3.3, based on the average soil temperature in the upper 5 cm during the warm season. In addition, to test the robustness of our findings, we tested 243 random combinations of the methane model parameters *r0*, *rq10*, *rkm*, *xvmax*, and *oxq10* (see Tables 3.1-3.3 for definitions) over the global ranges reported in literature (Walter and Heimann, 2000) (results not shown).

Finally, we derived methane emissions for the three schemes, using the procedure above, for several possible end-of-century climates spanning the approximate range of temperature and precipitation given by IPCC (2007) for West Siberia. The end-of-century scenarios were constructed (as by Bohn et al., 2007) by perturbing the meteorological forcings for the "baseline" period of 1980–1999 by adding a constant (0, 1, 2, 3, 4, or 5) °C to the daily air temperatures and a constant (0, 5, 10, or 15) percent to the daily precipitation. As in the baseline simulations, these future scenarios were first run with m = 41.8 cm (σ_{zwt} = 38 cm), and the resulting A_{sat} values were taken to be reasonable estimates of future conditions. Then, the simulations were re-run for the other values of m, and a time-varying spatially-uniform offset was added to z_{wt} to force the values of A_{sat} to match those of the m = 41.8 cm (σ_{zwt} = 38 cm) case.

Table 3.1: Values of methane emissions model parameters that varied in this study[a]

		Parameter Set		
Parameter	**Definition**	**Boreal Wetland[b]**	**Global[c]**	**Abisko[d]**

r0 (-)	Tuning parameter for methanogenesis	1.3	1.0	1.0
rq10 (-)	Q10 value for methanogenesis	4.5	3.3	2.6
xvmax (µmol/Lh)	Maximum oxidation rate at mean temperature	15	20	20
oxq10 (-)	Q10 value for oxidation	1.9	2.0	2.0

[a]Walter and Heimann (2000).
[b]Zhuang et al. (2004).
[c]Gedney et al. (2004).
[d]Ringeval et al. (2010)

Table 3.2: Values of methane emissions model[a] parameters that were held constant in this study.

Parameter	Definition	Value
ns (cm)	Height of soil surface above bottom of soil column	251
nday (-)	Number of time steps per day	24
h (dm)	Soil layer thickness	0.1
rk (h)	Time step length	1
rkm (umol/L)	Michaelis-Menten constant for oxidation	5
diffair (dm^2/h)	Diffusion coefficient of methane in bulk air	7.2
pox (-)	Fraction of CH4 that is oxidized in plant roots (rhiszosphere)	0.5
Dveg	Scaling parameter in plant-mediated transport equation	0.001
catm (umol/L)	Atmospheric CH4 concentration	0.076
nroot (cm)	Rooting depth	50
scmax (umol/L)	Threshold concentration for methane bubble formation	500
tveg (-)	Number (from 0 to 15) indicating efficiency of plant-mediated transport	7
rpv (-)	Volumetric fraction of coarse pore space	0.39
dtmean (°C)	Annual mean soil column temperature	5.11
ibare (%)	Percent of grid cell that is unvegetated	0
ifrin (%)	Percent of grid cell that is inundated (this parameter is ignored in the methane model code)	0
iother (%)	Percent of grid cell covered by non-wetland	0

[a]Walter and Heimann (2000).

Table 3.3: Minimum and maximum biases of the wet-dry and uniform schemes and missions of the distributed scheme and values of A_{sat} and A_{trans} corresponding to those biases.

			Min Bias					Max Bias				
S(zwt)	Scheme	Param. Set	Bias (% of Dist. CH_4)	Bias (mg/m^2d)	Dist. CH_4 (mg/m^2d)	Asat	Atrans	Bias (% of Dist. CH_4)	Bias (mg/m^2d)	Dist. CH_4 (mg/m^2d)	Asat	Atrans
38 cm	Wet-Dry	1	-28.4	-13.7	48.2	0.082	0.48	-18.1	-4.66	25.7	0.047	0.37
		2	-13	-3.51	27	0.082	0.42	14.3	1.78	12.5	0.047	0.33
		3	-3.42	-0.61	17.9	0.082	0.43	49.6	3.43	6.9	0.047	0.33
	Uniform	1	-104	-26.6	25.7	0.047	0.37	151	54.3	36	0.12	0.65
		2	-138	-17.2	12.5	0.047	0.33	182	39.7	21.8	0.12	0.55
		3	-171	-11.8	6.92	0.047	0.33	188	31.8	17	0.12	0.55
19 cm	Wet-Dry	1	-60.8	-41	66.9	0.059	0.85	-52.6	-31.2	59.3	0.12	0.87
		2	-52.3	-25.7	49.3	0.082	0.82	-43.1	-15.4	35.6	0.12	0.82
		3	-50	-17.2	34.5	0.082	0.83	-39.9	-8.01	20.1	0.083	0.81
	Uniform	1	-38.4	-20.2	52.5	0.047	0.83	49.1	29.1	59.3	0.12	0.87
		2	-38.3	-10.4	27.3	0.047	0.77	57.9	20.7	35.6	0.12	0.82
		3	-24.7	-4.44	18	0.047	0.77	57.5	16.2	28.2	0.12	0.81
9.5 cm	Wet-Dry	1	-85.7	-126	147	0.047	0.95	-75.8	-87.9	116	0.12	0.88
		2	-82.3	-66.3	80.6	0.047	0.95	-71.2	-50.1	70.4	0.12	0.88
		3	-81.6	-46	56.4	0.047	0.94	-69.9	-39.2	56.1	0.12	0.88
	Uniform	1	-10.3	-15.2	147	0.047	0.95	13.4	15.6	116	0.12	0.88
		2	-10.4	-8.35	80.6	0.047	0.95	15	10.6	70.4	0.12	0.88
		3	-9.63	-5.43	56.4	0.047	0.94	14.6	8.18	56.1	0.12	0.88
4.8 cm	Wet-Dry	1	-93	-281	302	0.047	0.95	-85	-158	187	0.12	0.88
		2	-91.7	-157	171	0.047	0.95	-82.9	-98.4	119	0.12	0.88
		3	-91	-105	115	0.047	0.95	-82.2	-77.9	94.8	0.12	0.88
	Uniform	1	-7.19	-21.7	302	0.047	0.95	3.6	6.73	187	0.12	0.88
		2	-7.66	-13.1	171	0.047	0.95	2.9	3.43	119	0.12	0.88
		3	-8.79	-10.1	115	0.047	0.95	2.62	2.49	94.8	0.12	0.88
2.4 cm	Wet-Dry	1	-94.8	-386	407	0.047	0.95	-87	-188	216	0.12	0.88
		2	-94.3	-234	248	0.047	0.95	-86.2	-126	147	0.12	0.88
		3	-93.9	-160	170	0.047	0.95	-85.8	-102	119	0.12	0.88
	Uniform	1	0	0	226	0.083	0.92	2.58	10.5	407	0.047	0.95
		2	-0.69	-1.01	147	0.12	0.88	0.81	2.01	248	0.047	0.95
		3	-0.57	-0.68	119	0.12	0.88	0.77	1.36	176	0.082	0.92

3.3 Results

All schemes' emissions depended on A_{sat}, z_{wt}, and A_{trans} (the fractional area of the "transition zone" denoted in Figure 3.1c), which are plotted in Figures 3.2a-c. The warm season average A_{sat} values for the various end-of-century climate scenarios are plotted in Figure 3.2a as a function of changes in precipitation and air temperature relative to the baseline climate. A_{sat} clearly is largest for the coolest, wettest scenarios and smallest for the warmest, driest scenarios. Figure 3.2b shows spatial average z_{wt} as a function of A_{sat} for selected values of standard deviation σ_{zwt}. It can be seen that, for a given value of A_{sat}, a smaller value of σ_{zwt} requires a shallower average z_{wt}. Similarly, A_{trans} depends on both z_{wt} and σ_{zwt} (Figure 3.2c) and increases dramatically, from 0.4–0.6 to 0.88–0.95 (i.e., (1- A_{sat})), as σ_{zwt} decreases and z_{wt} becomes shallower. Selected values of A_{sat} and A_{trans} are listed in Table 3.2.

The responses of the three schemes' CH_4 emissions over the warm season (May–October) to changes in climate exhibited similar patterns across not only the three methane model parameter sets under discussion, but also all but the most oxidative of the 243 randomly-selected parameter sets. As an example, results from the boreal wetland parameter set of Zhuang et al. (2004) are illustrated in Figures 3.2d–l. As σ_{zwt} decreased from 38 to 2.4 cm, and spatial average z_{wt} became shallower, the distributed scheme's emissions increased by almost a factor of 10, from 25–45 mg/m^{2}d at to 220–400 mg/m^{2}d (Figures 3.2d–f).

At large values of σ_{zwt}, the wet-dry scheme's emissions (Figure 3.2g) fall within 5–10% of the distributed scheme's emissions for most climate scenarios (exact values of min and max biases are listed in Table 32). However, because the wet-dry scheme only takes

account of emissions within the saturated zone, its emissions do not change with σ_{zwt}. Thus, the wet-dry scheme's emissions become increasingly biased as σ_{zwt} diminishes, dropping to essentially [A_{sat} * (the distributed scheme's emissions)], i.e. biases of −85% to −95%, when σ_{zwt} = 2.4 cm (Figure 3.2i). For the more typical σ_{zwt} value of 19 cm (Figure 3.2h), biases are between −50% and −60%. For the boreal wetland parameter set, this translates to biases of −31 mg/m^{2}d (at current temperatures) to −41 mg/m^{2}d (at temperatures 5°C warmer than current climate). This pattern is consistent across methane model parameter sets (see Table 3.2).

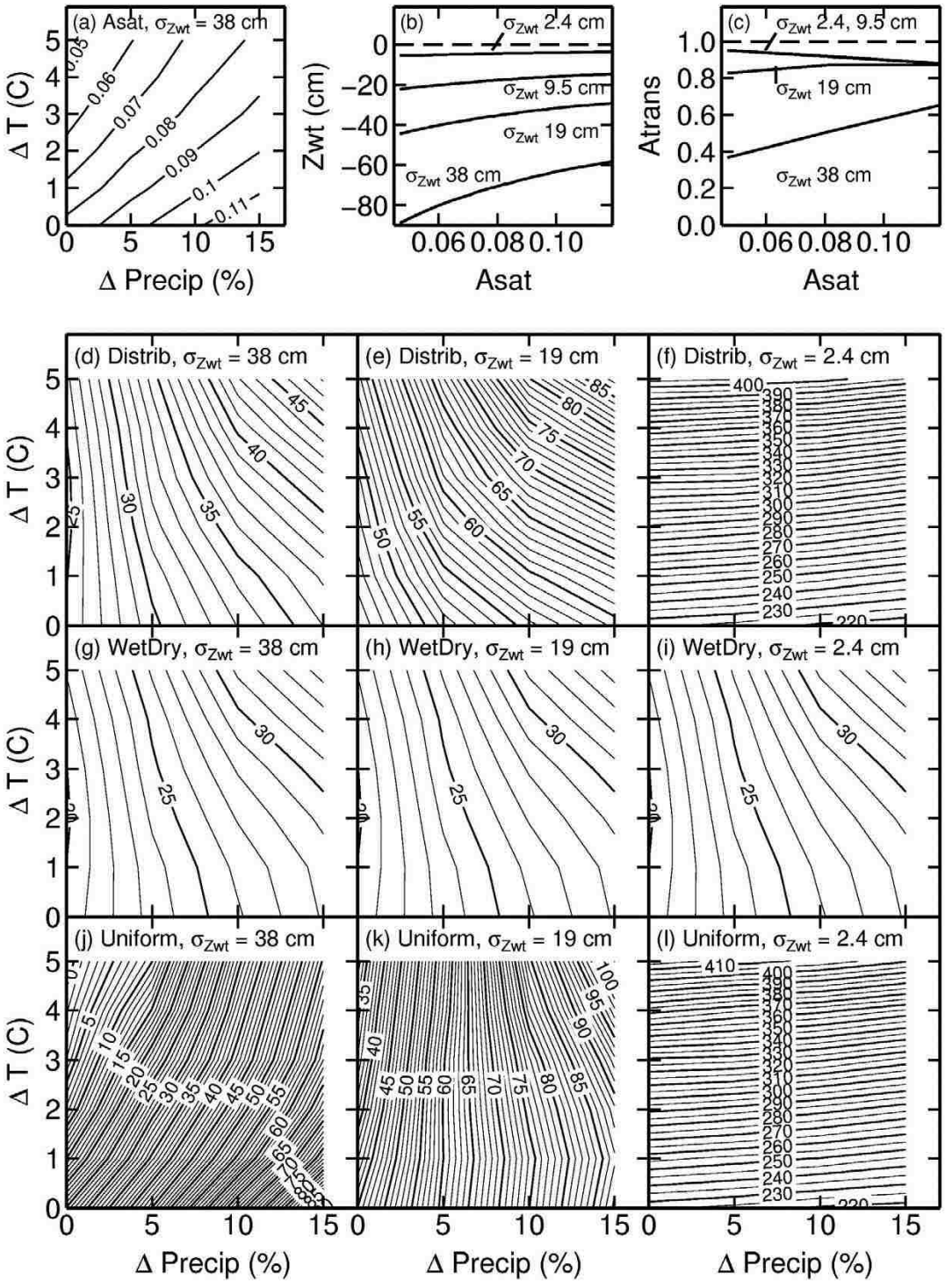

Figure 3.2: (a) Fractional saturated area (A_{sat}), (b) spatial average water table depth (z_{wt} (cm)), (c) fractional area of transition zone (A_{trans} and (d–l) average warm season CH_4 emissions (mg/m^{2}d) of the distributed, wet-dry, and uniform schemes, as a function of changes in precipitation and air temperature relative to baseline climate of 1980–1999, for σ_{zwt} = 38 cm, 19 cm, and 2.4 cm, for the boreal wetland parameter set of Zhuang et al. (2004, 2006).

In contrast, the uniform scheme's emissions exhibit their largest bias when σ_{zwt} is large (38 cm, Figure 3.2j) and vanish as σ_{zwt} approaches 0 (Figures 3.2k and l). For large σ_{zwt} (Figure 3.2j), the uniform scheme's biases depend on climate conditions: when the water table falls/rises, the uniform scheme tends to be biased low/high. For the baseline simulation, biases are 0 by design. For other climates, biases can range between +100% and −100% or more (i.e., net methane sink) when σ_{zwt} is large (38 cm); and between +55% and −40% for the more typical σ_{zwt} value of 19 cm. Exact numbers vary with the methane model parameter set (see Table 3.2). For the boreal wetland parameter set, and σ_{zwt} = 19 cm, biases range from +30 mg/m^{2}d for the coolest, wettest scenario to −20 mg/m^{2}d for the warmest, driest scenario.

3.4 Discussion and Conclusions

Over a wide range of methane model parameter sets, the biases of both the wet-dry and uniform schemes can be substantial, and depend on the spatial variability of the water table depth in opposite ways. To explain this, we refer to the "wet", "transition", and "dry" zones denoted in Figure 3.1c. The wet-dry scheme ignores the emissions of the transition and dry zones. In contrast, the uniform scheme's emissions are representative of the transition zone, because z_{wt} * and CH_4* (Figures 3.1b and c) tend to fall near the center of that zone. Thus the biases of the two schemes depend on the relative contribution of the transition zone, whose area A_{trans} and average water table depth depend on σ_{zwt} (Figures 3.2b and c). Where σ_{zwt} is large (e.g., 38 cm), the transition zone is relatively small, with a deep water table and low emissions. In this case, the wet-dry scheme is relatively accurate and the uniform scheme's biases are at their largest. As σ_{zwt} approaches 0, the transition

zone occupies most of the wetland, with a shallow water table and high emissions. In this case, the wet-dry scheme's biases approach [(1- A_{sat}) * distributed scheme's emissions] and those of the uniform scheme vanish.

These results imply that previous studies have been subject to systematic bias in their estimates of wetland methane emissions and their response to possible end-of-century climates. In particular, Zhuang et al. (2006) used a uniform scheme to predict more than a doubling of high-latitude methane emissions by 2100 under certain future climate scenarios. Assuming a σ_{zwt} of 19 cm, Zhuang et al.'s doubled wetland emissions could be 10–30% too large. Alternatively, Gedney et al. (2004) used a wet-dry scheme to predict similarly large increases in global methane emissions by the end of the century. Assuming that the saturated area fraction of the wetlands in our study is typical of high-latitude wetlands; and assuming that their contribution to global methane emissions is proportional to wetland area; Gedney et al.'s emissions could be too low, by a factor of 0.7 to 0.8. The fact that both studies predict comparable large increases in wetland methane emissions despite using methods with opposite biases implies compensation by other factors.

These results are also relevant to recent attempts to explain substantially lower atmospheric methane concentrations observed in ice cores at the Last Glacial Maximum (LGM). Some authors (e.g., Kaplan, 2002; Valdes et al., 2005; Kaplan et al., 2006) have explained this with a combination of a larger atmospheric methane sink and lower wetland methane emissions under the cooler climate of the LGM. However, these approaches may have been biased because they used a uniform water table scheme, calibrated to match current-day emissions. The net bias depends on the poorly-constrained global distribution

and saturated area of LGM wetlands. Nevertheless, our results suggest that the sizes of other LGM methane sources and sinks may need to be reevaluated.

Clearly, more accurate predictions of wetland methane emissions would result from accounting for the effects of spatial variability in water table depth. However, the distributed scheme suffers from two disadvantages: extra computation and the lack of a priori knowledge of the shape of the water table distribution. While the distribution given by the topographic wetness index shows promise, it is not yet clear that this approach will work at the scales at which microtopography (e.g., hummocks and hollows) occurs. Another option is an appropriate probability distribution (e.g., normal), with effective σ_{zwt} determined by calibration. In contrast, the simplified schemes are fast and involve fewer assumptions. In lieu of intensive water table depth observations, the complementary strengths of the two simplified schemes could be exploited (e.g., replacing the non-emitting portion of the wet-dry scheme with emissions from the uniform scheme). Another approach could be to model the water table distribution as two discrete points: an average hummock and an average hollow, although this would require knowledge of the proportions and relative heights of hummocks and hollows.

Acknowledgments

This work was funded by grant NNX08AH97G from NASA's ROSES program.

IV. MODELING THE LARGE-SCALE EFFECTS OF SURFACE WATER HETEROGENEITY ON WETLAND CARBON FLUXES IN THE WEST SIBERIAN LOWLAND

This chapter is currently in review as a discussion paper in *Biogeosciences Discussions* (Bohn et al., 2013b).

4.1 Introduction

As the world's largest natural source of methane (CH_4), wetlands are an important component of the global carbon cycle (Fung et al., 1991). Northern wetlands additionally have been a large net sink of carbon dioxide (CO_2) since the last Ice Age (Smith et al., 2004). Because the fluxes of both of these greenhouse gases are highly sensitive to soil moisture and temperature, there is concern that wetland CH_4 and CO_2 emissions could provide a positive feedback to climate change (Ringeval et al., 2011; Wania et al., 2009; Tang et al., 2008). Of particular concern are carbon-rich boreal and arctic wetlands, which comprise up to 50% of the total global wetland area (Lehner and Döll, 2004) and occupy one of the world's hotspots of historic and projected climate change (Serreze et al., 2000; Diffenbaugh and Giorgi, 2012). Despite the importance of these ecosystems to the global carbon cycle, substantial uncertainties remain in estimates of their current and future greenhouse gas emissions, due to uncertainties in both their emissions per unit area and the extents of their contributing areas.

Soil moisture's control on wetland carbon fluxes is complex and spatially heterogeneous. Because anoxic conditions in water-saturated soil promote methanogenesis and inhibit aerobic respiration, the water table position controls the partitioning of decomposition into CO_2 and CH_4 (Walter and Heimann, 2000) and, therefore, decomposition's net greenhouse warming contribution. In northern peatlands, photosynthesis in mosses is also inhibited when the water table reaches the surface (Frolking et al., 2002). Within boreal wetlands, a mosaic of lakes (Repo et al., 2007; Smith et al., 2005), seasonally-varying inundation (Schroeder et al., 2010), and spatially-varying water table depth on the scale of meters (Eppinga et al., 2008) gives rise to a *saturated zone*, whose area varies in time, and where CH_4 fluxes are at their maximum (Bohn et al., 2007).

Because the dependence of carbon fluxes on soil moisture is nonlinear, it is important to account for their spatial distribution in estimating these fluxes (Baird et al., 2009), especially their response to climate change (Bohn and Lettenmaier, 2010). To date, large-scale models have not accounted for all of the effects of heterogeneity on carbon fluxes, nor have they agreed on consistent definitions of the fluxes' contributing areas (Melton et al., 2013). As described in Bohn and Lettenmaier (2010), most models have employed one of two schemes to describe wetland surface and subsurface water: either a *uniform* water table scheme (which ignores the saturated zone as well as the distribution of water table depths within the wetland) (e.g., Zhuang et al., 2004) or a *wet-dry* scheme (which neglects the contribution of the unsaturated wetlands to methane fluxes) (e.g., Ringeval et al., 2010; Gedney et al., 2004). When applied to a typical boreal wetland, these schemes' predictions of the response of methane emissions to future climate change can be

subject to biases of up to ±30%, compared to a distributed water table scheme (Bohn and Lettenmaier, 2010). At large scales, different assumptions about local methane emissions and contributing areas can result in large differences in the spatial distribution of methane emissions (Petrescu et al. 2010; Melton et al., 2013). However, the impact of moisture heterogeneity on the total carbon budget at regional and global scales is still poorly known.

Given the sensitivity of wetland carbon fluxes to sub-grid heterogeneity in surface and sub-surface water, our goal was to assess the influence of this heterogeneity on the carbon budget of boreal wetlands over the last half-century. We focused our study on the West Siberian Lowland, where recent intensive field campaigns across large areas (Sheng et al., 2004; Peregon et al., 2009; Glagolev et al., 2011) enabled us to evaluate the performance of models in reproducing the large-scale spatial patterns of carbon fluxes. We used a combination of large-scale models, remote sensing, and in situ measurements to examine the spatio-temporal distributions and carbon fluxes of the region's saturated and unsaturated wetlands.

4.2 Methods

4.2.1 Study Domain

The Western Siberian Lowland (WSL, Figure 4.1) is a low-lying region bounded by the Ural Mountains to the west, the Yenisei River and Central Siberian Plateau to the east, the Arctic Ocean to the north, and the Central Asian steppe to the south (Kremenetski et al., 2003). Containing between 590,000 and 680,000 km^2 of wetlands, and 70 Pg of carbon in its peat soils (10-15% of the world's boreal carbon reservoir), the WSL is the world's largest high-latitude wetland region (Kremenetski et al., 2003; Sheng et al., 2004; Peregon

et al., 2009). As shown in Figure 4.1, permafrost occurs in the northern half of the domain (north of about 61° N). Interspersed among the region's wetlands are thousands of lakes and ponds, ranging in morphology from bog pools to thaw lakes (Eppinga et al., 2008; Repo et al., 2007; Smith et al., 2005; Lehner and Döll, 2004). Portions of the wetlands of the WSL undergo seasonal inundation after the region's snow melts in late spring and early summer (Schroeder et al., 2010).

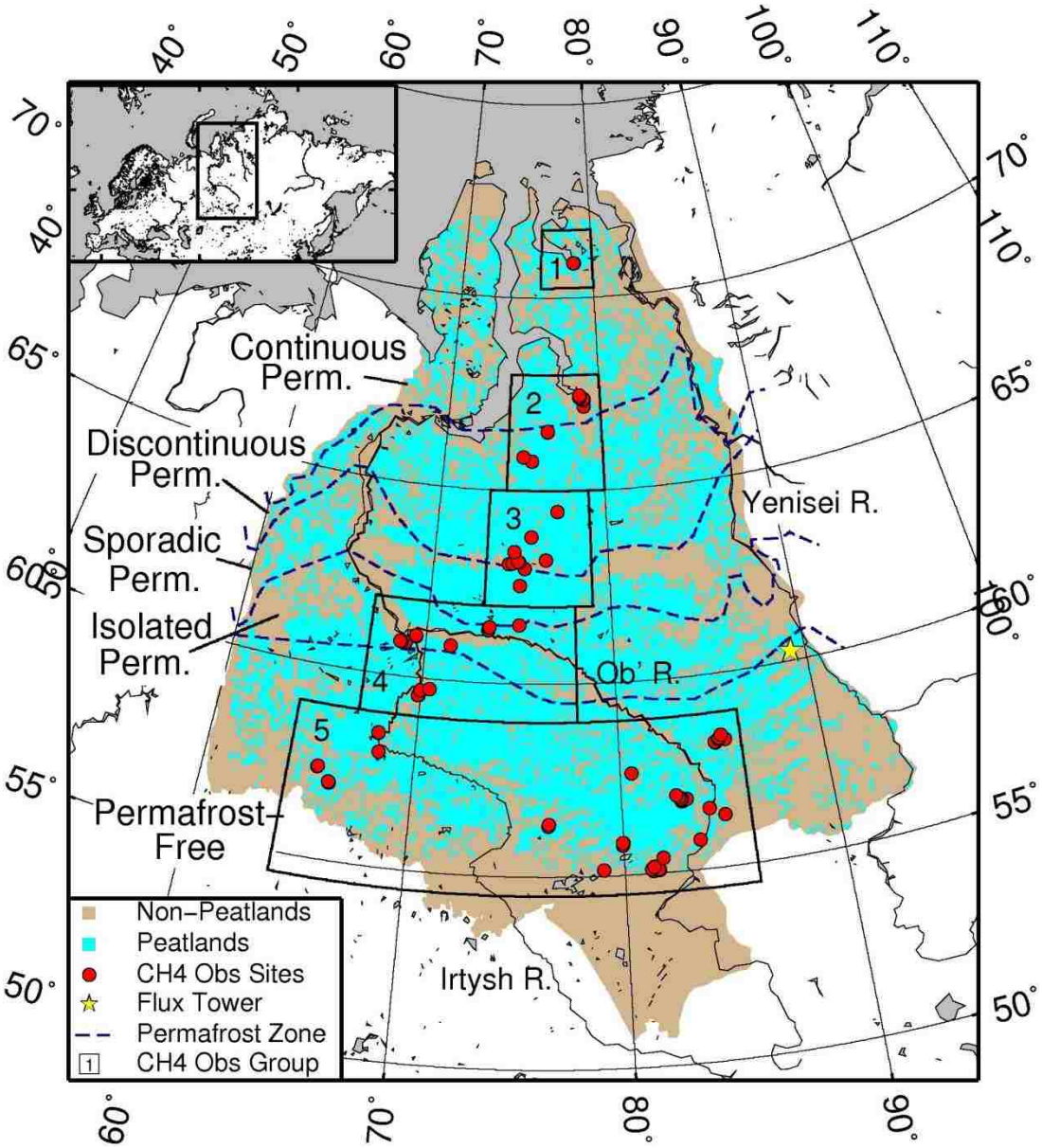

Figure 4.1: Map of the West Siberian Lowlands. Peatland distribution taken from Sheng et al. (2004). Methane flux observation sites (red circles) taken from Glagolev et al. (2011). Permafrost zones after Kremenetski et al. (2003).

4.2.2 Modeling Framework

To account for all of the major components of the wetlands of the WSL accurately (lakes, inundated wetlands, and exposed wetlands, as depicted in Figure 4.2), we employed a modified version of the Variable Infiltration Capacity (VIC) model (Liang et al., 1994), version 4.1.2 as the land surface component of the modeling framework. The relevant features of VIC 4.1.2 include simulation of permafrost using the scheme of Cherkauer and Lettenmaier (1999), thermal properties of organic soils (taken from Farouki, 1981), and a dynamic lake/wetland model that accounts for impoundment of surface water, thermal stratification, mixing, and ice cover (Bowling and Lettenmaier, 2010). Special enhancements include computation of carbon cycle processes such as net primary productivity (*NPP*) and soil respiration (*Rh*), with inhibition of both of these fluxes under saturated conditions and a parameterization of wetland microtopography. The modified VIC model was linked to the wetland methane emissions model of Walter and Heimann (2000) for calculation of methane fluxes, as described in Bohn et al. (2007). In addition, we made a small modification to the Walter and Heimann (2000) methane emissions model to allow sensitivity to spatial variation in *NPP*. These features are described in detail in Appendices A1 and A2.

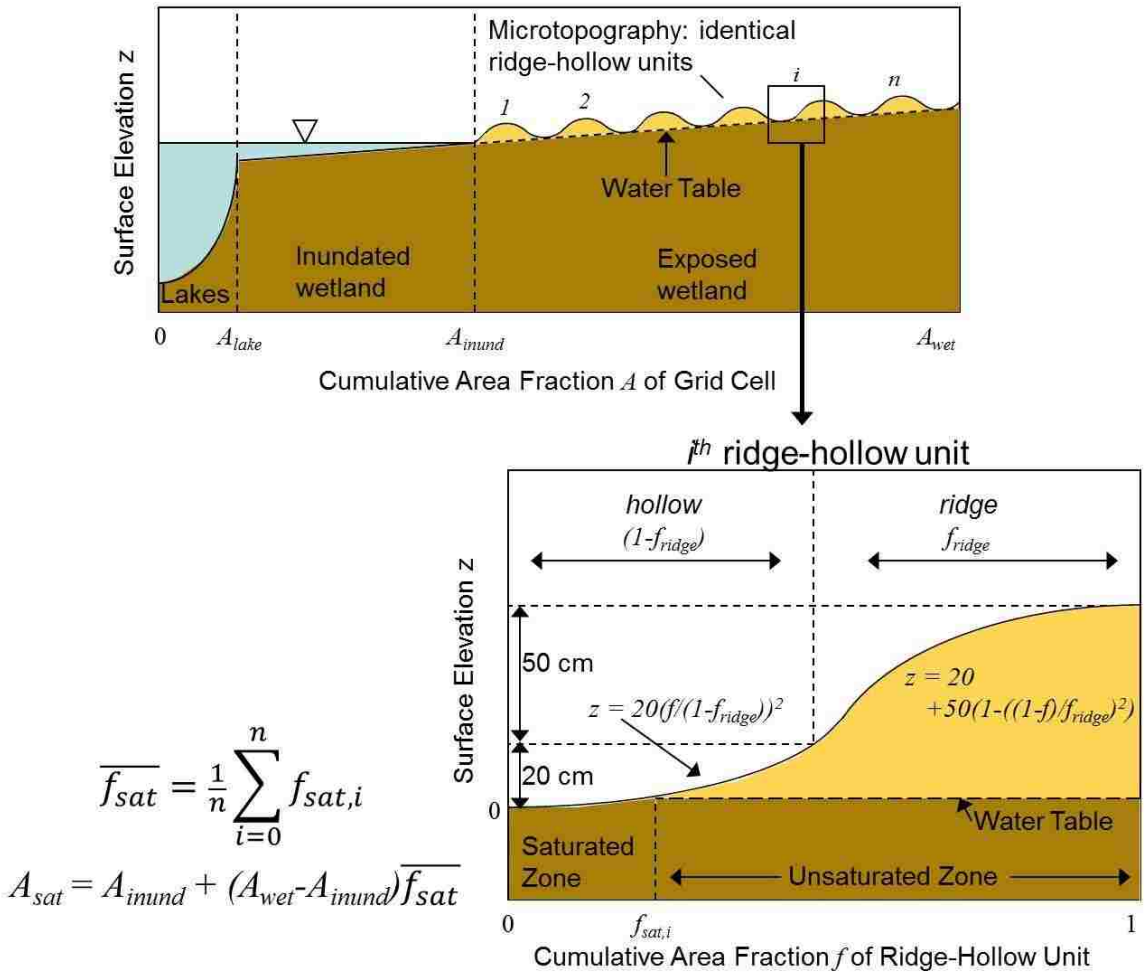

Figure 4.2: Components of lake-wetland system considered in this study.

4.2.3 Meteorological Forcings and Spinup

Daily meteorological forcings for the period 1948-2010 were created by rescaling the NCAR/NCEP reanalysis-derived fields of Sheffield et al. (2006) to match the monthly statistics of gridded monthly observations (precipitation and wind speed from Willmott and Matsuura, 2001; air temperature from Mitchell and Jones, 2005), with corrections to precipitation for gauge undercatch (Adam and Lettenmaier, 2003) and orographic effects

(Adam et al., 2006). Daily short- and longwave radiation and humidity, and hourly values of all meteorological forcings, were derived using methods described in Bohn et al. (2013).

To achieve realistic initial soil temperatures without a lengthy spin-up, soil temperatures were initialized with soil temperature profiles from Troy et al. (2011). This initialization was followed by a second 30-year spinup using forcings from the period 1948-1957 three times. Soil carbon pools required a different approach, because they are likely only 50-90% of their long-term equilibrium size, assuming an average wetland age of 10,000 years (Sheng et al., 2004) and drawing from Figure 6 of Wania et al. (2009). Therefore, we first iteratively ran our soil respiration model offline over the period 1947-1958 to find the long-term equilibrium carbon pool densities (defined by a net change in carbon pool storage of less than 0.1 g C/m^2 over the 10-year period). Then we rescaled the carbon densities by a constant factor (equal to 0.818 for simulations using optimal parameters) across the entire domain, so that the total storage in 1948 equaled the estimate of 70.2 Pg C from Sheng et al. (2004).

4.2.4 Model Parameters

4.2.4.1 Hydrology

As shown in Figure 4.3, we divided the domain into 278 cells using the EASE-Grid 100 km polar azimuthal equal area grid (Brodzik and Knowles, 2002). To account for different soil textures and flow regimes in lake-wetland systems versus uplands, we further divided these cells into dry and wet portions. The wet portion of each cell consisted of the cell's peatlands, taken from the database of Sheng et al. (2004); permanent lakes, taken from the Global Lake and Wetland Database (GLWD; Lehner and Döll, 2004); and wet

tundra land cover classes, taken from Bartalev et al. (2003). Each cell's wet portion was modeled as a single lake-wetland tile, underlain by peat soil, with peat depth taken from Sheng et al. (2004) and hydraulic properties taken from Letts et al. (2000). Exposed land within the lake-wetland tile was assigned to one of three VIC land cover classes (bog, forested bog, or evergreen needleleaf forest), according to the proportions of forest and non-forest pixels from Bartalev et al. (2003). Parameters for these classes are listed in Table 4.1. LAI values were prescribed by the monthly average over all pixels from the MODIS LAI product (Myneni et al., 2002) within the wet portion of each cell. Because this study focused on wetland behaviors, all descriptions hereafter refer only to the wet portions of the domain.

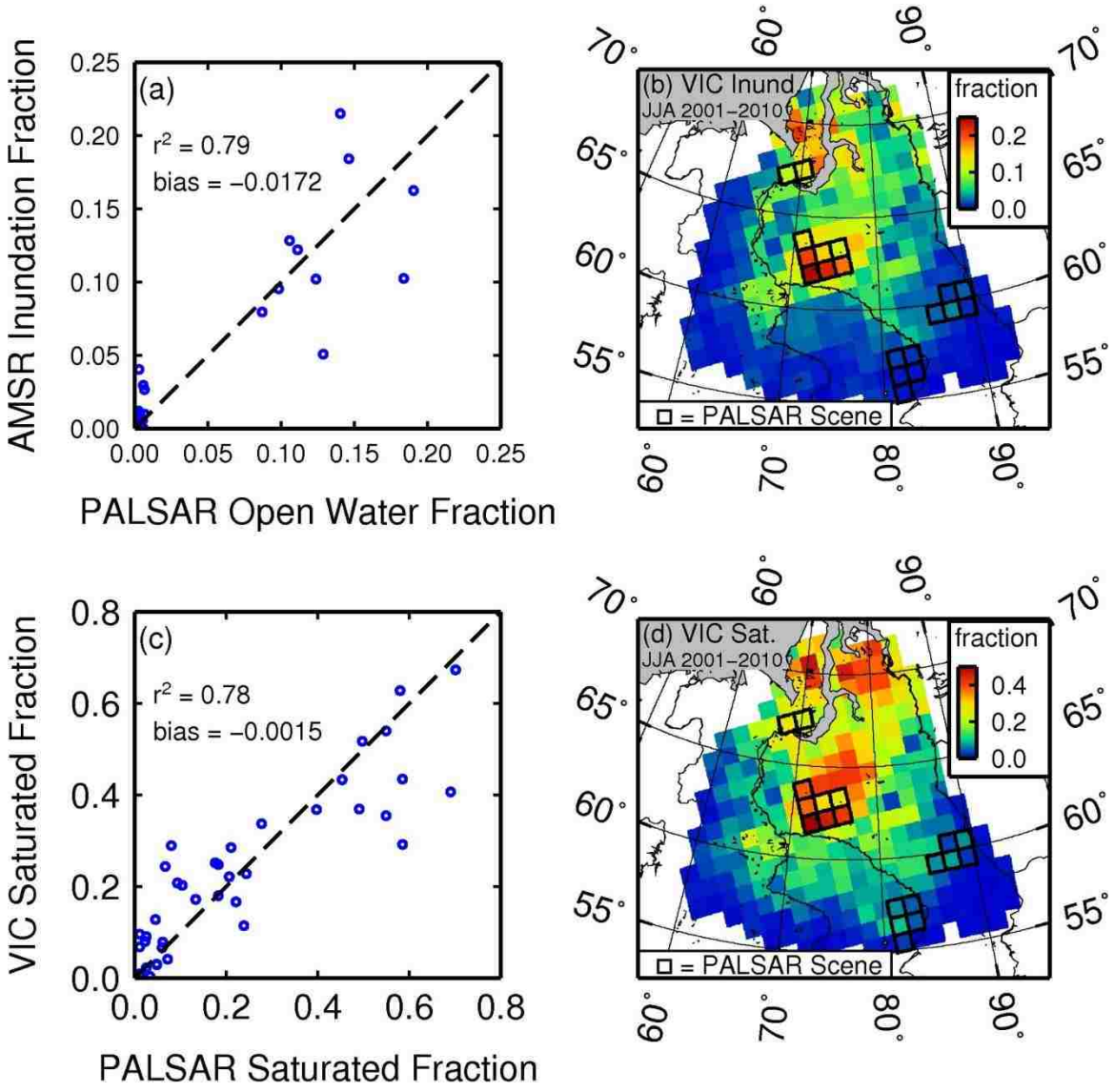

Figure 4.3: Observed and simulated fractional extents of inundation and saturation over the West Siberian Lowlands. Units are the fraction of the entire grid cell area (wetland plus upland).

Table 4.1: Photosynthesis parameters for land cover classes in this study. Units are $\mu molCO_2 m^{-2} s^{-1}$.

Parameter	Bog	Forested Bog	Evergreen Needleleaf Forest
V_m	20	29	29
J_m	37	52	52

Because VIC's *NPP* and *Rh* are inhibited under saturated conditions and reduced to zero under inundated conditions (when low-lying vegetation is completely submerged), it was important to constrain the fractional areas of inundation and saturation (A_{inund} and A_{sat}, respectively). To do so, we used two remote sensing products: the coarse-resolution (25 km) AMSR-E/QuikSCAT-based passive-active microwave global inundation product of Schroeder et al. (2010), extended to all snow-free days from July 2002 through 2009 (available at http://wetlands.jpl.nasa.gov); and high-resolution (30 m) ALOS/PALSAR active microwave imagery from four main focus regions (delineated by boxes in Figures 4.3b and 4.3d) on several dates from 2006 and 2007. The PALSAR pixels were classified into various categories, including open water (no emergent vegetation) and wet soil (emergent vegetation, with the water surface ranging from a few cm above the soil surface to just below the soil surface), via the random forest method described in Whitcomb et al. (2009). The extent of the saturated zone was computed as the sum of open water and wet soil extents. Comparison of the PALSAR classifications to the Schroeder et al. product over each 100-km ease grid cell where they overlapped (Figure 4.3a) indicated a good match between the Schroeder et al. product and the PALSAR open water extents (bias 0.0172, R^2 of 0.79). Therefore, we chose to treat the Schroeder et al. product as a measure of A_{inund}.

For VIC's dynamic simulation of A_{inund}, we created a two-part depth-area relationship for each grid cell. The first part, which describes the composite bathymetry of

permanent water bodies, was computed by assigning a depth to each of the cell's lakes, as a function of the lake's size, and computing the cumulative surface area of lakes deeper than each of several pre-selected depths. Lake depths were computed via a linear regression of log(depth) vs. log(area) using data reported for bog pools (Belyea and Lancaster, 2002; McEnroe et al., 2009), Alaskan thaw lakes (Bowling et al., 2003), and larger West Siberian lakes from the International Lake Environmental Committee World Lake Database (ILEC, 1988-1993). The areas of this depth-area relationship were then rescaled so that the total lake area fraction A_{lake} matched the minimum monthly average value of A_{inund} given by the Schroeder et al. product. The second part of the depth-area relationship described the additional surface area (A_{inund} between A_{lake} and A_{wet}) covered by seasonal inundation, as a function of excess water depth above the lake surface. This part of the relationship was generated by integrating the distribution of surface slopes from either the Shuttle Radar Topography Mission (SRTM) DEM (Farr et al., 2007) south of 60° N, or the Advanced Spaceborne Thermal Emission and Reflection (ASTER) DEM (NASA, 2001) north of 60° N.

The remaining lake parameter *wfrac* (outlet width as a fraction of the lake perimeter) was calibrated separately at each grid cell to minimize the bias between local simulated and observed JJA average A_{inund} over the period 2002-2007. JJA average simulated A_{inund} over the period 2001-2010 is shown in Figure 4.3b.

Within the wetland, two primary parameters (to which water table depth is sensitive) needed to be determined: the fraction of the wetland covered by ridges (f_{ridge}) and the maximum subsurface flow rate (*Dsmax*). We held these parameters constant across the domain. We sampled f_{ridge} and *Dsmax* uniformly across the ranges of their plausible

values: 0.4 to 0.6 for f_{ridge}, based on the findings of Peregon et al. (2009); and 0.0 to 0.8 mm/day for *Dsmax*, with the upper bound determined empirically by the maximum value of *Dsmax* for which $A_{sat} > A_{inund}$. We designated as "optimal" the values that approximately minimized the total bias between simulated and observed (via PALSAR) A_{sat} across the locations and times of PALSAR observations. Optimal values for both f_{ridge} and *Dsmax* equaled 0.5. As shown in Figure 4.3c, for these optimal parameter values, VIC's A_{sat} matched the PALSAR A_{sat} reasonably well, with R^2 of 0.78 and bias -0.0015. The resulting JJA average simulated A_{sat} values for the period 2001-2010, shown in Figure 4.3d, tend to be much higher in the north of the WSL than in the south. Boxes in Figure 4.3d delineate the grid cells used in the comparison of Figure 4.3c.

4.2.4.2 Biogeochemistry

Where possible, parameters for photosynthesis were taken from the BETHY model (Knorr, 2000). Values of the parameters V_m and J_m chosen for the new bog and forested bog land cover classes are listed in Table 4.1. Most parameters for aerobic soil respiration and methane emissions were taken from Sitch et al. (2003) and Walter and Heimann (2000), respectively.

Three parameters associated with photosynthesis and soil respiration required calibration: the wetland photosynthesis inhibition parameter f_{inhib} (eqn A.2.2), the soil respiration inhibition factor r_{sat} (eqn A.2.4), and the soil respiration scaling factor k (eqn A.2.3). These parameters were held constant across the domain. We calibrated these parameters using CO_2 flux observations for the year 2000 from the Zotino Bog flux tower (Arneth et al., 2002), denoted with a yellow star in Figure 4.1. We assessed the joint

likelihoods of 1000 uniformly-sampled parameter combinations with respect to two objective functions: 1. the joint likelihoods of the time series of simulated vs. observed 10-day mean net ecosystem exchange (*NEE*); and 2. the mean soil carbon density of 90 ± 30 kg/m^2 for the region around the flux tower, based on Sheng et al. (2004). Percentiles of the posterior distributions of parameter values are listed in Table 4.2.

Table 4.2: Posterior distributions of calibrated parameters.

Region	Parameter [units]	Percentile		
		1	**50**	**99**
WSL	f_{ridge} [-]	0.4	0.5	0.6
	Dsmax [mm/d]	0.2	0.5	0.8
	f_{inhib} [-]	0.00	0.25	0.50
	k [-]	0.18	0.24	0.49
	r_{sat} [-]	0.15	0.34	0.50
North	*r0* $[(gC/m^2/d)^{-1}]^*$	0.015	0.020	0.026
	xvmax [µmol/l/h]	0.059	0.135	0.316
	rkm [µmol/l]	4.20	10.95	13.89
	rq10 [-]	2.52	3.42	5.21
	oxq10 [-]	1.34	4.94	5.91
South	*r0* $[(gC/m^2/d)^{-1}]^*$	0.016	0.020	0.025
	xvmax [µmol/l/h]	0.054	0.245	0.293
	rkm [µmol/l]	1.63	14.78	18.57
	rq10 [-]	9.57	10.69	11.71
	oxq10 [-]	1.60	2.05	3.41

*The units of *r0* differ from those in Walter and Heimann (2000); see Appendix B for details.

For the Walter and Heimann wetland methane emissions model, we calibrated five parameters: *r0*, *xvmax*, *rkm*, *rq10*, and *oxq10*. We used in situ observations of methane flux, soil temperatures, and water table depth from over 750 locations across West Siberia for the period 2006-2010 (Glagolev et al., 2011; Glagolev et al., 2012; Sabrekov et al., 2012), most of which were only monitored for a period of 1-2 days. To generate simulated fluxes at each site, soil temperatures, *NPP*, and water table distributions simulated by VIC for the grid cell containing the site were used as inputs to the methane emissions model. To form an objective function, we grouped the observations into five regional groups (depicted in Figure 4.1). Within each regional group, we divided the observations into four water table depth categories (shown in Figure 4.4) and computed the mean of the log-transformed simulated and observed fluxes for each category. For each regional group, our

objective function was the joint likelihood of the categories' means. We found that using a single parameter set for all observation groups resulted in substantial positive biases in groups 2 and 3 (Figures 4.1 and 4.4), and a substantial negative bias in group 1. However, these biases were due in part to sample error: groups 1-3 only contained 196 observations total; further subdividing these groups into sub-groups based on water table range resulted in some sub-groups having fewer than 10 observations. To check this, we consolidated groups 1-3 into a single northern group (not shown in Figure 4.4) and re-ran the calibration. This resulted in a substantial negative bias in the combined northern group. Therefore, we calibrated groups 1-3 (consolidated into a single group) and 4-5 separately, resulting in separate north and south parameter sets (the optimal southern parameter set was very similar to the optimal whole-domain parameter set, due to the larger numbers of observations, and correspondingly smaller uncertainties, in the South). Posterior distributions of values for these two parameter sets are listed in Table 4.2. The likely ranges (1^{st} to 99^{th} percentiles) of rq10 (methanogenesis seasonal temperature dependence parameter) in the two sets exhibited no overlap. We applied the south parameter set to grid cells having July wetland LAI values ≥ 2.5, and the north parameter set to all other cells. The boundary between these two sets of cells fell approximately at 61° N, roughly coinciding with both the northern boundary of the middle Taiga (Glagolev et al., 2011) and the southern limit of permafrost. The resulting distributions of observed and simulated soil temperatures and CH_4 fluxes are shown in Figure 4.4. Simulated soil temperature profiles (left column) matched observations reasonably well across all groups, except for a warm bias of 1-2 °C from 0 to 20cm depth in the north (groups 1-2). Simulated CH_4 fluxes (right column) matched observed fluxes reasonably well in the south (groups 4 and 5), but less so

in the north. In particular, the simulations still substantially overestimated fluxes under saturated conditions at sites in the central WSL (groups 3-4), and still substantially underestimated fluxes in the far north (group 1).

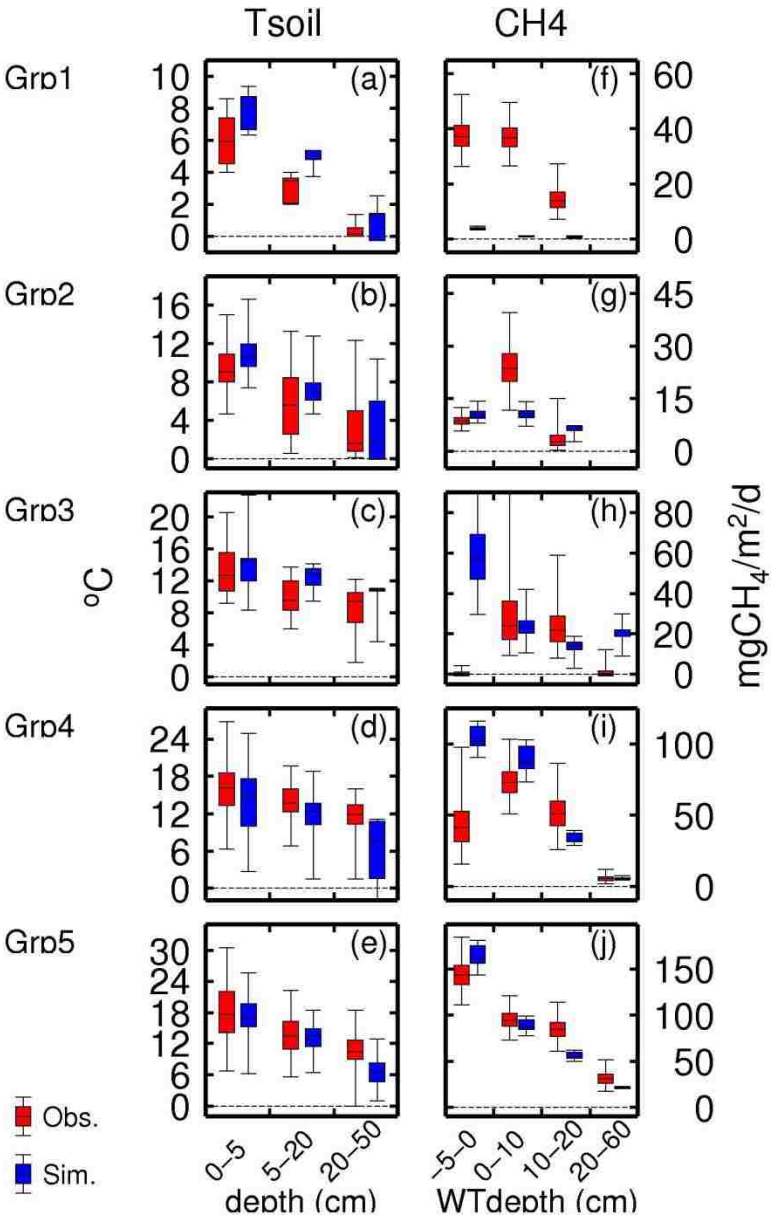

Figure 4.4: Observed (red) and simulated (blue) soil temperature profiles (left column) and methane fluxes (right column), for each of the five observation groups delineated in Figure 1 (rows 1-5, respectively).

4.2.5 Historical Simulations

Historical simulations covered the period 1948-2010, using the optimal (median posterior) values for all calibration parameters. To assess parameter uncertainty, we then randomly sampled calibration parameter values to generate 1200 simulations at a

randomly-selected subset of 50 cells across the domain, the results of which were spatially interpolated to the other cells. To assess the influence of saturated area on carbon fluxes, we performed an additional control simulation employing a uniform water table scheme, in which each grid cell's water table depth distribution was replaced by its spatial average and fractional inundated and saturated areas were set to 0.

4.3 Results

4.3.1 Present-day Extents and Carbon Fluxes

In terms of both area and total carbon fluxes, unsaturated wetlands were the dominant hydrologic zone in the WSL. Estimates of the current JJA average extents (chosen because the vast majority of carbon fluxes occur during the summer) of the wetland zones over the period 2001-2010 are listed in Table 4.3. The total JJA saturated area (excluding permanent lakes) had a median value of 235,000 km^2 (with 1st and 99th percentiles of 165,000 km^2 and 332,000 km^2, respectively). This represents 34% (24% to 47%) of the non-lake wetland area of the WSL (and 13% of the total area of the WSL). The remainder (66%) (53% to 76%) of the non-lake wetland area, was unsaturated. Inundated wetlands occupied 25,250 km^2, or 4% of the non-lake wetland area.

Table 4.3: Estimates of JJA average areas (km2) of wetland zones, totaled across the WSL, over the period 2001-2010.[a]

Zone	Percentile		
	1	50	99
Permanent Lakes	100,750	100,750	100,750
Non-lake Inundated	25,050	25,250	25,810
Exposed and Saturated	135,160	209,500	306,040
Non-lake Saturated	165,020	234,750	331,860

Total Saturated	265,770	335,500	432,600
Total Wetland	801,500	801,500	801,500

[a]Note that areas in each column do not sum to the total wetland area in general, because a given percentile of one area does not correspond to the same percentile of the other areas.

The unsaturated zone dominated the area of the WSL wetlands, as well as the region's carbon budget. As shown in Table 4.4, the total annual wetland *NPP* and *Rh* across the WSL are 163 and 149 Tg C/y, respectively, and the contribution from unsaturated wetlands (129 and 119 Tg C/y, respectively) comprises about 80% of the total flux in both cases. Similarly, unsaturated wetlands emit 64% of the total methane flux of 3.6 Tg CH_4/y. Because *NPP* exceeds *Rh*, the WSL wetlands as a whole are a net carbon sink of 11.5 Tg C/y (sinks are listed as negative in Table 4.4); unsaturated wetlands account for 8.0 Tg C/y, or 70% of the region's wetland carbon sink. Assuming that CH_4 has a greenhouse warming equivalence of 21 over the span of a century (IPCC, 2007), CH_4 emissions dominate the region's total greenhouse warming potential (*GHWP*), leading to a total *GHWP* of 24.7 Tg CO_2/y; unsaturated wetlands account for 56% of the total.

Table 4.4: Annual average carbon budget terms over the period 2001-2010.

Term	**Percentile**			**Components (for median case)**	
	1	**50**	**99**	**Saturated**	**Unsaturated**
Soil Carbon (Pg C)	42.8	70.7	129	N/A	N/A
NPP (Tg C/y)	85.3	163	176	33.6	129.3
Rh (Tg C/y)	63.1	149	167	29.2	119.5
CH_4 (Tg CH_4/y)	1.69	3.65	5.96	1.28	2.37
Cnet (Tg C/y)	-15.9	-11.5	-8.55	-3.44	-8.02
GHWP (Tg CO_2/y)	-4.55	24.7	58.65	10.8	13.9

The dominance of unsaturated wetlands in the region's *NPP* and *Rh* may not come as a surprise, given that saturated wetlands should exhibit lower rates for these fluxes (rates

per unit area in saturated wetlands tended to be 50-60% of their rates in adjacent unsaturated wetlands). In contrast, the dominance of unsaturated wetlands in CH_4 and *GHWP* fluxes is counterintuitive, because CH_4 fluxes per unit area tended to be much larger (by about 40%) in the saturated zone. A second surprising result was that the control simulations, for which non-lake saturated area was always 0, yielded similar results to the primary simulations: an increase of only 5% in *NPP*, *Rh*, and C_{net}, and a decrease of only 2% in CH_4 and *GHWP*, over the totals from the distributed scheme. The large area of the unsaturated zone was partly responsible for these results.

4.3.2 Spatial Distributions

Not only did unsaturated wetlands occupy a larger total area than saturated wetlands, but also the majority of the WSL's carbon fluxes occurred in the drier parts of the domain, where the saturated area fraction is small. To illustrate this, maps of the simulated 2001-2010 annual average states and fluxes (expressed as fluxes or densities per unit area of non-lake wetland) are shown in Figure 4.5. JJA average A_{sat} (Figure 4.5a) is concentrated in the central and northern portions of the domain (north of 60° N).

In contrast, the spatial distributions of *NPP*, *Rh*, and soil carbon density (C_{dens}), shown in Figures 4.5b-d, were all anti-correlated with A_{sat} (correlation coefficients of -0.72, -0.71, and -0.64, respectively). Control runs using a uniform water table scheme with no seasonal inundation allowed (not plotted) yielded similar spatial distributions to the distributed water table scheme. Thus, the spatial distribution of these terms appears to have been primarily a reflection of the spatial distribution of VIC's MODIS-prescribed LAI,

which had a correlation coefficient with A_{sat} of -0.71 (although this distribution of LAI may itself be the cumulative result of thousands of years of *NPP* inhibition).

The spatial distributions of CH_4, C_{net}, and *GHWP* (Figure 4.5e-g) demonstrated weaker dependence on A_{sat} (correlations of -0.43, +0.30, and -0.30, respectively). However, even in these cases, fluxes above the median rate tended to fall outside the region of greatest A_{sat}. In particular, the CH_4 emissions (Figure 4.5e) were substantially higher south of 61° N than to the north, due to the use of different CH_4 model parameter sets in the South and the North of the domain (addressed in section 4.3.3.). Even within the separate northern and southern halves of the domain, CH_4 exhibited only very weak positive correlations with A_{sat} (0.27 and 0.18, respectively), due to the competing influence of NPP (which was negatively correlated with A_{sat}). For C_{net} (Figure 4.5f), the largest carbon uptake rates (> 40 g $C/m^2/y$) occurred at the western edge of the domain, between 57° and 66° N. Still, the majority of uptake rates greater than the median rate of 20 g $C/m^2/y$ fell in cells where A_{sat} was less than 0.5. The distribution of *GHWP* (Figure 4.5g) was more complex, with the large C_{net} uptake rates in the West driving *GHWP* negative, and the large CH_4 emissions rates in the South and East driving *GHWP* positive. Still, the largest positive or negative fluxes once again occurred outside the wetter center of the WSL.

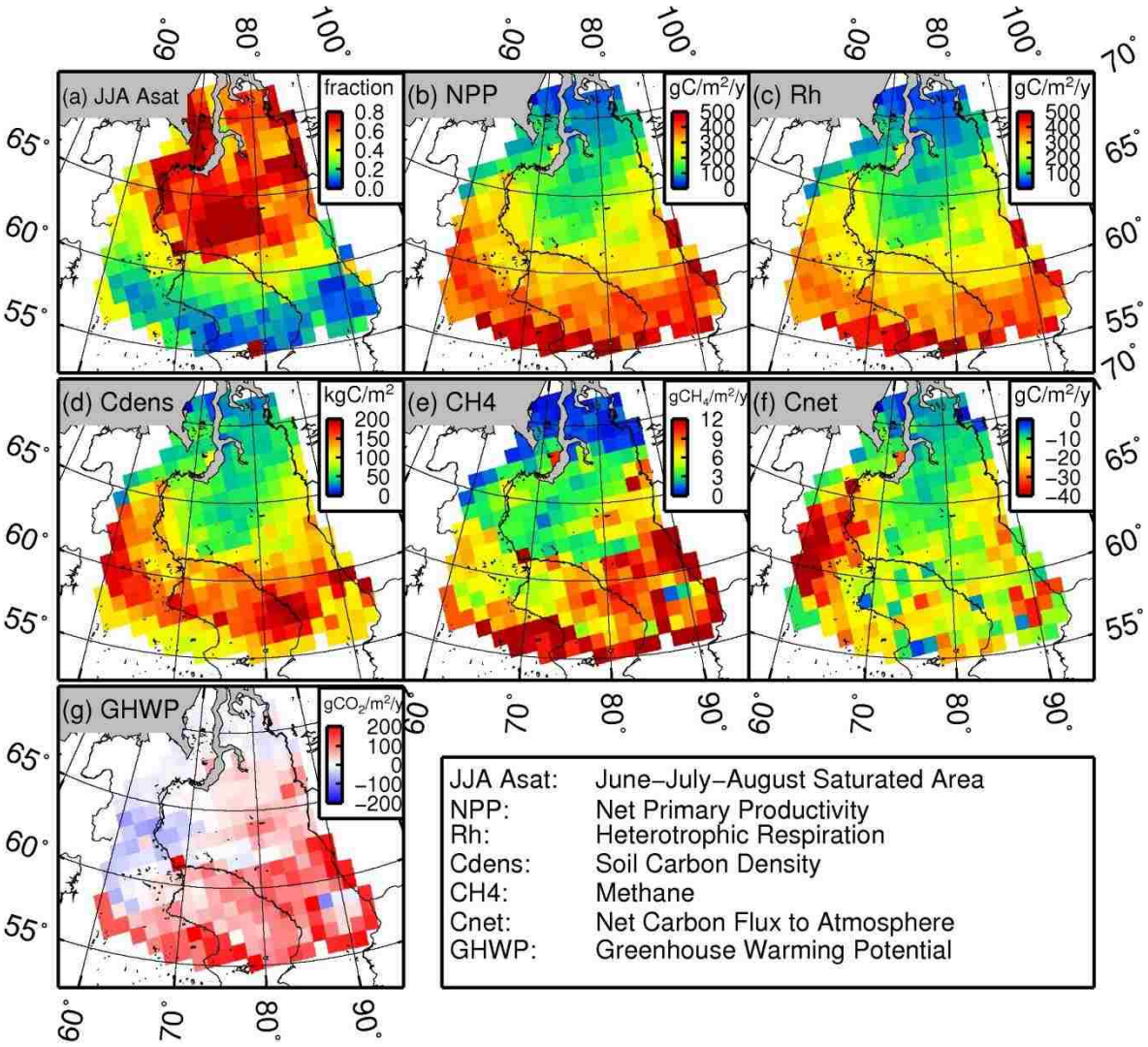

Figure 4.5: 2001-2010 annual average simulated states and fluxes, per unit wetland area.

Our simulated C_{dens} distribution was somewhat corroborated by the distribution of observed soil carbon densities reported by Sheng et al. (2004) (Figure 4.6). With the exception of an underprediction of soil carbon density in the North (66-70° N, 75-90° E), the two distributions compared favorably ($R^2 = 0.53$ for cells outside the region of the mismatch). The cause of the mismatch was not clear: the MODIS LAI values there were not substantially different from those of their neighbors, and none of our Monte Carlo simulations reproduced this feature. By design, our estimate of the total wetland carbon

storage in the WSL, 70.7 Pg C (42.8-129 Pg C), matched the figure from Sheng et al. (2004) (70.2 Pg C) quite closely.

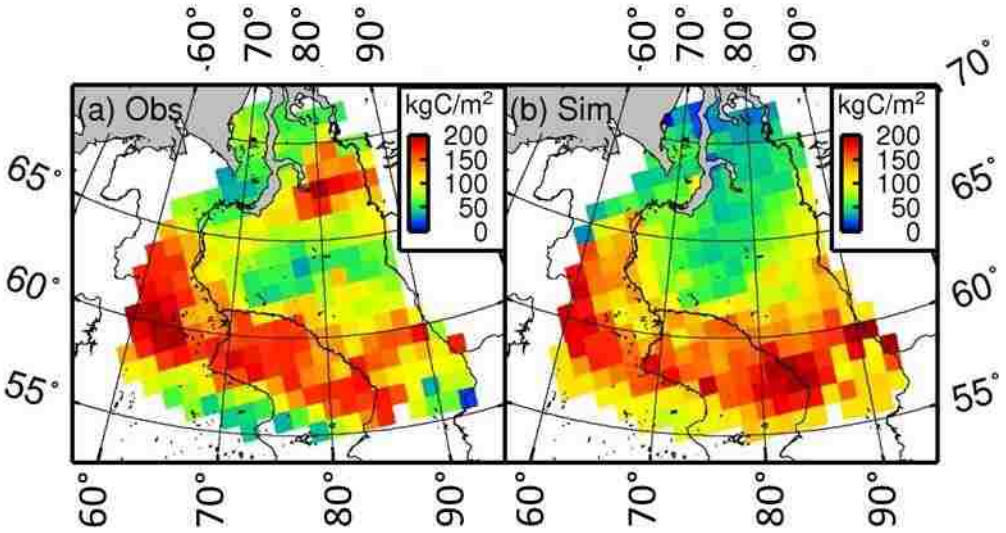

Figure 4.6: Observed and Simulated soil carbon density, per unit wetland area, from Sheng et al. (2004).

4.3.3 Spatial Distribution of CH_4 Emissions per Grid Cell Area

For comparison with our simulated CH_4 distribution, the spatial distributions of Glagolev et al. (2011) and Fung et al. (1991) are shown in Figures 4.7a-b. The distribution of Glagolev et al., derived by mapping their observed CH_4 flux rates to the landcover classifications of Peregon et al. (2008 and 2009), places the vast majority of CH_4 emissions south of 60° N, where wetlands are predominantly unsaturated. In contrast, the Fung et al. distribution (as well as many other subsequent estimates, e.g., Schuldt et al., 2013) places the majority of its emissions north of 60° N, where saturated area fractions are larger and permafrost occurs. This difference in spatial distribution has important implications for the response of these wetlands to future climate change, as discussed in section 4.4.

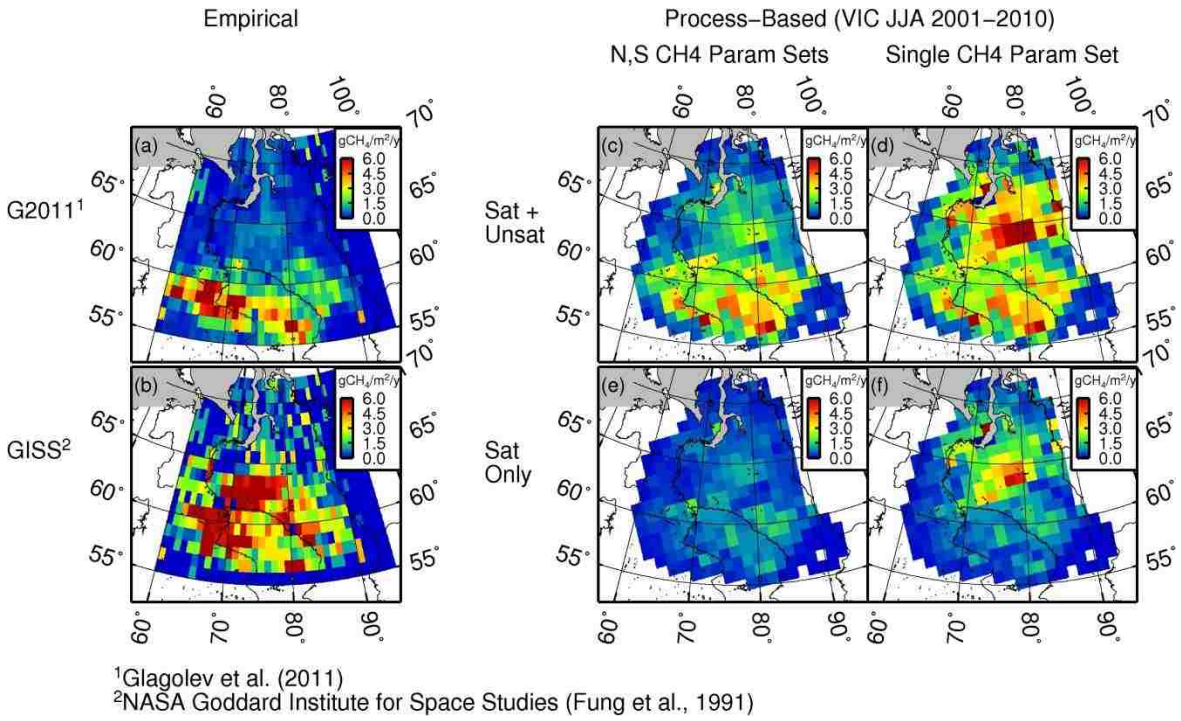

Figure 4.7: Spatial distributions of various estimates of annual methane emissions per unit area of grid cell (wetland plus upland).

To compare our simulated CH_4 emissions with these other estimates, we converted from flux per unit area of non-lake wetland to flux per unit area of the entire grid cell. The resulting distribution (Figure 4.7c) placed the majority (70%) of the domain's annual emissions south of 60° N, with maximum values of 5-6 g $CH_4/m^2/y$ confined to the region 65-85° E, 57-59° N. The broad features of this distribution agree with those estimated by Glagolev et al. (2011), although the emissions of Glagolev et al. were even more narrowly focused in the south than ours (likely due to our overestimation of saturated flux rates in the central WSL, shown in Figure 4.4h). Our underestimation of per-unit-area emissions in the far north (Figure 4.4f) did not produce large overall errors in the spatial distribution. Our estimate of total annual CH_4 emissions over the entire WSL, 3.65 Tg CH_4/y (1.69-5.96

Tg CH_4/y), is reasonably close to that of Glagolev et al. (3.9 Tg CH_4/y). This agreement is not surprising, since both studies used the same in situ observations from locations spanning the WSL. In contrast, Fung et al. and Schuldt et al. estimated substantially larger total annual emissions for the region (6-7 Tg CH_4/y)

To gain insight into the difference in spatial distribution between the Glagolev et al. and Fung et al. estimates, we performed control simulations in which either a) the single optimal CH_4 parameter set was applied across the entire domain, or b) the emissions from unsaturated wetlands were neglected (equivalent to a wet-dry scheme), or both a) and b) were applied. All of the control simulations (Figures 4.7d-f) led to a substantially greater proportion of emissions in the northern half of the domain. Thus, to avoid larger CH_4 emissions in the central and northern WSL, it appears that simulations must account for both the lower methanogenesis rates north of 61° N and the emissions from unsaturated wetlands.

4.3.4 Seasonal Cycle

The mismatch between the region's carbon fluxes and saturated soil is not only spatial in nature; it is also temporal. The seasonal cycles of the meteorological forcings, wetland zone area fractions, and carbon fluxes, for the entire domain and the southern and northern halves are plotted in Figure 4.8. While air temperature (T_{air}, Figure 4.8a-c) peaked in July, A_{sat} (Figure 4.8g-i) peaked in May-June, in response to snowmelt inputs and the drawdown from evapotranspiration (*Melt* and *ET*, respectively; Figure 4.8d-f). Across the entire WSL and particularly in the south, all carbon fluxes (Figure 4.8j-o) with the exception of CH_4 from the saturated wetlands (blue line, Figure 4.8m-o) peaked in July (or

July-August in the case of CH_4). In the south, where the bulk of the carbon fluxes were generated, July-August A_{sat} values averaged only 0.2, or 30-40% of their peak values.

To assess the degree to which the July peaks in carbon fluxes were caused by inhibition of *NPP* and *Rh* during the June peak of A_{sat}, we compared the seasonal cycles from the primary (distributed water table) simulations to those of control runs using a uniform water table scheme (so that A_{sat} was always 0). The resulting carbon fluxes (denoted by dashed lines in Figure 4.8j-o) were similar to the seasonal cycles of the non-control fluxes. Thus, it would appear that the carbon fluxes responded primarily to the July peak in T_{air}, with A_{sat} losing most of its potential influence over the fluxes by the time of their peak values.

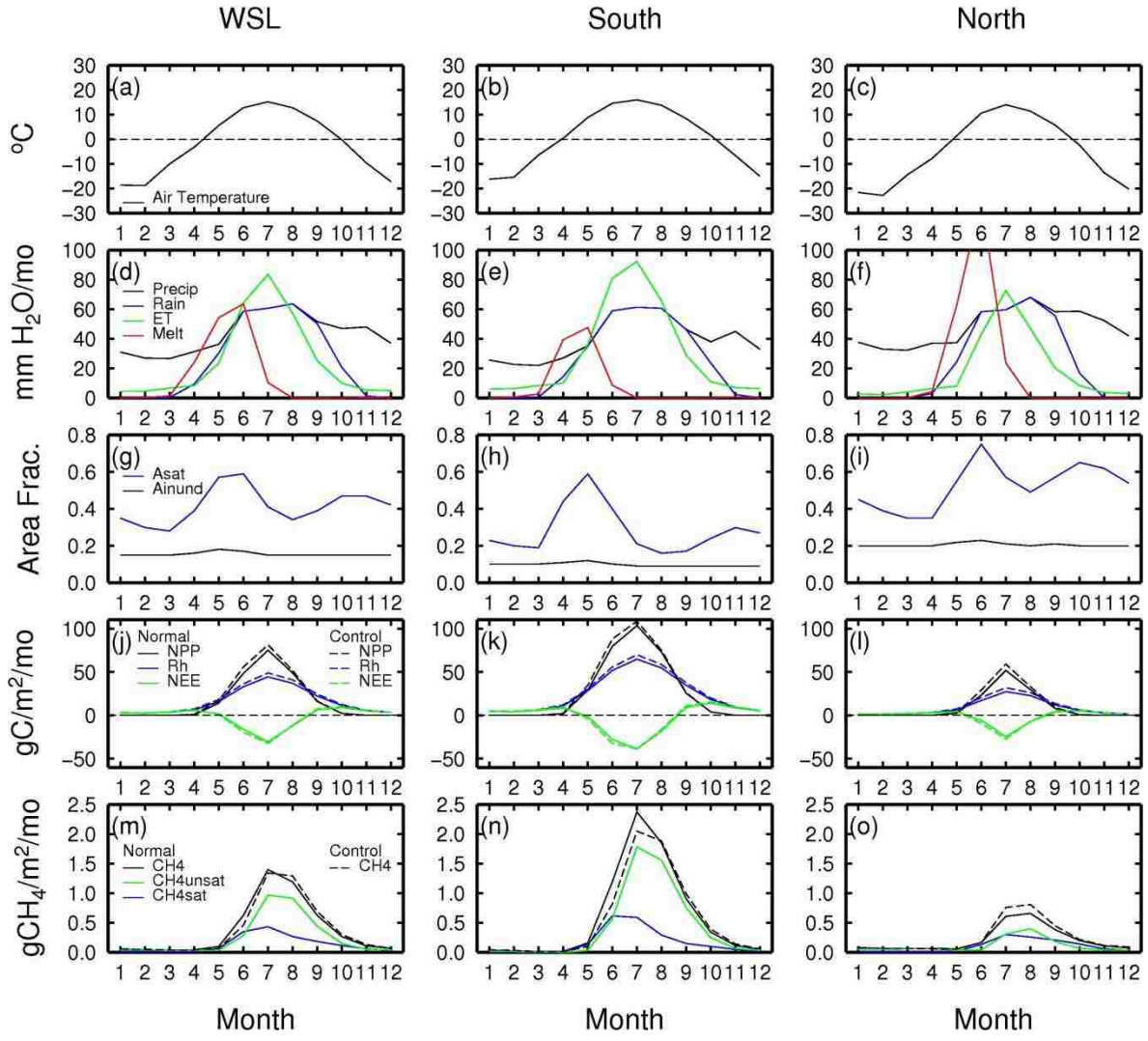

Figure 4.8: 2001-2010 monthly average meteorological forcings and simulated states and fluxes, per unit wetland area.

4.3.5 Interannual Variations (Historical Reconstruction)

As a consequence of the spatio-temporal mismatch between A_{sat} and carbon fluxes, A_{sat} had little influence over the interannual variability of carbon fluxes in the WSL. Correlations among the domain's annual carbon fluxes and JJA T_{air}, precipitation, and A_{sat} are listed in Table 4.5. As we might expect, JJA A_{sat} displayed a negative correlation with JJA T_{air} (via evaporative losses) of -0.63 and a strong positive correlation of 0.77 with JJA

precipitation. Despite the fact that *NPP* and *Rh* both showed strong negative correlations with JJA A_{sat} (-0.76 and -0.78, respectively), the net carbon flux (in which CH_4 plays only a minor role) showed very little correlation (0.16) with JJA A_{sat}. Similarly, while CH_4 emissions from saturated and unsaturated wetlands displayed clear correlations with JJA A_{sat} (0.72 and -0.49, respectively), their opposing signs and the larger area of unsaturated wetlands resulted in a very low correlation (-0.09) of total CH_4 with JJA A_{sat}. *GHWP* also displayed little correlation (0.09) with JJA A_{sat}, once again due to the opposing influences of its component fluxes. As a result, the domain's carbon fluxes displayed stronger correlations with JJA T_{air} than with either JJA A_{sat} or JJA precipitation. Control runs using a uniform water table scheme showed similar correlations between carbon fluxes and JJA T_{air} and precipitation.

Table 4.5: Temporal correlations of domain-wide annual carbon fluxes with JJA hydrologic conditions over the period 1948-2010.

Water Table Scheme	Dep. Variable	Correlation Coefficient		
		JJA Tair	JJA Precip.	JJA Asat
Distributed	JJA Asat	-0.63	0.77	1.0
	NPP	0.61	-0.58	-0.76
	Rh	0.78	-0.45	-0.78
	CH_4 Saturated	-0.13	0.80	0.72
	CH_4 Unsaturated	0.58	-0.21	-0.49
	CH_4 Total	0.46	0.19	-0.09
	Cnet	0.19	0.40	0.16
	GHWP	0.30	0.36	0.09
Uniform	*NPP*	0.60	-0.53	n/a
	Rh	0.80	-0.46	n/a
	CH_4	0.30	0.28	n/a
	Cnet	0.42	0.12	n/a
	GHWP	0.43	0.18	n/a

Historical time series of these terms, plotted in Figure 4.9, tell a similar story. JJA T_{air} (Figure 4.9a) displayed a general upward trend between the mid-1960s and 2010;

performing a Mann-Kendall trend test on the time series for all segments of at least 20 years in length yielded positive trends at the 95% confidence level ranging from 0.023 °C/y to 0.080 °C/y for most segments having a starting year in the 1960s and an ending year between 1990 and 2010. Fewer trends in precipitation, evapotranspiration, and snowmelt (Figure 4.9b) were significant over this period, but precipitation did have negative trends ranging from -1.1 to -2.2 mm/y for some segments beginning in the 1960s and ending in the 1990s. JJA A_{sat} (Figure 4.9c) had significant negative trends ranging from -0.0004 to -0.0018 y^{-1} for roughly half of the segments starting in the 1960s and ending between 1990 and 2010. *NPP* and *Rh* (Figure 4.9d) both had significant positive trends ranging from 0.55 to 1.7 Tg C/y and 0.47 to 1.2 Tg C/y, respectively, over most segments in this period. Because control runs with a uniform water table also yielded similar positive trends in *NPP* and *Rh* (Figure 4.9d, dashed lines), these trends were presumably in response to the positive trends in T_{air}. Yet *NEE* (Figure 4.9e) did not have any significant trends in segments starting in the 1960s, although *NEE* did have significant trends ranging from -0.09 to -0.23 Tg C/y for some segments starting in the 1950s and ending in the 1990s. Similarly, CH_4 emissions from saturated and unsaturated wetlands (Figure 4.9f) had significant trends of -0.005 to -0.023 Tg CH_4/y and 0.009 to 0.017 Tg CH_4/y, respectively, for many segments starting in the 1960s, presumably in response to the decline in JJA A_{sat}, but total CH_4 emissions (Figure 4.9f) and *GHWP* (Figure 4.9g) do not had any significant trends.

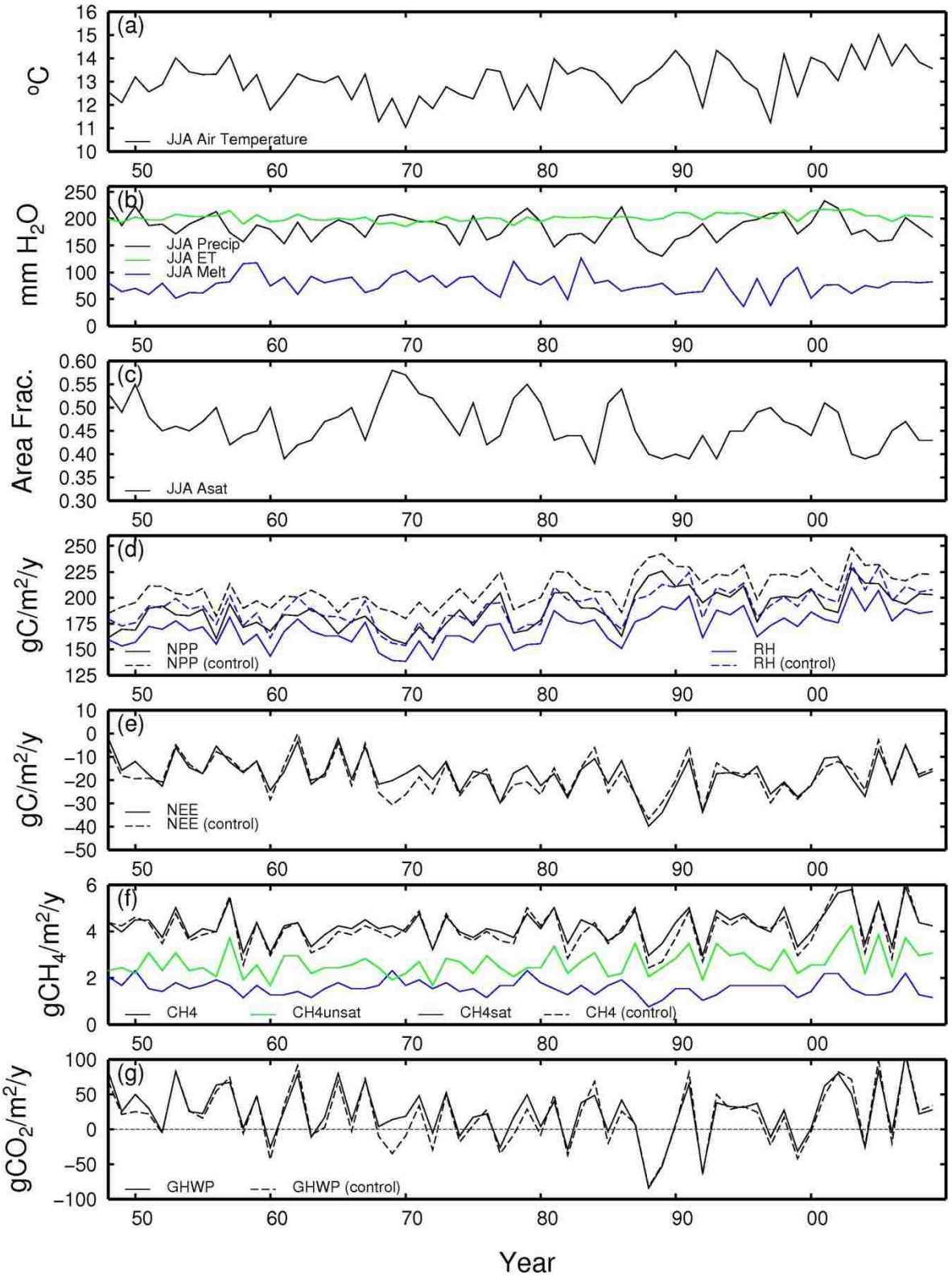

Figure 4.9: 1948-2010 annual meteorological forcings and simulated states and fluxes.

4.4 Discussion

The most striking result of our work is the markedly different spatial distribution of methane emissions in the WSL given by this study, in comparison with most previous estimates. Both the in situ observations of CH_4 fluxes and the spatial distribution estimated by Glagolev et al. (2011) indicate a dramatic drop in emission rates from South to North in the WSL, with the most pronounced gradient occurring between 58° and 62° N. This region coincides with both the southern limit of permafrost and a zone of large fractional extents of lakes, inundation, and saturated wetlands in the center of the WSL. As shown in Figures 4.7d-f, we were unable to match this drop in methane emissions without both a) using a less productive methane emissions parameter set in the permafrost zone (lowering northern emissions) and b) accounting for emissions from unsaturated wetlands (raising southern emissions).

These factors can plausibly explain the differences between our spatial distribution and those of most previous estimates, which did not have access to the observations of Glagolev et al. (2011). For example, most previous bottom-up estimates (e.g., Schuldt et al., 2012; Zhu et al., 2012; Ito and Inatomi, 2012; Meng et al., 2012; Spahni et al., 2011; Riley et al., 2011; Ringeval et al., 2011; Ringeval et al., 2010; Petrescu et al., 2010; Zhuang et al., 2004; Gedney et al., 2004; Fung et al., 1991) applied the same methane emissions parameters to all boreal wetlands (although Zhuang et al. and Zhu et al. distinguished between boreal and tundra wetlands), and consequently overestimated methane emissions in the central WSL. Curiously, Shindell et al. (2004), using the results of Walter et al (2001), also overestimated methane emissions in the central WSL, despite allowing one of the methane emissions parameters (r0) to vary spatially as a function of mean annual

temperature and NPP. The reason may be because this function was derived from a relatively sparse set of global in situ observations. In addition, some studies (e.g., Ringeval et al., 2011 and 2010; Gedney et al., 2004) employed wet-dry schemes that ignored the contributions from unsaturated wetlands (although Ringeval et al. did account for emissions from areas where the water table was within 5 cm of the surface), thereby underestimating emissions in the southern WSL.

Two previous estimates that did agree generally with our spatial distribution were those of Eliseev et al. (2008) and one of the simulations of Petrescu et al. (2010). However, instead of accounting for emissions from unsaturated wetlands, Eliseev et al. assumed all wetlands were 100% saturated, and prescribed wetland saturated extents statically from a map-based inventory rather than estimating them dynamically. Petrescu et al. (2010) used five different estimates of potential wetland areas as inputs to a process-based model, which accounted for emissions from unsaturated wetlands, but applied a uniform methane emissions parameter set to all boreal wetlands. One of the five wetland area estimates did not overestimate methane emissions from the central WSL, but this seems to reflect the prescribed wetland areas rather than the model formulation.

This geographic discrepancy could have important consequences for predicting the response of wetland methane emissions in the WSL (and elsewhere in the high latitudes) to future climate change. Recently, concern has arisen in the cryosphere community that the thawing of permafrost could place previously frozen soil carbon at risk of decomposition (Koven et al., 2011; Schaefer et al., 2011; Walter et al., 2006). How much of this carbon is respired anaerobically as methane depends on rates of methanogenesis and oxidation, estimates of which depend on assumed model parameters. Given that our single-

parameter-set control simulation (Figure 4.7d) yielded annual CH_4 emissions 2-3 times larger than our normal simulations in the central WSL (Figure 4.7c) for the same amount of labile carbon, use of the same parameters in the permafrost zone as in the south could therefore lead to as much as a 2- to 3-fold overestimation of the response to permafrost thaw. While this assumes that methane emissions parameters (which depend to some extent on the composition of the soil microbial communities, which, in turn, may depend on environmental conditions) will remain constant in time, most studies to date have made such an assumption.

It is not clear how best to represent the spatial variation evident in the Glagolev et al. methane flux observations in a global process-based model. Our wetland LAI threshold of 2.5 for the more productive southern CH_4 parameter set was intended to contain the productive eutrophic mires found in the subtaiga, southern taiga, and middle taiga zones (Glagolev et al., 2011). At the very least, this suggests that global models may need to apply distinct methane emissions parameter sets at eutrophic mires, using specialized wetland land cover classifications similar to Peregon et al. (2008 and 2009). A more process-based approach may require incorporating other spatially-varying factors, including soil pH, redox potential, substrate quality, and nutrient concentrations, although soil pH may play only a small role in spatial variability, due to the adaptations of microbial communities to local average pH (Glagolev, 2004). Some existing models already account for various combinations of some of these factors (e.g., Zhuang et al., 2004; Wania et al., 2010; Riley et al., 2011; Spahni et al., 2011; Meng et al., 2012; Zhu et al., 2012), but the inability of these models to reproduce the observed spatial distribution of emissions suggests that incorporating these factors may not be sufficient. Similarly, the low

emissions under inundated conditions observed by Glagolev et al. in the central WSL (Figures 4.4g-i) may indicate another process that is not currently accounted for in large-scale models and may help explain the spatial distribution of emissions.

Carbon fluxes from our control simulations employing a uniform water table (for which A_{sat} was always 0) differed only slightly from our fully-distributed simulations. However, it may be dangerous to interpret this as a validation of uniform water table schemes. The lack of influence of fractional saturation over current carbon fluxes appears to be the result of mismatches between the current spatial and temporal distributions of saturated soil and carbon fluxes. The current configurations of these spatial distributions indicate a substantial cumulative reaction to thousands of years of *NPP* inhibition under saturated conditions, which may not persist under projected future changes in the WSL's climate. Indeed, Bohn and Lettenmaier (2010) found that the differences between the uniform and distributed water table schemes were most pronounced in their response to the climate projected for the end of the 21st century, rather than present-day fluxes.

Nevertheless, it is important to constrain the fractional saturated area, if for no other reason than it is one of the few large-scale observations that can be used to calibrate a model's soil moisture storage and water table depth (to which carbon fluxes are extremely sensitive). However, as Figure 4.3a shows, passive-active microwave products such as Schroeder et al. (2010) appear to be primarily sensitive to inundated extent, which is typically much smaller than the extent of saturated soil. While the SSMI-based product of Papa et al. (2010) exhibited better agreement with the PALSAR saturated fraction in some portions of the central WSL, where forest cover is low, the Papa et al. product dropped to 0 in many locations south of 60° N. Thus, neither product alone is a reliable measure of

saturated soil extent. Therefore, it would be very helpful to the modeling community for remote sensing specialists to generate products that combine both passive microwave and other (e.g., SAR-based) data.

4.5 Conclusions

We examined the role of spatial heterogeneity of surface and sub-surface water on the carbon budget of the wetlands of the WSL. We conclude that:

- Sub-surface moisture heterogeneity played an important role in both the overall magnitude and spatial distribution of estimates of the region's carbon fluxes, whereas surface heterogeneity had little overall effect. This was primarily because the bulk of the region's carbon fluxes occurred in the portion of the region where fractional saturated areas were lowest.
- To reproduce the observed spatial pattern of CH_4 emissions, in which very little CH_4 is emitted north of 60° N, it was necessary to account for CH_4 emissions from unsaturated wetlands, and to use a methane model parameter set that reduced estimated CH_4 emissions in the northern half of the domain.
- Previous estimates of the response of the WSL to thawing permafrost may have overestimated future increases in methane emissions in the permafrost zone.

Appendix A: Model Formulation

A.1 Hydrology

We used a modified version of VIC 4.1.2, an early version of which was described in Bohn et al. (2007). The model divides the land surface of each grid cell into separate land cover "tiles"; one of these tiles may be reserved to contain lakes and wetlands. Within the lake-wetland tile (with fractional area A_{wet}), lakes and wetlands are simulated as a continuous, connected system representing a single composite of all lakes and wetlands within the grid cell (Figure 2). At any given time, some portion of the lake-wetland system (A_{inund}) may be inundated with standing water on the surface, while the remainder of the system ($A_{wet} - A_{inund}$) is exposed. The inundated portion may include both "permanent" lakes (A_{lake}) and seasonally-inundated wetlands ($A_{inund} - A_{lake}$).

As described in Bowling and Lettenmaier (2010), A_{inund} varies with time as a function of topography (or lake basin bathymetry) and the volume of impounded surface water. Surface runoff and sub-surface drainage from the exposed wetland flow into the inundated portion. Sub-surface drainage from the inundated portion of the lake-wetland flows into the channel network. All sub-surface drainage is controlled by VIC's baseflow parameters *Ws*, *Ds*, and *Dsmax*. When the water level in the inundated portion is above the lip of the permanent lake basin, the impounded water may also flow over the lip into the local channel network (controlled by the effective outlet width parameter, *wfrac*). If the inundated portion expands into the unsaturated wetland, some of the impounded water must recharge the newly-flooded wetland area until its soil is saturated.

Within the exposed wetland, field observations (e.g., Eppinga et al., 2008; Glagolev et al., 2011) indicate that microtopography exerts the single strongest control on local water

table depth, with variations in water table depth over small scales nearly equal to variations in surface elevation relative to a datum. Therefore, we assume the landscape is composed of a mix of identical mounds (*ridges*) and depressions (*hollows*), as shown in Figure 2. Following the observations of Eppinga et al. (2008), we assume the soil surface elevation within a hollow uniformly spans a range of 20 cm, while the surface of a ridge rises to a maximum to 50 cm above the edge of the hollow, for a total elevation range of 70 cm. The fraction of the landscape covered by ridges (f_{ridge}) is a calibration parameter. This topographic distribution is then sampled at regular intervals. Local water table elevation Z_{WT_i} is then computed at these same points via the equation

$$Z_{WT_i} = \overline{Z_{WT}} + \left(Z_{surf_i} - \overline{Z_{surf}}\right) \quad \text{(A1.1)}$$

where $\overline{Z_{WT}}$ is the spatial mean water table elevation, Z_{surf_i} is the local microtopographic elevation, and $\overline{Z_{surf}}$ is the spatial mean of the microtopographic elevation distribution. The spatial mean water table depth is computed from total soil column water storage by following the method of Frolking et al. (2002), in which the water in peat soils is assumed to be in equilibrium between the forces of gravity and matric tension.

The locus of all points where the water table is at or above the surface is called the *saturated zone*, with fractional area A_{sat}. Thus, A_{sat} is the time-varying sum of permanent lake area, inundated wetlands, and saturated exposed wetlands:

$$A_{sat} = A_{inund} + (A_{wet} - A_{inund})\,\overline{f_{sat}} \quad \text{(A1.2)}$$

where $\overline{f_{sat}}$ is the mean saturated area fraction across all ridge-hollow pairs in the exposed wetland.

A.2 Biogeochemistry

In the modified VIC model, photosynthesis and aerobic soil respiration are simulated in the exposed wetland (and set to 0 under inundation). Separate carbon fluxes are computed individually at each point on the water table distribution, but these fluxes interact with a common soil carbon reservoir. For photosynthesis, a Farquhar-based scheme taken from the BETHY model (Knorr, 2000) is employed, as described in Bohn et al. (2007):

$$A = f_M(w) \cdot A_{unlim}(V_m, J_m) \qquad \text{(A2.1)}$$

where A is the photosynthesis rate; A_{unlim} is the photosynthesis rate in the absence of moisture limitation; V_m and J_m are the plant-specific maximum carboxylation rate and electron transport rate, respectively; and $f_M(w)$ is a moisture dependence function.

However, to inhibit photosynthesis under saturated conditions, we replaced the moisture dependence function $f_M(w)$ from Knorr (2000) with the following simplification of the moisture dependence function from Frolking et al. (2002):

$$f_M(w) = \begin{cases} 2w, & 0 < w < 0.5 \\ 1 - f_{inhib}(w - 0.5), & 0.5 \le w < 1.0 \end{cases} \qquad \text{(A2.2)}$$

where w is the volumetric soil moisture content and f_{inhib} is the fractional reduction in photosynthesis under saturated conditions, whose value must be calibrated.

Vegetation carbon storage is not explicitly simulated; daily litterfall is set equal to the previous year's total net primary productivity (*NPP*), distributed uniformly in time and space. In VIC's soil respiration scheme, based on that of the LPJ model (Sitch et al.,

2003), soil carbon storage is divided into litter, intermediate, and slow pools. Soil respiration (*Rh*) from the i^{th} pool is given by

$$Rh_i = k \cdot f_T(T_i) \cdot f_M(w_i) \cdot C_i / \tau_i \qquad \text{(A2.3)}$$

where k is a scaling factor that we added to account for the effects of soil pH and redox potential, f_T is the Lloyd-Taylor (1994) temperature dependence function; T_i , w_i, C_i, and τ_i, are the temperature, volumetric soil moisture, carbon density, and turnover time, respectively, of the i^{th} pool (Sitch et al., 2003), and f_M is a moisture dependence function modified from Yi et al. (2010):

$$f_M(w) = \begin{cases} \left[\dfrac{(w - w_{\min})(w - w_{\max})}{(w - w_{\min})(w - w_{\max}) - (w - w_{opt})^2} \right], w \le w_{opt} \\ \left(\dfrac{w - w_{opt}}{w_{\max} - w_{opt}} \right) \cdot r_{sat} + \left[\dfrac{(w - w_{\min})(w - w_{\max})}{(w - w_{\min})(w - w_{\max}) - (w - w_{opt})^2} \right], w > w_{opt} \end{cases} \qquad \text{(A2.4)}$$

where w_{min} is 0, w_{max} is 1, w_{opt} is the optimal soil moisture content of 0.5 (at which peak respiration occurs), and r_{sat} is the ratio of the respiration rate at saturation (w = 1) to the peak respiration rate (w = 0.5). k and r_{sat} are calibration parameters. The total soil column *Rh* is integral of equation A2.3 across all 10-cm intervals between the surface and 2.5m depth. The litter C pool exists only at the surface, while the intermediate and slow C pools co-exist throughout the remainder of the soil column.

Wetland methane emissions are computed using the model of Walter and Heimann (2000), driven by daily *NPP*, soil temperature profile, and water table depths from VIC (as described in Bohn et al., 2007 and Bohn and Lettenmaier, 2010). Methane emissions are computed separately for each point in the water table distribution. Lake methane emissions are not simulated.

We modified the model of Walter and Heimann (2000) to respond to spatial variation in *NPP*. In the original model, the time series f_{in} of substrate availability was given by:

$$f_{in}(t) = 1 + f_{NPP}(t)/NPP_{max} \quad \text{(A2.5)}$$

where NPP_{max} is the local historical maximum daily *NPP* rate and f_{NPP} (t) is a time series of substrate flux into the soil equal to daily *NPP*(t) during the growing season and a time-varying fraction of the previous growing season's total *NPP* during the subsequent winter. We replaced equation A2.5 with:

$$f_{in}(t) = NPP_{max} + NPP(t) \quad \text{(A2.6)}$$

As a consequence, the units of the tuning parameter *r0* became $(gC/m^2/d)^{-1}$.

Acknowledgments

Sasha Richey (University of California, Irvine), Kaiyu Guan (Princeton University), and Xiaodong Chen (University of Washington) assisted in development of the modeling framework and parameter sets. Laura C. Bowling (Purdue University) provided valuable advice in application of the VIC lake/wetland model to boreal wetlands.

This work was funded by grants NNX08AH97G and NNX09AK57G from NASA to the University of Washington. ALOS/PALSAR imagery courtesy of JAXA.

V. EXPLORING THE RESPONSE OF WEST SIBERIAN WETLAND METHANE EMISSIONS TO FUTURE CHANGES IN CLIMATE, VEGETATION, AND SOIL MICROBIAL COMMUNITIES

This chapter is in preparation for submission to *Biogeosciences* (Bohn and Lettenmaier, 2013).

5.1 Introduction

Global wetlands have been the subject of increased attention from the climate modeling community because their large, temperature-dependent methane (CH_4) emissions may provide a positive feedback to future warming (Melton et al., 2013; Eliseev et al., 2008; Gedney et al., 2004). Boreal and arctic wetlands are of particular concern, due to their large extent (Lehner and Döll, 2004), pronounced historic and projected climate warming at high latitudes (Serreze et al., 2000; Diffenbaugh and Giorgi, 2012) and the possibility that previously-frozen soil carbon will decompose (Koven et al., 2011; Schaefer et al., 2011; Walter et al., 2006; Zimov et al., 2006) or be exported to the Arctic Ocean (Raymond et al., 2007; Frey and Smith, 2005) as permafrost thaws. Despite its importance to the global carbon cycle, the response of northern wetland methane emissions to climate change is fraught with uncertainties due to uncertain projections of future climate and geographic distribution of vegetation, and the response of soil microbial communities to these changes.

Climate change can influence methane emissions directly through several mechanisms. Wetland CH_4 emissions have been observed to depend strongly on soil temperature and moisture conditions (Olefeldt et al., 2013; Limpens et al., 2008; Christensen et al., 2003; Saarnio et al., 1997; Dise et al., 1993). Model projections (IPCC, 2007) suggest that, by the end of this century, high-latitude annual temperatures will rise by 2.8-7.8 °C and annual precipitation will increase by 10-28%; most global climate models agree that changes will be greater in winter than summer. But whether wetland soils become drier or wetter depends on the local trade-off between increased air temperature, and hence (in most climate models) increased evapotranspiration (ET) and water table drawdown; and increased precipitation, and hence shallower water tables (Bohn et al., 2007). In addition, warmer conditions and greater atmospheric CO_2 concentrations can be expected to lead to greater net primary productivity (NPP) (Wania et al., 2009), thereby supplying more labile carbon substrate for the production of methane (via root exudates, Riley et al., 2011; Walter and Heimann, 2000). If the drying is sufficiently large, the net wetland response to warming can be a reduction in methane emissions, leading to a negative climate-wetland CH_4 feedback (Ringeval et al., 2011).

In response to these changes in climate, dynamic global vegetation models (DGVMs) generally have predicted a northward shift in the geographic ranges of boreal and arctic biomes by the end of this century, with forests displacing tundra and, within tundra, taller shrublands displacing prostrate shrub tundra (Kaplan and New, 2006; Alo and Wang, 2008a; Jiang et al., 2012; Sitch et al., 2008), resulting in a corresponding increase in average leaf area index (LAI) between 1 and 4 m^2/m^2 throughout most of the high latitudes (Alo and Wang, 2008a,b). Assuming these changes apply equally to wetland vascular

plants, this could have multiple effects on wetland carbon cycling. First, greater LAI could lead to further increases in NPP (Alo and Wang, 2008a), providing more labile carbon to the soil via root exudates (a positive feedback, Riley et al., 2011). Second, greater LAI could lead to further increases in ET (Alo and Wang, 2008b), potentially increasing the negative feedback on wetland greenhouse gas emissions (Ringeval et al., 2011). Thus, increases in LAI bring another set of trade-offs between NPP and ET. Third, the distribution of plants with aerenchyma (a conduit of both CH_4 to the atmosphere and oxygen to the root zone) may change, affecting the relative strengths of different pathways of methane to the atmosphere (Riley et al., 2011; Berrittella and van Huissteden, 2011; Christensen et al., 2004).

Not only do uncertainties in future climate and vegetation distributions lead to uncertainties in future ambient soil conditions, but the possible responses of soil microbial communities to these long-term changes are also poorly known (Graham et al., 2012; Conant et al., 2011). Some evidence exists for acclimatization (reduction in response over time) to elevated temperatures (Allison et al., 2010). However, the underlying mechanism for this has not been determined conclusively, and not all studies agree (e.g., Contosta et al., 2013). Another factor in the microbial response is the shifting of species abundances as local climate conditions and vegetation change. It has been noted that most species of microbes have essentially global geographic distributions (Finlay and Clarke, 1999), due to their ease of geographic dispersal (e.g., airborne dispersal; DeLeon-Rodriguez et al., 2013). Indeed, evidence from temperate bogs and elsewhere suggests that differences in microbial community composition over large geographic areas depend more on local environmental conditions than on the distance between them, implying that dispersal has not encountered

a major barrier (Yavitt et al., 2012; Dumbrell et al., 2010). Similarly, there is evidence of a strong correlation between the strength of CH_4 emissions and plant species assemblages in peatlands across the U.K. (Levy et al., 2012), the pan-Arctic (Olefeldt et al., 2013) and the West Siberian Lowland (Glagolev et al., 2011). Taken together, these findings suggest that, as vegetation patterns shift, species abundances in microbial communities might shift with them (albeit not all at the same rates; Pickles et al., 2012). Whether these shifts will replicate the plant and microbial assemblages (and their characteristic responses to soil conditions) to the south or create entirely new assemblages (and new responses to soil conditions) is an open question.

Various individual aspects of the influence of vegetation distribution and soil microbial responses at large scales have been explored (Ringeval et al., 2011; Koven et al., 2011; Riley et al., 2011; Berrittella and van Huissteden, 2011) but, to our knowledge, no large-scale modeling studies have considered the effects of microbial population shifts on future land surface methane emissions. This is due in part to the application of a single set of methane emissions parameters across large portions of the globe in most studies (Bohn et al., 2013b). Similarly, no studies have compared the relative magnitudes of climate-, vegetation-, and soil microbe-based uncertainties in methane emissions.

The West Siberian Lowland (WSL) provides an interesting arena for testing the possible effects of microbial acclimatization and population shifts, in conjunction with changes in climate and vegetation. Intensive observations over a 2000-km transect of the region (Glagolev et al., 2011) demonstrated that the eutrophic mires in the south of the region emit far more methane per unit area than the tundra wetlands in the north. Bohn et al. (2013b) applied the methane emissions model of Walter and Heimann (2000) to the

WSL and found little overlap between the likely parameter values (primarily the temperature dependence of methanogenesis) in the northern and southern wetlands, implying substantially different responses to climate change between the two subregions' plant and microbial communities. Thus, in the WSL, a northward shift in vegetation and microbial communities might bring with it a northward shift in the response to climate change, resulting in an additional increase in methane emissions. In contrast, acclimatization might be expected to reduce the response of methane emissions to climate change.

In this study we attempt to determine the range of possible end-of-century methane emissions from the WSL, characterize the dominant factors (climate, vegetation, microbial response) that influence them, and identify the mechanisms by which they act, including trade-offs between them. To this end, we ran the Variable Infiltration Capacity (VIC) land surface model (Liang et al., 1994), linked to the wetland methane emissions model of Walter and Heimann (2000), forced in off-line simulations with the outputs of CMIP5 21st century climate projections (Taylor, et al., 2012) for the RCP 4.5 pathway (essentially a middle-of-the-road future scenario for global greenhouse gas emissions).

5.2 Methods

5.2.1 Study Domain

The West Siberian Lowland (WSL; Figure 5.1a) which includes approximately 800,000 km^2 of lakes and wetlands, is the largest high-latitude wetland region in the world (Kremenetski et al., 2003; Sheng et al., 2004; Peregon et al., 2009). Spanning 18 degrees of latitude (55-73° N) from the Eurasian Steppe to the Arctic Ocean, the WSL contains

both permafrost and permafrost-free wetlands (Figure 5.1a). These lakes and wetlands are interspersed with boreal forest (taiga) in the south and tundra in the north. Leaf Area Index (LAI) values derived from MODIS imagery (Myneni et al., 2002) vary accordingly from south to north, with values (one-sided and/or projected) ranging from 3 to 5 in the taiga declining northward to the treeless tundra above 70° N (Figure 5.1b).

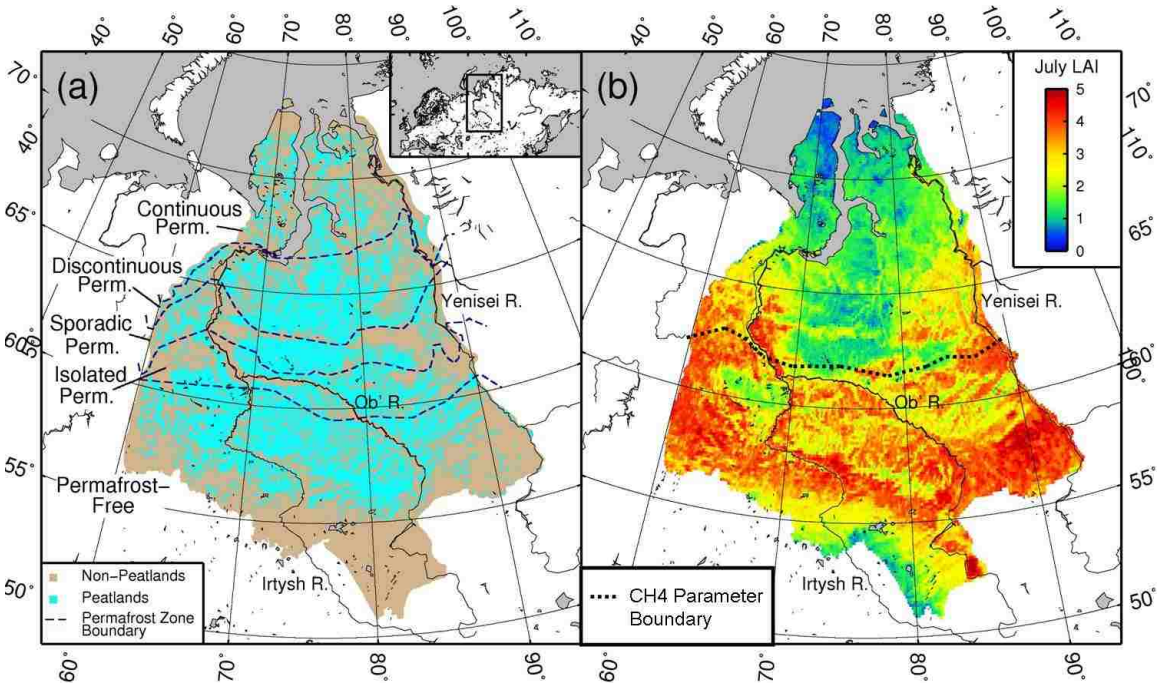

Figure 5.1: The West Siberian Lowland (WSL). Panel a: peatland distribution (from Sheng et al., 2004) and permafrost zone boundaries (after Kremenetski et al., 2003). Panel b: average July LAI for the period 2003-2010 derived from MODIS (Myneni et al., 2002). Dashed line denotes the boundary between northern and southern CH_4 parameter sets.

5.2.2 Model Formulation

Our study builds on the historical simulations of Bohn et al. (2013b) and uses the model formulation described therein. That study used a modified version of the Variable Infiltration Capacity model (VIC, Liang et al., 1994) land surface model, release 4.1.2. VIC 4.1.2 contains a frozen soil physics model (Adam and Lettenmaier, 2008; Cherkauer and Lettenmaier, 1999) and a dynamic lake-wetland model (Bowling and Lettenmaier, 2010). As described in Bohn et al. (2013b), VIC 4.1.2 was extended to include a distributed water table depth (WTD) scheme that accounts for wetland microtopography, such that wetlands contain a time-varying inundated area fraction A_{inund} (where standing water exists above the soil surface) which is a subset of a time-varying saturated area

fraction Asat (where the water table is at or above the soil surface). Another modification to VIC 4.1.2 included formulations for carbon cycle processes such as NPP and aerobic soil respiration (Rh), both of which are inhibited under saturated conditions (Bohn et al., 2013b). Additionally, the version of VIC 4.1.2 we used was coupled to the wetland CH_4 emissions model of Walter and Heimann (2000). As in Bohn et al. (2013b), all carbon fluxes were computed at several points along each grid cell's water table distribution and integrated to account for the net effect of fractional saturation on the cell's carbon fluxes.

Model parameter values were taken from Bohn et al. (2013b). As in Bohn et al., (2013b), wetland fractional areas were derived primarily from Sheng et al. (2004). Monthly historical wetland LAI values were computed as the average MODIS (Myneni et al., 2002) LAI value for all pixels that fell within the wetland portion of each grid cell.

For those parameters that were calibrated, we used the median values from Bohn et al. (2013b). In that study, parameters for the wetland methane emissions model were calibrated to match the in situ observations of Glagolev et al. (2011). Because wetlands in the southern half of the domain are much more productive than those in the northern half of the domain, we used separate CH_4 parameter values in the southern and northern halves, with the geographic boundary at approximately 62° N (denoted in Figure 5.1b), corresponding to northern boundary of the Middle Taiga zone (Glaglolev et al., 2011). The primary difference between the two parameter sets was the range of values for rq10 (which governs methanogenesis temperature sensitivity as in Walter and Heimann 2000), which ranged from 9.57 to 11.71 (median 10.69, unitless) in the South and from 2.52 to 5.21 (median 3.42) in the North. An even wider range of values for this parameter has been reported in the literature for wetlands globally (1.7 to 16; Walter and Heimann, 2000). The

values used in this study for these methane emissions model parameters are listed in Table 5.1.

Table 5.1: Median parameter values from Bohn et al. (2013b) for the wetland methane emissions model of Walter and Heimann (2000).

Parameter	Units	Value	
		South	North
r0[1]	$(gC/m^2/d)^{-1}$	0.020	0.020
xvmax	µmol/l/h	0.245	0.135
rkm	µmol/l	14.78	10.95
rq10	unitless	10.69	3.42
oxq10	unitless	2.05	4.94

[1]As documented in Bohn et al. (2013b), we modified the NPP dependence of the methane emissions model, resulting in the originally unitless *r0* parameter taking on units of $[(gC/m^2/d)^{-1}]$.

5.2.3 Meteorological Forcings

Meteorological forcings were derived for the periods 1948-2010 (historical) and 2011-2100 (future). VIC requires hourly values of air temperature, precipitation, wind speed, humidity, shortwave and longwave radiation, and atmospheric CO_2 concentration as inputs. We used methods described in Bohn et al (2013a) to derive hourly values of all of these variables (except CO_2) from daily values of precipitation, minimum and maximum temperature, and wind speed. Historical observations of these daily variables were derived over the 100-km EASE polar azimuthal equal-area grid (Brodzik and Knowles, 2002) from a combination of the daily meteorological fields of Sheffield et al. (2006) and gridded monthly observations (Willmott and Matsuura, 2001; Mitchell and Jones, 2005) via the methods of Adam and Lettenmaier (2003) and Adam et al. (2006). Future values of these variables were derived from model projections from the fifth phase of the Coupled Model Intercomparison Project (CMIP5, Taylor et al., 2012), for the Integrated Assessment Modeling Consortium (IAMC) RCP4.5 scenario (Moss et al., 2010) via what is commonly termed the "delta" approach (Hamlet and Lettenmaier, 1999). In the delta approach, fractional changes in monthly precipitation (future/historic) and differences in monthly

average temperature are applied, on a fixed seasonal cycle, to historic observations to form future scenarios. In our implementation, for each grid cell and each of 32 CMIP5 models (listed in Table 5.2), we computed a long-term climate trajectory from the 31-year moving average of monthly air temperature and precipitation for the years 2010-2100 from the CMIP5 projections), assigned to the year at center of window. We then converted these time series into monthly additive (temperature) or multiplicative (precipitation) anomalies relative to the model's local monthly mean over the historical scenario for the period 1975-2005 (because CMIP5 historical simulations end at year 2005). These anomalies were then regridded to the 100-km EASE grid. For each year in this time series, we then applied that year's monthly temperature and precipitation anomalies to one year of the historical daily forcings described above, randomly sampled from the period 1980-2010. For atmospheric CO_2 concentrations, we used the CMIP5 ensemble mean values.

Table 5.2: CMIP5 model outputs used in this study[1].

Model	Dynamic Vegetation	Model	Dynamic Vegetation
ACCESS1-0	No	GISS-E2-H-CC	No
ACCESS1-3	No	GISS-E2-R	Yes
BCC-CSM1-1	Yes	GISS-E2-R-CC	No
BCC-CSM1-1-m	Yes	HadGEM2-AO	No
BNU-ESM	No	HadGEM2-CC	Yes
CanESM2	Yes	HadGEM2-ES	Yes
CCSM4	Yes	INMCM4	Yes
CESM1-BGC	Yes	IPSL-CM5A-LR	Yes
CESM1-CAM5	No	IPSL-CM5A-MR	Yes
CMCC-CM	No	IPSL-CM5B-LR	Yes
CMCC-CMS	No	MIROC5	Yes
CNRM-CM5	No	MIROC-ESM	Yes
CSIRO-Mk3-6-0	No	MIROC-ESM-CHEM	Yes
GFDL-ESM2G	Yes	MRI-CGCM3	No
GFDL-ESM2M	Yes	NorESM1-M	Yes
GISS-E2-H	No	NorESM1-ME	Yes

[1]For more information, visit http://cmip-pcmdi.llnl.gov/cmip5/

5.2.4 Changes in LAI

Many CMIP5 models contained a dynamic vegetation component (Table 5.2) and predicted changes in the geographic distribution of vegetation over the next century. To account for the effects of these changes on LAI and consequently on carbon fluxes (NPP, RH, CH_4) as well as hydrology (ET, saturated area, water table depth), we converted each model's predicted end-of-21st-century (whole-gridcell) LAI to an equivalent end-of-century VIC (wetland) LAI via quantile mapping (Panofsky and Brier, 1968), under the assumption that the afforestation predicted by each dynamic vegetation model for the entire grid cell will apply in wetlands, too, relative to their own distribution of LAI. For each CMIP5 projection with a DGVM, we computed the percentile of each EASE-grid cell's wetland average LAI with respect to all the cells in the domain, for two periods: historical (1981-2010) and future (2071-2100). Similarly, we computed the percentile of each grid cell's average present-day wetland LAI as given by MODIS with respect to all cells. Then, for each CMIP projection, we mapped the CMIP5 historical and future LAI values to the corresponding MODIS LAI value of the corresponding percentile of the MODIS LAI distribution. The difference between these two MODIS LAI values was then added to the present-day MODIS LAI value as an estimate of the future wetland-average LAI for the grid cell. Grid cells for which the future CMIP5 LAI had no present-day analog were assigned the average change in LAI of their neighbors. No other vegetation-specific parameters were changed.

5.2.5 Simulations

To investigate the effects of changes in temperature, soil moisture, and LAI separately and in combination, we performed several sets of simulations (listed in Table 5.3). "Warming+Drying+LAI" consisted of 32 separate simulations, one per CMIP5 model, using the model's meteorological outputs and either the model's predicted LAI, if the model contained a dynamic vegetation component, or (for models without a DGVM), the median LAI of the models with DGVMs, to force our modified VIC LSM. "Warming+Drying" was the same as Warming+Drying+LAI, but held the seasonal cycle of LAI constant at historical MODIS values. Similarly, "Warming+LAI" was the same as Warming+Drying+LAI but with Asat and WTD in our LSM prescribed by repeating their daily values over the period 1981-2010 for the three 30-year periods 2011-2040, 2041-2070, and 2071-2100. Finally, "Warming" prescribed the historical values of LAI, Asat, and WTD. All simulations used the final state of the historical simulation of Bohn et al. (2013b) as the initial state of our LSM runs.

Table 5.3: Names and characteristics of simulations.

Simulation Name	N	Climate (T, P)	Soil Moisture	LAI
Historical	1	Gridded meteorology of Adam and Lettenmaier (2003) and Adam et al. (2006)	Prognostic	MODIS (Myneni et al., 2002)
Warming+Drying+LAI	32	CMIP5 outputs	Prognostic	LAI of corresponding CMIP5 model[1]
Warming+Drying	32	CMIP5 outputs	Prognostic	Historical LAI
Warming+LAI	1	CMIP5 ensemble mean	Historical Asat and WTD from 1981-2010 repeated for 2011-2040, 2041-2070, 2071-2100	Median CMIP5 LAI
Warming	1	CMIP5 ensemble mean	Historical Asat and WTD from 1981-2010 repeated for 2011-2040, 2041-2070, 2071-2100	Historical LAI

[1]For CMIP5 models that did not have a dynamic vegetation component, the median (seasonal cycle, for each grid cell) of the other models' LAI values was used.

To bracket the range of possible responses of soil microbial communities to changes in ambient soil conditions, we performed three variations of each of the above simulations (Table 5.4): one without acclimatization or population shifts ("NoAcc+NoShift"), one with acclimatization ("Acc+NoShift"), and one with both acclimatization and population shifts ("Acc+ShiftShift"). Acclimatization was modeled by replacing the constant Tmean parameter in the methane emissions model (Walter and Heimann, 2000) with the 10-year moving average of the vertically-averaged temperature in the top 1 m of the soil column. Population shifts were modeled as a complete replacement of northern microbial species abundances with those of the south. Accordingly, we replaced all instances of the northern values of the methane emissions parameters *r0*, *xvmax*, *rkm*, *rq10*, and *oxq10* with their southern counterparts.

Table 5.4: Names of soil microbial response cases.

Name	Acclimatization	Population Shift
NoAcc+NoShift	No	No
Acc+NoShift	Yes	No
Acc+Shift	Yes	Yes

5.3 Results

5.3.1 Future Climate and LAI

Because the majority of carbon fluxes take place in the WSL during the summer months (June-August), we focused our analysis on summer climate and LAI values. Changes over the 21st century in summer air temperature (ΔT_{JJA}) and summer precipitation (ΔP_{JJA}) predicted by the CMIP5 models are plotted in Figure 5.2 for the southern (south of 62° N) and northern (north of 62° N) halves of the domain (Figures 5.2a and b,

respectively). Predicted increases in summer air temperature (ΔT_{JJA}) were similar over the two halves of the domain, ranging from 1 to 5 °C (median approximately 3 °C) with the exception of one model (GFDL-ESM2M) predicting essentially no change in summer temperature in the South. In contrast, predicted changes in summer precipitation (ΔP_{JJA}) were more negative in the South (-19.6% to +29.1%, with a median of 0.0%) than in the North (-7.2% to +22.6%, with a median of +7.7%). In the South, ΔT_{JJA} and ΔP_{JJA} were moderately negatively correlated (Pearson's r of -0.53).

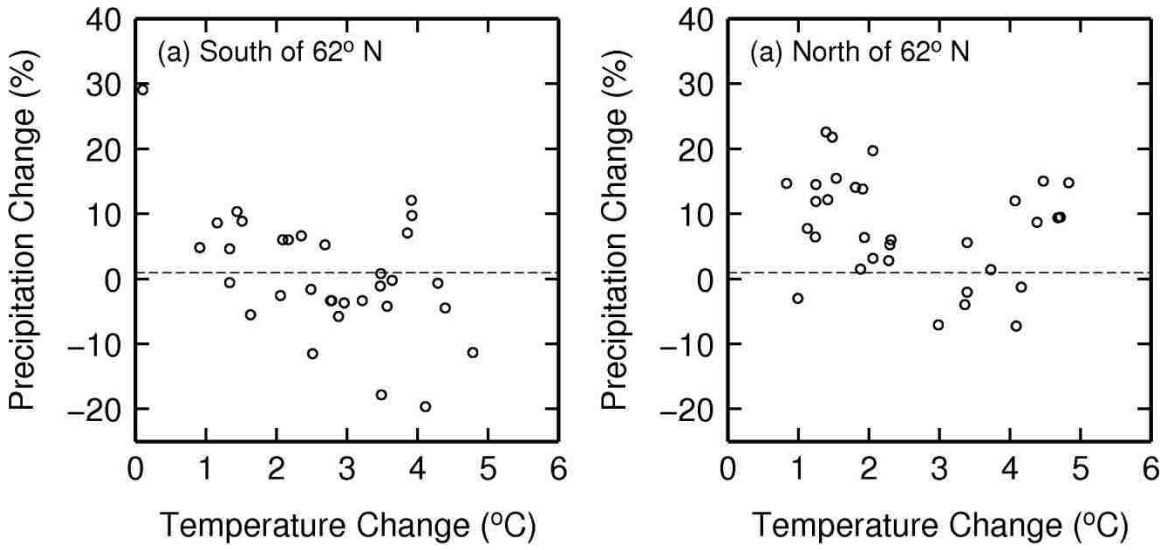

Figure 5.2: Differences between end-of-century (2071-2100) and historical (1981-2010) June-August climate given by each of the 32 CMIP5 climate projections, for the West Siberian Lowland, a) south of 62° N, and b) north of 62° N.

Profiles of JJA LAI (LAI_{JJA}) values for CMIP5 models (whole-gridcell) and VIC (wetland only) are shown in Figure 5.3. The original CMIP5 historical LAI_{JJA} values (Figure 5.3a) displayed a large degree of scatter, especially north of 60° N. The median LAI_{JJA} peaked at approximately 3 m^2/m^2 between 58 and 60° N and declined to the north. Among the CMIP5 models, projected 21st century changes in LAI_{JJA} (ΔLAI_{JJA}) were positive everywhere (median of approximately 0.5 m^2/m^2) and only exceeded 1 m^2/m^2 at the 75th percentile or higher (Figure 5.3b). Uncertainty in ΔLAI_{JJA} increased from south to north, as a result of disagreement among models about the amount of northward expansion of the boreal forest. The resulting end-of-century LAI_{JJA} values (Figure 5.3c) displayed greater uncertainty north of 60° N than their historical values.

Historical MODIS wetland LAI_{JJA} values (Figure 5.3d) also peaked at 3 m^2/m^2 at 56° N and declined northward, but tended to fall 0.5-1 m^2/m^2 below the median historical CMIP5 LAI_{JJA} values in the northern half of the domain. The values of ΔLAI_{JJA} derived

from quantile mapping (Figure 5.3e) were broadly similar to the ΔLAI_{JJA} values from the individual CMIP5 models (Figure 5.3b), with the exception of lower variability in the highest percentiles. Similar to the CMIP5 values, the end-of-century VIC wetland LAI_{JJA} values (Figure 5.3f) displayed more uncertainty in the North (1-2 m^2/m^2, or approximately 50-200% of the median values) than the South (1 m^2/m^2, or 30-50% of the median values). But at all latitudes the uncertainty in VIC LAI_{JJA} values was less than half that of the CMIP5 models, due to our application of the ΔLAI_{JJA} values to a single set of historical (MODIS) values. Spatial average ΔLAI_{JJA} was moderately correlated with ΔT_{JJA} in both the southern ($\rho = 0.67$) and northern ($\rho = 0.56$) halves of the domain.

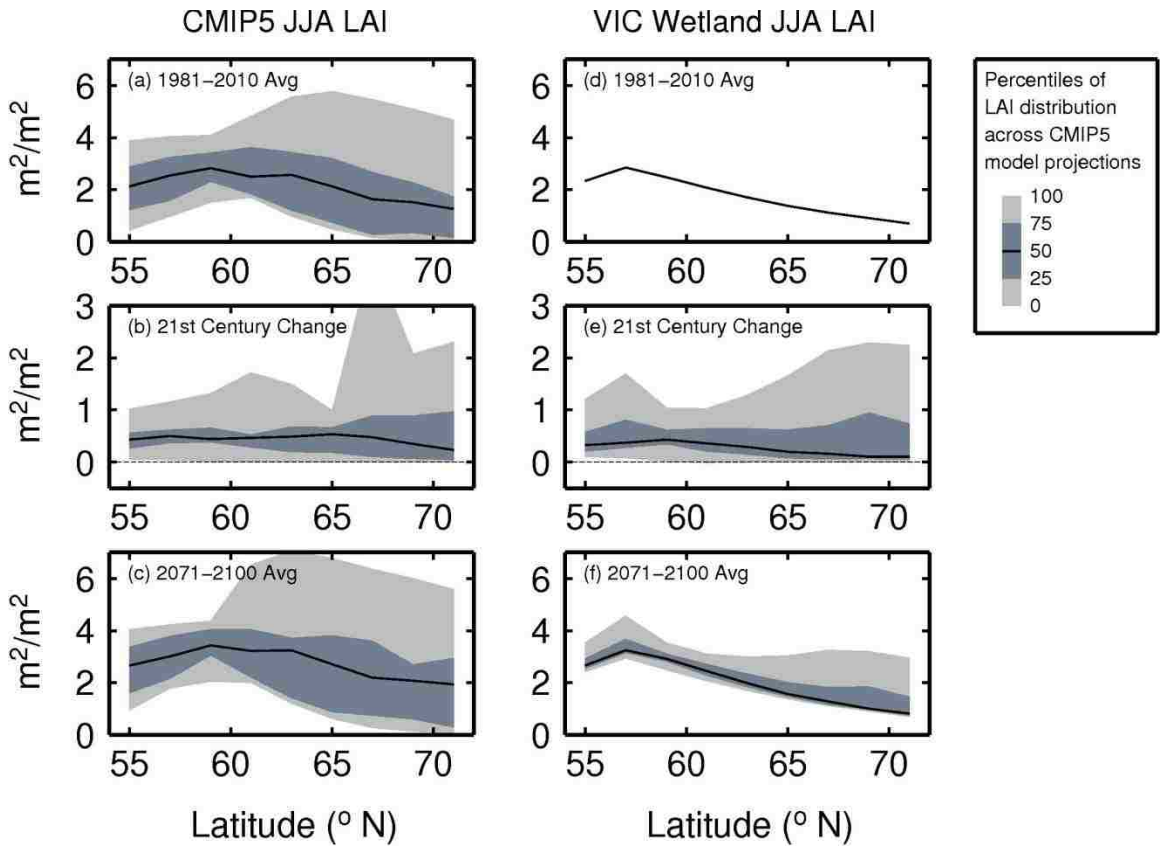

Figure 5.3: Distributions of historical and future zonal mean June-August (one-sided) LAI values for CMIP5 models (average LAI over all vegetation types) and VIC simulations (wetland LAI only).

5.3.2 Effects of Changes in Climate and LAI

Our results (summarized in Figure 5.4, for the NoAcc+NoShift case, and in Table 5.5) indicated that, for the most important greenhouse fluxes, warming will act in opposition to drying and increasing LAI. In the Warming simulation (blue bars in Figure 5.4), LAI, summer saturated area ($Asat_{JJA}$) and water table depth (WTD_{JJA}) were all prescribed at historical values (Figures 5.4a and b). This resulted in substantial increases in NPP, Rh, and especially CH_4 fluxes (end-of-century totals over the WSL of 199 Tg C/y, 191 Tg C/y, and 7.80 Tg CH_4/y, respectively; Figures 5.4c-e). Because Rh is more sensitive to temperature than NPP in our model (see Bohn et al., 2013b for parameter values), Rh increased faster than NPP, increasing the net flux of carbon to the atmosphere (Cnet; negative of carbon uptake) from its historical value of -14 Tg C/y to just -2.2 Tg C/y (Figure 5.4f). The large increase in CH_4 emissions and reduced carbon uptake drove a large increase in greenhouse warming potential (GHWP) emissions from 12 to 135 Tg CO_2/y (Figure 5.4g). Most terms responded similarly in the southern and northern halves of the domain. Thus, warming alone resulted in large increases in net fluxes to the atmosphere.

Increasing LAI (without drying) reduced net fluxes to the atmosphere, despite causing increases in individual fluxes. In the Warming+LAI simulation (green bars), end-of-century NPP rose to 240 Tg C/y (due to larger photosynthesizing area), and Rh rose to 2910g C/y (due to more carbon substrate entering the soil). Because NPP is more sensitive to LAI than Rh over decadal time scales, NPP increased more than Rh, causing carbon

uptake to surpass historical levels (Cnet of -22 Tg C/y, Figure 5.4f), and reducing GHWP to 66 Tg CO_2/y (Figure 5.4g). CH_4 was relatively insensitive to increased LAI.

Climate-induced drying (Warming+Drying; yellow bars) also acted in opposition to warming alone. In this simulation, the summer saturated area as a fraction of wetland area, $Asat_{JJA}$ (Figure 5.4a) decreased from 0.46 to 0.42, and WTD_{JJA} (Figure 5.4b) increased from 17 to 20 cm. The reduction of saturated area led to increases in NPP and Rh (to 220 and 210 Tg C/y, respectively) relative to warming alone, due to their inhibition under saturated conditions (Figures 5.4c and d). In contrast, the drier soils yielded a smaller end-of-century CH_4 flux (7.2 Tg CH_4/y) than for warming alone (Figure 5.4e). Carbon uptake increased (Cnet decreased), leading to a Cnet of -7.6 Tg C/y (Figure 5.4f). The net effect on GHWP was a larger increase from its historical value (to 100 Tg CO_2/y) than for Warming+LAI (Figure 5.4g), but still smaller than for warming alone.

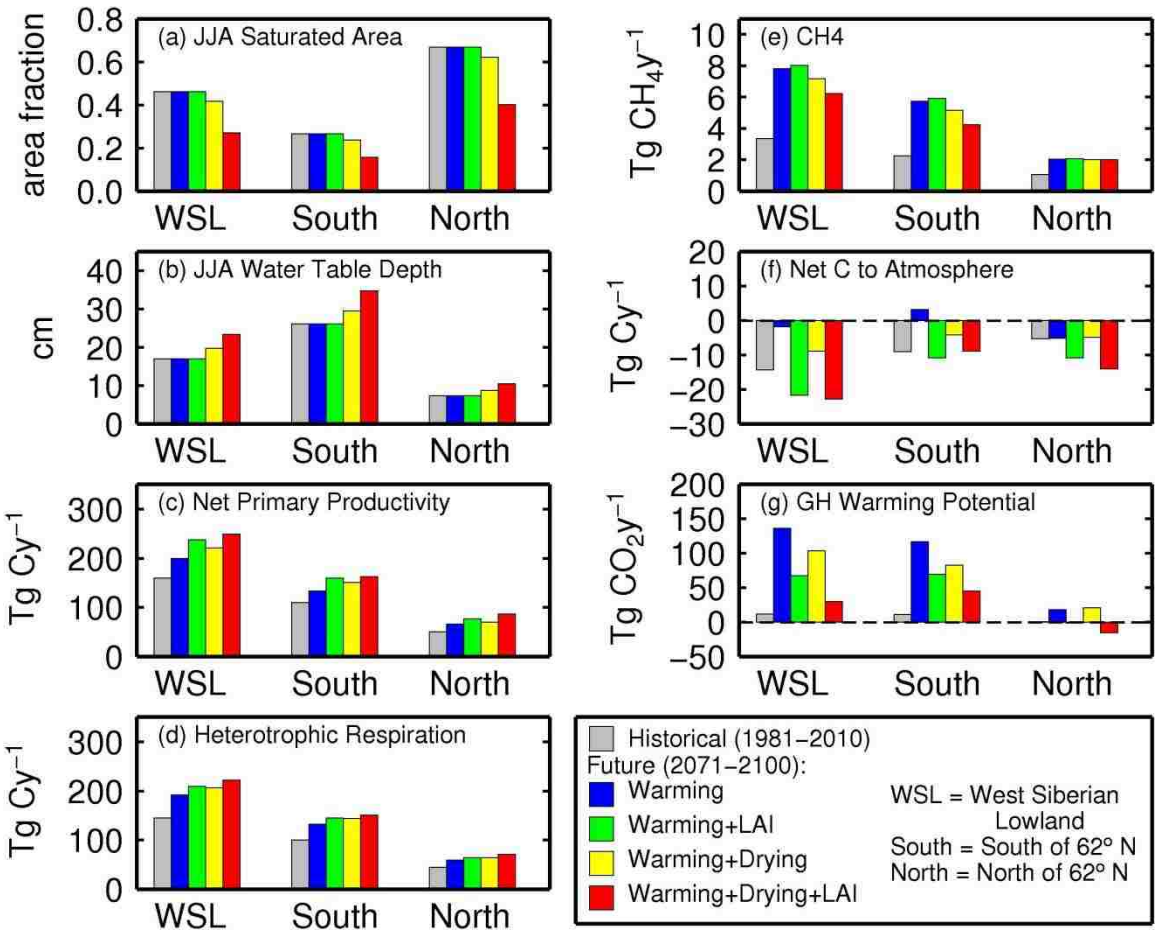

Figure 5.4: Simulated historical and end-of-century water and carbon cycle terms over the WSL (average over 32 GCMs) and its southern and northern halves.

The combination of drying and increased LAI (Warming+Drying+LAI; red bars) also acted in opposition to warming alone. This simulation predicted greater drying than Warming+Drying: end-of-century values of $Asat_{JJA}$ and WTD_{JJA} were 0.27 and 23 cm, or 42% less and 36% greater than their historical values, respectively (Figures 5.4b and c). Drier soils and greater photosynthesizing area led to the largest increases in NPP and Rh of all simulations, with values of 250 and 220 Tg C/y (Figures 5.4c and d). In contrast, drier soils led to the smallest increase in end-of-century CH_4 of all simulations, to 6.2 Tg CH_4/y (86% above historical, Figure 5.4e). Greater carbon uptake (Cnet of -23 Tg C/y, Figure

5.4f) and lower CH_4 emissions led to the smallest increase in end-of-century GHWP of all simulations, of 29 Tg CO_2/y (approximately 2.6 times its historical value; Figure 5.4g).

Thus, the combination of drier soils and greater photosynthesizing area only partially offset the effects of warming on CH_4 and GHWP, but surpassed the effects of warming on carbon uptake (Cnet). For these fluxes, warming increased the flux of carbon to the atmosphere, while drying (both LAI- and climate-driven) reduced the flux to the atmosphere. While increased LAI (without drying), had little influence over CH_4, it played a major role in reducing the net flux to the atmosphere for Cnet and GHWP. There were two exceptions to these patterns. In the South, the drying due to both climate and LAI caused some grid cells to experience water limitation, which slowed the increase of NPP and carbon uptake (Figures 5.4c and f). In contrast, in the North, wetlands were more likely to be temperature-limited than water-limited; thus, CH_4 fluxes there responded primarily to warming, and showed a small but positive response to increased LAI with drying (Figure 5.4e and Table 5.5).

For CH_4, the opposing influences of warming and drying are consistent with the negative climate-wetland CH_4 feedback explored by Ringeval et al. (2011) and Koven et al. (2011). To estimate its size, Ringeval et al. and Koven et al. compared simulations with fixed wetland extent (analogous to our Warming+LAI simulations, because they used a DGVM) to simulations with varying wetland extent (analogous to our Warming+Drying+LAI simulations). Koven et al. found that drying reduced the 21st century increases in CH_4 yielded by warming by 60-80% over the Arctic. Based on the difference between the predictions of our Warming+LAI (green) and Warming+Drying+LAI (red) simulations, we estimate the size of this effect over the WSL

to be -1.8 Tg CH_4/y, or only 38% of the size of the effect of future warming (Warming+LAI minus Historical).

Table 5.5: End-of-century water- and carbon-cycle terms.

Variable	Units	Soil Microbe Response	Simulation	Mean WSL	Mean S	Mean N
ET_{JJA}[1]	mm H_2O	n/a	Historical	204	238	161
		NoAcc+NoShift	Warming+Drying	243	291	188
			Warming+Drying+LAI	258	305	206
$Asat_{JJA}$	Fraction	n/a	Historical	0.462	0.266	0.669
		NoAcc+NoShift	Warming	0.462	0.266	0.669
			Warming+LAI	0.462	0.266	0.669
			Warming+Drying	0.419	0.239	0.622
			Warming+Drying+LAI	0.274	0.158	0.402
WTD_{JJA}	Cm	n/a	Historical	17.0	26.1	7.4
		NoAcc+NoShift	Warming	17.0	26.1	7.4
			Warming+LAI	17.0	26.1	7.4
			Warming+Drying	19.7	29.6	8.7
			Warming+Drying+LAI	23.4	34.8	10.5
NPP	Tg C/y	n/a	Historical	160	110	50
		NoAcc+NoShift	Warming	199	133	66
			Warming+LAI	237	160	77
			Warming+Drying	220	150	70
			Warming+Drying+LAI	249	162	87
Rh	Tg C/y	n/a	Historical	144	100	44
		NoAcc+NoShift	Warming	191	131	60
			Warming+LAI	209	144	65
			Warming+Drying	207	143	64
			Warming+Drying+LAI	221	150	71
CH_4	Tg CH_4/y	n/a	Historical	3.36	2.29	1.06
		NoAcc+NoShift	Warming	7.80	5.75	2.05
			Warming+LAI	8.04	5.95	2.09
			Warming+Drying	7.20	5.19	2.01
			Warming+Drying+LAI	6.25	4.24	2.02
		Acc+NoShift	Warming	4.16	2.54	1.61
			Warming+LAI	4.63	2.95	1.68
			Warming+Drying	4.20	2.63	1.57
			Warming+Drying+LAI	3.57	1.97	1.59
		Acc+Shift	Warming	7.79	2.55	5.25
			Warming+LAI	8.48	2.97	5.51
			Warming+Drying	7.92	2.77	5.15
			Warming+Drying+LAI	7.36	2.01	5.36
Cnet	Tg C/y	n/a	Historical	-13.5	-8.3	-5.2
		NoAcc+NoShift	Warming	-2.2	2.3	-4.5
			Warming+LAI	-22.0	-11.5	-10.4
			Warming+Drying	-7.6	-3.1	-4.5
			Warming+Drying+LAI	-23.3	-8.8	-14.5

		Acc+NoShift	Warming	-4.9	-0.1	-4.8
			Warming+LAI	-24.5	-13.8	-10.7
			Warming+Drying	-9.9	-5.0	-4.8
			Warming+Drying+LAI	-25.3	-10.5	-14.8
		Acc+Shift	Warming	-2.2	-0.1	-2.1
			Warming+LAI	-21.6	-13.8	-7.9
			Warming+Drying	-7.1	-4.9	-2.1
			Warming+Drying+LAI	-22.5	-10.5	-12.0
GHWP	Tg CO_2/y	n/a	Historical	11.9	11.4	0.3
		NoAcc+NoShift	Warming	134.5	113.4	21.0
			Warming+LAI	66.2	66.3	-0.1
			Warming+Drying	103.5	83.3	20.2
			Warming+Drying+LAI	28.6	45.0	-16.2
		Acc+NoShift	Warming	58.0	46.0	11.8
			Warming+LAI	-5.0	3.5	-8.5
			Warming+Drying	40.5	29.6	11.0
			Warming+Drying+LAI	-27.7	-2.6	-25.3
		Acc+Shift	Warming	134.3	46.2	88.2
			Warming+LAI	75.4	3.7	71.7
			Warming+Drying	118.7	32.5	86.1
			Warming+Drying+LAI	51.9	-1.8	53.9

[1]ET_{JJA} was not explicitly computed for the Warming and Warming+LAI simulations.

5.3.3 Acclimatization and Population Shifts

Acclimatization and population shifts proved to be potentially more important than climate and LAI as a factor in our results. Figure 5.5 shows the predicted CH_4 and GHWP emissions for the same set of simulations as Figure 5.4, for the three cases of soil microbial response (Cnet was relatively insensitive to soil microbe response and is not plotted). Relative to the NoAcc+NoShift simulations (Figures 5.5a and b), applying acclimatization but not population shifts (Acc+NoShift; Figures 5.5c and d) dramatically reduced the end-of-century CH_4 emissions over the WSL to 3.57 Tg CH_4/y (only 6% greater than historical emissions), and turned the domain into a net GHWP sink of -28 Tg CO_2/y. This is consistent with Koven et al. (2011), who found that acclimatization eliminated 50-75% of

the increases predicted by simulations that did not account for acclimatization (note that the curves in their Figure 5.4 for fixed and varying Tmean were mis-labeled; Koven and Ringeval, pers. comm., 2013). These changes were most pronounced in the South, where warming in the presence of acclimatization led to only a meager increase in CH_4 emissions, for which climate- and LAI-induced drying more than compensated, leading to future CH_4 emissions (1.97 Tg C/y) that were 15% lower than historical. In the North, acclimatization had only a slight effect on CH_4 and GHWP.

In contrast, adding population shifts to the acclimatization simulations (Acc+Shift; Figures 5.5e and f) yielded larger increases in CH_4 emissions over the WSL (7.36 Tg CH_4/y, or 119% above historical values) than the NoAcc+NoShift case (6.25 Tg CH_4/y, or 85% above historical values). Similarly, GHWP emissions rose to 52 Tg CO_2/y, compared to 29 Tg CO_2/y for the NoAcc+NoShift case. However, unlike the NoAcc+NoShift case, in which approximately 2/3 of future CH_4 emissions were generated in the South, 73% of future CH_4 emissions were generated in the North (where emissions increased by a factor of five over historical values) for the Acc+Shift case. The reason for this is that we modeled population shifts as a complete replacement of the northern species abundances (and their response to temperature) with those of the southern microbial communities. Thus, in the South, there was no change in the CH_4 parameter set; acclimatization worked as it did in the acclimatization/no population shift simulations. In the North, the introduction of the greater Southern temperature sensitivity allowed for larger emissions during the growing season, despite the elevated Tmean. Population shifts also amplified the North's small but positive response to increased LAI with drying.

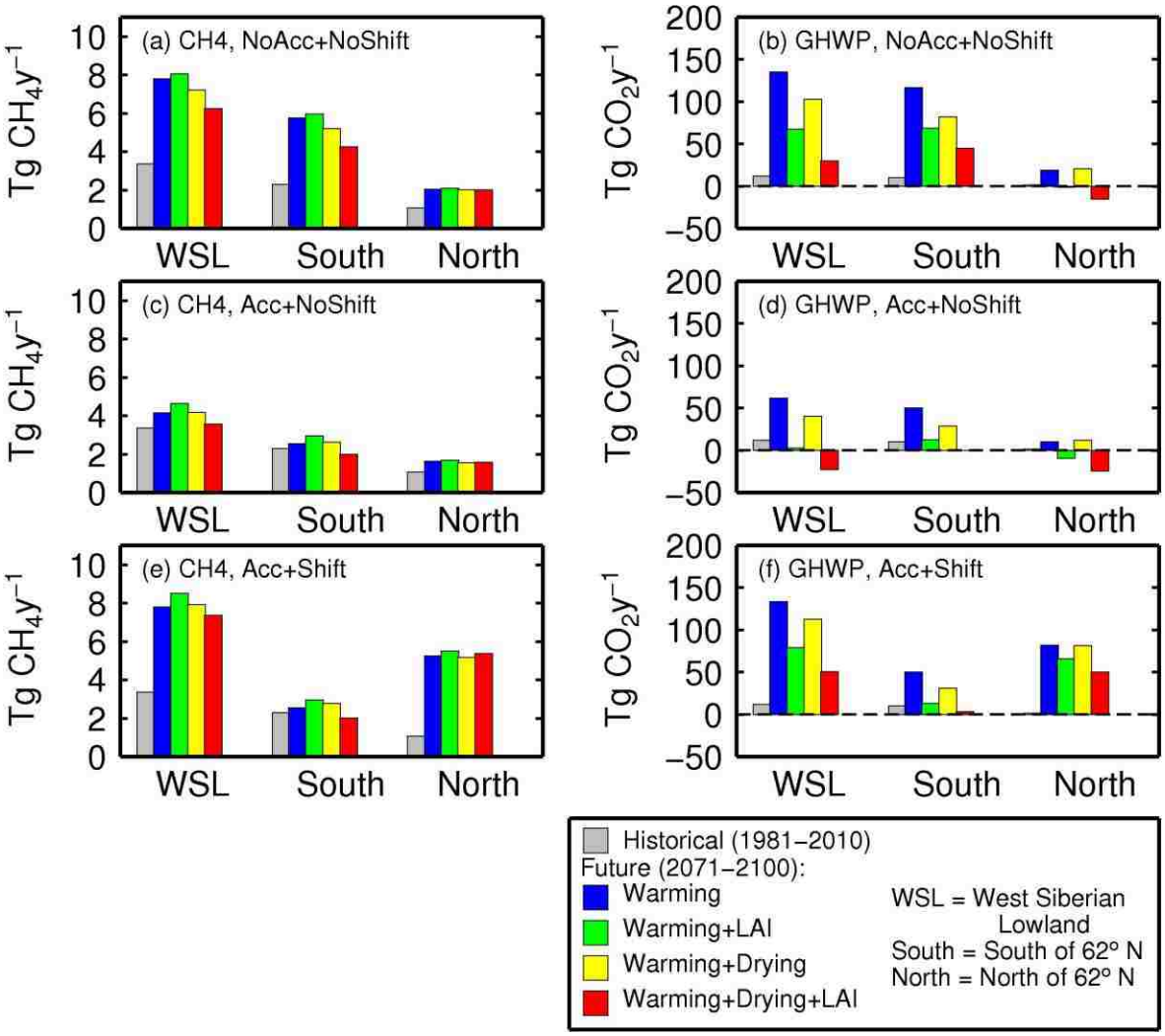

Figure 5.5: Simulated historical and end-of-century methane (CH_4) emissions and greenhouse warming potential (GHWP) over the WSL and its southern and northern halves, for the cases of a,b) no acclimatization or population shifts ("NoAcc+NoShift"), c,d) acclimatization but no population shifts ("Acc+NoShift"), and e,f) acclimatization plus population shifts ("Acc+ShiftShift").

For the WSL as a whole, the range of CH_4 emissions bracketed by the median results for the presence or absence of acclimatization and population shifts was nearly as large (3.8 Tg CH_4/y) as the effect of warming alone in the NoAcc+NoShift simulations (which added 4.2 Tg CH_4/y), and more than twice the size of the effect of the climate-wetland CH_4 feedback for the NoAcc+NoShift case (1.8 Tg CH_4/y). For the North in particular, the range of values bracketed by the soil microbial response cases (3.8 Tg

CH_4/y) was almost four times the size of the effect of warming alone in the NoAcc+NoShift case (1.0 Tg CH_4/y). It should be noted, however, that the primary mechanism by which population shifts and acclimatization acted was changing the temperature sensitivity, so that their effects constitute a modulation of the warming effect.

Acclimatization (with or without population shifts) reduced the size of the climate-wetland CH_4 feedback to -1.1 Tg CH4/y. At the same time, the warming (Warming+LAI minus Historical) effect decreased to 1.3 Tg CH4/y under acclimatization and increased to 5.1 Tg CH4/y under acclimatization plus population shifts. Thus, the various soil microbial responses caused the strength of the climate-wetland CH_4 feedback to be between 22 and 85% of the warming effect, the upper bound of which is more consistent with the estimate of Koven et al. (2011) for the entire Arctic (60-80% of the warming effect).

5.3.4 Effects on the Seasonal Cycle

Acclimatization and population shifts not only affected total annual CH_4 emissions, but also changed the shape of the seasonal cycle of emissions in the northern half of the WSL. Monthly spatial average methane emissions and hydrologic terms over the period 2071-2100 are plotted in Figure 5.6, for the southern and northern halves of the WSL. During snowmelt (Figure 5.6c and d), the upper soil layers begin to thaw (Figure 5.6e and f). Without acclimatization or population shifts, the North's lower temperature sensitivity (Q10) leads to lower CH_4 emissions throughout the growing season than in the South (solid black lines in Figure 5.6a and b), despite the North's wetter and more anoxic conditions (evidenced by larger saturated fraction and higher water table, Figure 5.6g-h and Figure 5.6i-j, respectively) and the presence of labile carbon substrate (to which NPP is a

contributor, Figure 5.6k and l). By raising Tmean, acclimatization reduces the temperature response in both the South and the North (dashed blue lines, Figure 5.6a and b), but in the North, the difference is relatively small due to the lower Q10 there.

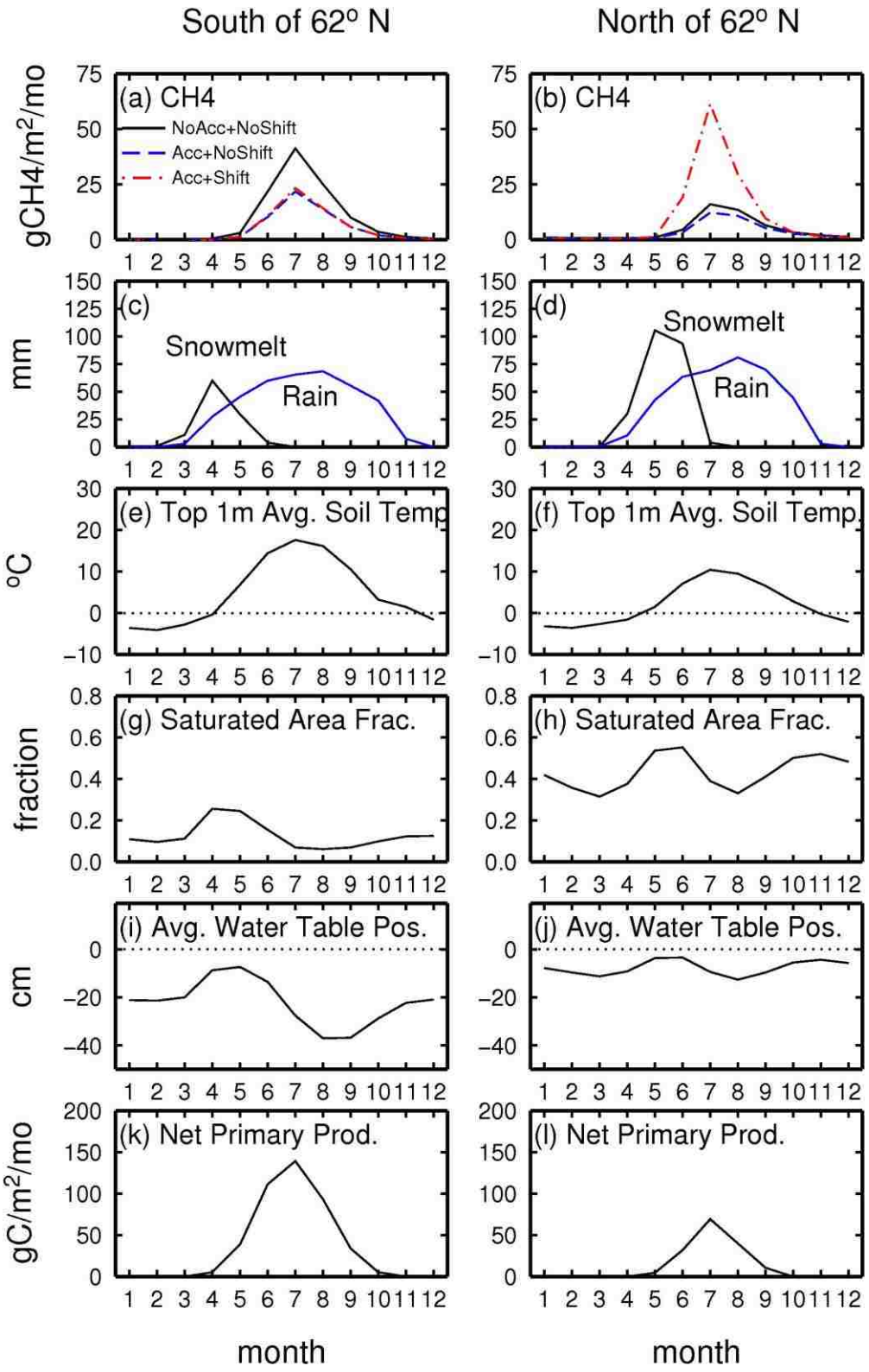

Figure 5.6: Monthly spatial average seasonal cycles of methane emissions and hydrologic terms for the period 2071-2100, for the CMIP5 ensemble mean climate forcings and median LAI, for the southern and northern halves

of the WSL, for the cases of no acclimatization or population shifts ("NoAcc+NoShift"), acclimatization but no population shifts ("Acc+NoShift"), and acclimatization plus population shifts ("Acc+ShiftShift").

Population shift (red dot-dashed lines, Figure 5.6a and b) has little effect in the South, but makes a large difference in the North, where the increase in Q10 allows microbes to take advantage of both the warming temperatures and the wetter conditions, leading to larger emissions than were achieved in the South even without acclimatization. In addition, population shift disproportionately increases emissions (by a factor of 3.8 to 4.2, relative to no population shifts) in the first half of the growing season, during and immediately after snowmelt (Figure 5.6b), when conditions are wettest. Later in the growing season, increases in emissions are smaller (only a factor of 1.5 to 2 relative to no population shifts) due to drier soils and their accompanying methanotrophy. The net result is to shift the peak emissions forward in time. The implications of increased methanogenic activity during and immediately after snowmelt are discussed further in section 5.4.

5.4 Discussion

Our results suggest that the potential response of soil microbial communities to changes in climate and vegetation is as important as climate change itself to predicting future high-latitude wetland methane emissions. More importantly, the soil microbial response has the potential to shift emissions to the northern portion of the WSL, where uncertainty about the potentially large amount of labile carbon that might be liberated by permafrost thaw (not explicitly considered in this study) is also a concern (Koven et al., 2011; Schaefer et al., 2011; Zimov et al., 2006). In particular, Schaefer et al. predicted a median cumulative flux to the atmosphere from present-day permafrost soils of about 80 Gt C between 2020 and 2100, and estimated it could lead to an increase in atmospheric carbon

of 25% over current levels. Whether this additional carbon will be respired as CO_2 or CH_4 depends crucially on the degrees of microbial acclimatization and population shifts that will occur. Futhermore, our findings indicate that population shift not only increases CH_4 emissions in the permafrost zone, but also increases uncertainty in those emissions via increased sensitivity to temperature.

The increased temperature sensitivity in the northern half of the domain brought about by population shifts, and the disproportionate increase in microbial activity during snowmelt that results, may result in a larger increase in CH_4 emissions than we have predicted. Studies have found that the dissolved organic carbon (DOC) in boreal and Arctic streams is most labile (easily consumable by microbes) during the snowmelt freshet, followed by a decline over the course of the summer (Mann et al., 2012; Holmes et al., 2008), suggesting that the onset of snowmelt liberates highly labile carbon from the soil. Observations suggest that, during the lower flow conditions after snowmelt, wetland microbes preferentially consume labile DOC faster than it is input by local plants (Olefeldt and Roulet, 2012), so that lability declines with distance downstream and with residence time in the wetland. Our modeling framework does not explicitly model the lability of carbon or its preferential consumption by microbes, and therefore likely underestimates the lability of the carbon available during snowmelt. Given that the labile DOC consumed by wetland microbes would otherwise be exported to the relatively oxic stream network, where it is metabolized and outgassed as CO_2 (Wallin et al., 2013), the degree to which soil microbes influence the export of labile DOC to streams is an important factor to constrain.

While our results corroborated both the climate-wetland CH_4 feedback and the acclimatization estimated by Ringeval et al. (2011) and Koven et al. (2011), our estimate of

the climate-wetland CH_4 feedback effect size was smaller than theirs (22-38% of the size of the warming effect, vs. 60-80%), and our estimate of acclimatization was larger (85% of the size of the warming effect, vs. 50%). One reason for this may be that our acclimatization approach set Tmean equal to the 10-year moving average of soil temperature, while Ringeval et al. and Koven et al. used a relaxation approach with a 365-day time constant, in which the previous winter's soil temperatures might have a larger influence than in our approach. Another potential reason for the discrepancy might be their neglect of emissions from wetlands where the water table depth is deeper than 5 cm, which could affect sensitivities to climate change (Bohn and Lettenmaier, 2010). Another reason may be that Ringeval et al. and Koven et al. applied a single methane emissions parameter set globally, which yielded a positive bias in historical methane emissions over the northern WSL (Bohn et al.; 2013b). The higher historical baseline emissions in the North might have reduced the size of the warming effect in their simulations. Their more productive northern emissions (and their use of a single parameter set globally) suggest that their end-of-century results might correspond more with our Acc+Shift simulation than with our Acc+NoShift simulation. Conversely, the historical/current net value of the climate-wetland CH_4 feedback over the high latitudes may be more negative than estimated by Ringeval et al.

Modeling population shift as an expansion of the range over which we apply the southern CH_4 parameter set may be an oversimplification in several ways:

1. The new microbial communities in the North will not necessarily be identical to those currently in the South, due to different local conditions (e.g., soil pH, subsurface flow, etc.). It is not clear whether our assumptions might effectively be

an upper bound, because we do not know if new combinations of species (especially different abundances of methanogens and methanotrophs) will produce larger or smaller net CH_4 emissions. Pickels et al. (2012) noted that fungi disperse at different rates, and that community dominance often depends on the order of species arrival. In addition, some microbes are symbiotic with plant hosts, which will also experience varying rates of dispersal. How microbe and plant abundances might evolve through time and space, and how that would affect carbon fluxes, is poorly known (e.g., Conant et al., 2011, Olsrud et al., 2004).

2. We modeled population shift as a complete replacement of species abundances across the entire domain; in reality population shifts might be limited by climate. Thus, we may have produced something close to an upper bound on the changes in the North.
3. We did not change the CH_4 parameters used in the South. It is possible that southern mires might also experience changes in species assemblages, perhaps evolving to resemble temperate communities, which are potentially more productive (e.g., Yavitt et al., 2012). Thus, this is a lower bound on the changes in the South.
4. We did not vary plant-aided transport parameters spatially and thus could not model any potential changes in geographic distribution of vascular plants that have aerenchyma. Nor did we consider factors like N, P, pH, or redox state. Previous studies (Riley et al., 2011; Berrittella and van Huissteden, 2011) found that CH_4 emissions were sensitive to plant-aided transport, and in particular, Berrittella and van Huissteden (2011) found that differences in the distributions of plants with

aerenchyma had a strong influence on Ice Age CH_4 emissions. However, any influence that plant-aided transport might have on the current distribution of CH4 emissions would presumably shift northward along with the plants themselves, contributing to the increase in emissions in the northern half of the domain.

Our results reinforce the findings of Bohn et al. (2013b), that spatial variation in soil microbial behavior (reflected in CH_4 emissions parameters) exerts an important control on large-scale wetland carbon fluxes. No other studies have examined microbial population shifts, in part because few large-scale models have applied spatially-varying parameters. This, in turn, is partly due to a lack of sufficient long-term in situ observations to support spatially-varying parameters. However, with the advent of intensive data sets such as Glagolev et al. (2011) and Peregon et al. (2009) in the WSL and Levy et al. (2012) in the UK, it should become possible to find linkages between vegetation and CH_4 parameters that enable parameter transfer over regions where few in situ observations have been made.

5.5 Conclusions

We used the Variable Infiltration Capacity (VIC) land surface model (Liang et al., 1994), linked to the wetland methane emissions model of Walter and Heimann (2000), forced off-line with outputs of CMIP5 projections (Taylor, et al., 2012) for the RCP 4.5 pathway to simulate changes in the surface hydrology and methane emissions of the wetlands of the West Siberian Lowland. We examined the effects on end-of-century CH_4

emissions of changes in climate and LAI, and the possible responses of soil microbes to these changes. We conclude that:

- By the end of this century, CH_4 emissions from the WSL will rise to 3.6-7.3 Tg CH_4/y, an increase of 6-119% over their historical values. Carbon uptake by the region's wetlands will increase to 23 Tg C/y from a historical level of 14 Tg C/y. The net greenhouse warming potential of the region's wetlands will range between -22 to 51 Tg CO_2/y.
- The potential response of soil microbes to future changes in climate and vegetation is as important as climate change in determining future greenhouse gas emissions from high-latitude wetlands. Acclimatization almost completely offset the increases in CH_4 emissions that arose from changes in climate and LAI, while population shifts led to a near doubling of the region's emissions. Crucially, while ignoring acclimatization and population shifts focused the majority of emissions in the southern half of the domain, acclimatization plus population shifts concentrated 73% of future emissions in the northern half of the domain, where the possible release of carbon with permafrost thaw is a concern.
- Population shifts increased microbial activity during and immediately following snowmelt, when highly labile carbon is thought to be first released from the soil. This may imply larger CH_4 emissions than we have predicted, and a possible reduction of the labile carbon exported to Arctic streams.

Our work indicates the importance of better constraining the responses of soil microbial communities to changes in climate and vegetation as they are critical determinants of the region's future methane emissions.

Acknowledgments

This work was funded by grants NNX08AH97G and NNX09AK57G from NASA to the University of Washington. Advanced computational, storage, and networking infrastructure was provided in part by the University of Washington's Hyak supercomputer system, supported in part by the University of Washington eScience Institute.

VI. CONCLUSIONS

The research reported in this dissertation addresses the four science questions from Chapter I, specifically: (i) What are the dominant mechanisms controlling the behavior of a heterogeneous water table in boreal wetlands, and how do they influence the response of high-latitude wetland carbon fluxes to future climate change?, (ii) Can a model that represents these mechanisms be used to characterize the errors inherent in previous global estimates of wetland carbon fluxes?, (iii) How does small-scale heterogeneity in water table depths and large-scale variability in methane productivity affect the large-scale behavior of high-latitude wetland carbon fluxes?, and (iv) What are the dominant factors affecting future carbon fluxes from high-latitude wetlands? To address these questions, I used a combination of large-scale hydrology and biogeochemistry models (primarily the VIC model and the wetland methane emissions model of Walter and Heimann, 2000), remote sensing products, and in situ observations.

To answer the first question, I implemented a distributed water table scheme in the VIC modeling framework, and ran it over a small test region in the southern West Siberian Lowland (WSL). I found that air temperature and precipitation exert opposing influences over the water table depth, and hence (for the values of methane parameters that were optimal at the calibration site) over methane emissions. Representation of spatial variations in water table depth gave rise to a saturated zone of time-varying area (Asat) where CH_4 emissions were at their maximum value. This affected the sensitivity of simulated methane emissions to climate. Holding precipitation at historical levels but increasing temperature

to the maximum end-of-century value predicted for the region (IPCC, 2007) increased per-unit area emissions in the saturated zone due to higher metabolic rates; but Asat decreased due to higher evapotranspiration rates, leading to a decrease in total emissions. In contrast, holding temperature at historical levels but increasing precipitation to the maximum predicted end-of-century value did not change per-unit-area emissions but increased Asat, leading to an increase in total emissions. This competition between temperature and precipitation resulted in a fairly consistent trade-off of 3° C increase in temperature per 5% increase in precipitation, for which methane emissions remained relatively constant, over most of the range of possible future climates. The median climate forecast of a 3 °C increase in temperature and a 10% increase in precipitation yielded roughly a doubling of current CH_4 emissions by the end of the century.

To answer the second question, I characterized the errors generated by other commonly-used water table formulations (i.e., *uniform* schemes, in which a single average water table depth is applied to the entire wetland; and *wet-dry* schemes, in which only emissions from the saturated portion of the wetland are considered), relative to my spatially distributed scheme, over the same test region in the southern WSL, for the same combinations of future changes in temperature and precipitation. The other schemes' biases depended on the spatial standard deviation of the water table depth, σ_{zwt}. For small values of σ_{zwt} (e.g., 2.4 cm), the uniform scheme's bias approached 0, but the wet-dry scheme's biases reached -85% of the distributed scheme's emissions (-(1-Asat)*100%), due to neglect of emissions from unsaturated wetlands. For large values of σ_{zwt} (e.g., 38 cm), the wet-dry scheme's bias approached 0, but the uniform scheme's bias reached up to

+/-100% of the distributed scheme's emissions (with the most extreme biases occurring under the most extreme changes in climate). For intermediate values of σ_{zwt} and the median predicted end-of-century climate, the uniform scheme's bias was 10-30% and the wet-dry scheme's bias was -20 to -30%. Thus, different water table formulations may explain a substantial amount of the variation among previously published model estimates of end-of-century CH_4 emissions from high latitude wetlands.

To answer the third question, I applied the modeling framework to the entire WSL for the period 1948-2010. As part of this effort, I replaced the TOPMODEL formulation used in Chapters II and III with a water table distribution based on observed microtopography, and added seasonal inundation. After calibrating the modeling framework to match remotely-sensed inundation and saturated soil and in situ observations of water table depth and methane emissions, I found that, while surface heterogeneity (fractional saturated area) had little overall effect on estimates of the region's carbon fluxes, sub-surface heterogeneity (spatial variations in water table depth) played an important role in both the overall magnitude and spatial distribution of estimates of the region's carbon fluxes. In particular, to reproduce the spatial pattern of CH_4 emissions recorded by intensive in situ observations across the domain, in which very little CH_4 is emitted north of 60° N, it was necessary to a) account for CH_4 emissions from unsaturated wetlands and b) use a methane model parameter set that reduced estimated CH_4 emissions in the northern half of the domain. My results suggest that previous estimates of the response of these wetlands to thawing permafrost may have overestimated future increases in methane emissions in the permafrost zone.

To answer the fourth question, I ran the modeling framework over the WSL, forced with outputs from 32 CMIP5 models for the RCP4.5 scenario, and compared the effects of changes in climate and vegetation (leaf area index in particular) on predicted wetland CH_4 emissions and other fluxes for the period 2071-2100, relative to the period 1981-2010. I also explored possible responses of soil microbial communities to these changes. My results suggest that, if soil microbial communities acclimatize to elevated temperatures without population shifts, end-of-century CH_4 emissions from the WSL will only rise to 3.6 Tg CH4.y (6% above historical emissions). In contrast, if substantial population shift takes place as well, CH_4 emissions will more than double, to 7.3 Tg CH_4/y. Crucially, while historical emissions have been concentrated in the southern half of the domain, acclimatization plus population shift would concentrate almost 3/4 of future emissions in the northern half of the domain, where the possible release of carbon with permafrost thaw is a concern. In addition, accounting for acclimatization and population shift reduced the region's net (negative) climate-wetland CH_4 feedback by 38%, and changed the sensitivity of the region's CH4 emissions to changes in LAI from negative to positive. This work indicates the importance of better constraining the responses of soil microbial communities to changes in climate and vegetation as they are critical determinants of the region's future methane emissions.

VII. REFERENCES

Adam, J. C., and D. P. Lettenmaier, 2003: Adjustment of global gridded precipitation for systematic bias, *J. Geophys. Res.-Atmos.*, **108**(D9), 1-14, doi: 10.1029/2002JD002499.

Adam, J. C., and D. P. Lettenmaier, 2008: Application of new precipitation and reconstructed streamflow products to streamflow trend and attribution in northern Eurasia, *J. Climate*, **21**(8), 1807-1828, doi: 10.1175/2007JCLI1535.1.

Adam, J. C., E. A. Clark, D. P. Lettenmaier, and E. F. Wood, 2006: Correction of global precipitation products for orographic effects, *J. Climate*, **19**(1), 15-38, doi: 10.1175/JCLI3604.1.

Allison, S. D., M. D. Wallenstein, and M. A. Bradford, 2010: Soil-carbon response to warming dependent on microbial physiology, *Nat. Geosci.*, **3**(5), 336-340, doi: 10.1038/NGEO846.

Alm, J., S. Saarnio, H. Nykänen, J. Silvola, and P. J. Martikainen, 1999: Winter CO2, CH4, and N2O fluxes on some natural and drained boreal peatlands, *Biogeochemistry*, **44,** 163–186, doi: 10.1023/A:1006074606204.

Alo, C. A., and G. Wang, 2008a: Potential future changes of the terrestrial ecosystem based on climate projections by eight general circulation models, *J. Geophys. Res.-Biogeo.*, **113(**G1), G01004, doi: 10.1029/2007JG000528.

Alo, C. A., and G. Wang, 2008b: Hydrological impact of the potential future vegetation response to climate changes projected by 8 GCMs, *J. Geophys. Res.-Biogeo.*, **113**(G3), G03011, doi: 10.1029/2007JG000598.

Arneth, A., J. Kurbatova, O. Kolle, O. B. Shibistova, J. Lloyd, N. N. Vygodskaya, and E.-D. Schulze, 2002: Comparative ecosystem-atmosphere exchange of energy and mass in a European Russian and a central Siberian bog II. Interseasonal and interannual variability of CO_2 fluxes, *Tellus B*, **54**(5), p. 514-530, doi: 10.1034/j.1600-0889.2002.01354.x.

Aurela, M., T. Laurila, and J.-P. Tuovinen, 2002: Annual CO2 balance of a subarctic fen in northern Europe: importance of the wintertime efflux, *J. Geophys. Res.-Atmos.*, **107** (D21), doi: 10.1029/2002JD002055.

Baird, A. J., L. R. Belyea, and P. J. Morris, 2009: Upscaling of peatland-atmosphere fluxes of methane: Small-scale heterogeneity in process rates and the pitfalls of "bucket-and-slab" models, Carbon Cycling in Northern Peatlands, *Geophys. Monogr. Ser.*, vol. 184, edited by A. J. Baird et al., pp. 37–53, AGU, Washington, D. C., doi:10.1029/2008GM000826.

Bartalev, S. A., A. S. Belward, D. V. Erchov, and A. S. Isaev, 2003: A new SPOT4-VEGETATION derived land cover map of Northern Eurasia, *Int. J. Remote Sens.*, **24**(9), 1977-1982, doi: 10.1080/0143116031000066297.

Belyea, L. R., and J. Lancaster, 2002: Inferring landscape dynamics of bog pools from scaling relationships and spatial patterns, *J. Ecol.*, **90**(2), 223-234, doi: 10.1046/j.1365-2745.2001.0647.x.

Berrittella, C., and J. van Huissteden, 2011: Uncertainties in modeling CH4 emissions from northern wetlands in glacial climates: the role of vegetation parameters, *Clim. Past*, **7**(4), 1075-1087, doi: 10.5194/cp-7-1075-2011.

Beven, K. J., and M. J. Kirkby, 1979: A physically based, variable contributing area model of basin hydrology, *Hydrol. Sci. Bull.*, **24**, 43–69, doi: 10.1080/02626667909491834.

Bohn, T. J., D. P. Lettenmaier, K. Sathulur, L. C. Bowling, E. Podest, K. C. McDonald, and T. Friborg, 2007: Methane emissions from western Siberian wetlands: heterogeneity and sensitivity to climate change, *Environ. Res. Lett.*, **2**(4), 045015, doi: 10.1088/1748-9326/2/3/045015.

Bohn, T. J., and D. P. Lettenmaier, 2010: Systematic biases in large-scale estimates of wetland methane emissions arising from water table formulations, *Geophys. Res. Lett.*, **37**, L22401, doi: 10.1029/2010GL045450.

Bohn, T. J., B. Livneh, J. W. Oyler, S. W. Running, B. Nijssen, and D. P. Lettenmaier, 2013a: Global evaluation of MTCLIM and related algorithms for forcing of ecological and hydrological models, *Agric. Forest Meteorol.*, **176**, 38-49, doi: 10.1016/j.agrformet.2013.03.003.

Bohn, T. J., E. Podest, R. Schroeder, N. Pinto, K. C. McDonald, M. Glagolev, I. Filippov, S. Maksyutov, M. Heimann, and D. P. Lettenmaier, 2013b: The effects of surface moisture heterogeneity on wetland carbon fluxes in the West Siberian Lowland, *Biogeosciences Discuss.*, **10**, 6517-6562, doi: 10.5194/bgd-10-6517-2013 (in review).

Bohn, T. J., and D. P. Lettenmaier, 2013: Exploring the response of West Siberian wetland methane emissions to future changes in climate, vegetation, and soil microbial communities (in preparation).

Bowling, L. C., D. L. Kane, R. E. Gieck, L. D. Hinzman, and D. P. Lettenmaier, 2003: The role of surface storage in a low-gradient Arctic watershed, *Wat. Resour. Res.*, **39**(4), doi: 10.1029/2002WR001466.

Bowling, L. C., and D. P. Lettenmaier, 2010: Modeling the Effects of Lakes and Wetlands on the Water Balance of Arctic Environments, *J. Hydromet.*, **11**(2), 276-295, doi: 10.1175/2009JHM1084.1.

Brodzik, M. J. and K. W. Knowles, 2002: "EASE-Grid: a versatile set of equal-area projections and grids", *Discrete Global Grids*, M. Goodchild (Ed.), Santa Barbara, California USA: National Center for Geographic Information & Analysis. http://www.ncgia.ucsb.edu/globalgrids-book/ease_grid/.

Brooks, R. H., and A. T. Corey, 1964: Hydraulic properties of porous media, *Hydrology Paper no. 3*, Civil Engineering Department, Colorado State University.

Butman, D., and P. A. Raymond, 2011: Significant efflux of carbon dioxide from streams and rivers in the United States, *Nature Geosci.*, **4**, 839-842, doi: 10.1038/NGEO1294.

Chen, C., A. Liaw, and L. Breiman, 2004: Using random forest to learn imbalanced data, *Technical Report Series*, Report no. 666, Version 1, Statistics Department, University of California at Berkeley.

Cherkauer, K. A., and D. P. Lettenmaier, 1999: Hydrologic effects of frozen soils in the upper Mississippi River basin, *J. Geophys. Res.-Atmos.*, **104**(D16), doi: 10.1029/1999JD900337.

Christensen, T. R., A. Ekberg, L. Strom, M. Mastepanov, N. Panikov, M. Oquist, B. H. Svensson, P. J. Martikainen, and H. Oskarsson, 2003: Factors controlling large scale variations in methane emissions from wetlands, *Geophys. Res. Lett.*, **30**(7), 1414, doi: 10.1029/2002L016848.

Christensen, T. R., R. T. Johansson, H. J. Akerman, M. Mastepanov, N. Malmer, T. Friborg, P. Crill, and B. H. Svensson, 2004: Thawing sub-arctic permafrost: Effects on vegetation and methane emissions, *Geophys. Res. Lett.*, **31**(4), L04501, doi: 10.1029/2003GL018680.

Conant, R. T., M. G. Ryan, G. I. Agren, H. E. Birge, E. A. Davison, P. E. Eliasson, S. E. Evans, S. D. Frey, C. P. Giardina, F. M. Hopkins, R. Hyvonen, M. U. F. Kirschbaum, J. M. Lavallee, J. Leifeld, W. J. Parton, J. M. Steinweg, M. D. Wallenstein, J. A. M. Wetterstedt, and M. A. Bradford, 2011: Temperature and soil organic matter decomposition rates – synthesis of current knowledge and a way forward, *Glob. Change Biol.*, **17**(11), 3392-3404, doi: 10.1111/j.1365-2486.2011.02496.x.

Contosta, A. R., S. D. Frey, S. V. Ollinger, and A. B. Cooper, 2013: Soil respiration does not acclimatize to warmer temperatures when modeled over seasonal timescales, *Biogeochemistry*, **112**, 555-570, doi: 10.1007/s10533-012-9748-6.

Crill, P. M., 1991: Seasonal patterns of methane uptake and carbon dioxide release by a temperate woodland soil, *Global Biogeochem. Cy.*, **5,** 319–334, doi: 10.1029/91GB02466.

DeLeon-Rodriguez, N., T. L. Lathem, L. M. Rodriguez-R, J. M. Barazesh, B. E. Anderson, A. J. Beyersdorf, L. D. Ziemba, M. Bergin, A. Nenes, and K. T. Konstantinidis, 2013: Microbiome of the upper troposphere: Species composition and prevalence, effects of tropical storms, and atmospheric implications, *Proc. Nat. Acad. Sci.*, **110**(7), 2575-2580, doi: 10.1073/pnas.1212089110.

Dickinson, R. E., A. Henderson-Sellers, C. Rozensweig, and P. Sellers, 1991: Evapotranspiration models with canopy resistance for use in climate models, a review, *Agric. For. Meteorol.*, **54,** 373–388, doi: 10.1016/0168-1923(91)90014-H.

Diffenbaugh, N. S., and F. Giorgi, 2012: Climate change hotspots in the CMIP5 global climate model ensemble, *Climatic Change*, **114**(3-4), 813-822, doi: 10.1007/s10584-012-0570-x.

Dise, N. B., E. Gorham, and S. Verry, 1993: Environmental factors controlling methane emissions from peatlands in Northern Minnesota, *J. Geophys. Res.-Atmos.*, **98**(D6), 10583-10594.

Dumbrell, A. J., M. Nelson, T. Helgason, C. Dytham, and A. H. Fitter, 2010: Relative roles of niche and neutral processes in structuring a soil microbial community, *ISME J.*, **4**, 337-345, doi: 10.1038/ismej.2009.122.

Eliseev, A. V., I. I. Mokhov, M. M. Arzhanov, P. F. Demchenko, and S. N. Denisov, 2008: Interaction of the methane cycle and processes in wetland ecosystems in a climate model of intermediate complexity, *Iz. An. SSSR. Fiz. Atm.+*, **44**(2), 139-152, doi: 10.1134/S0001433808020011.

Eppinga, M. B., M. Rietkerk, W. Borren, E. D. Lapshina, W. Bleuten, and M. J. Wassen, 2008: Regular surface patterning of peatlands: Confronting theory with field data, *Ecosystems*, **11**(4), 520-536, doi: 10.1007/s10021-008-9128-z.

Famiglietti, J. S., J. A. Devereaux, C. A. Laymon, T. Tsegaye, P. R. Houser, T. J. Jackson, S. T. Graham, M. Rodell, and P. J. van Oevelen, 1999: Ground-based investigation of soil moisture variability within remote sensing footprints during the Southern Great Plains 1997 (SGP97) Hydrology Experiment, *Water Resour. Res.*, **35,** 1839–1851, doi: 10.1029/1999WR900047.

Famiglietti, J. S., J. W. Rudnicki, and M. Rodell, 1998: Variability in surface moisture content along a hillslope transect: Rattlesnake Hill, Texas, *J. Hydrol.*, **210,** 259–281, doi: 10.1016/S0022-1694(98)00187-5.

Farouki, O. T., 1981: The thermal properties of soils in cold regions, *Cold Reg. Sci. Technol.*, **5**(1), 67-75, doi: 10.1016/0165-232X(81)90041-0.

Farquhar, G. D., S. von Caemmerer, J. A. and Berry, 1980: A biochemical model of photosynthesis in the leaves of C3 species, *Planta*, **149,** 78–90, doi: 10.1007/BF00386231.

Farr, T. G., and M. Kobrick, 2000: Shuttle radar topography mission produces a wealth of data, *Eos Trans. AGU*, **81**, 583–585, doi: 10.1029/EO081i048p00583.

Farr, T. G., P. A. Rosen, E. Caro, R. Crippen, R. Duren, S. Hensley, M. Kobrick, M. Paller, E. Rogriguez, L. Roth, D. Seal, S. Shaffer, J. Shimada, J. Umland, M. Werner, M. Oskin, D. Burbank, and D. Alsdorf, 2005: The shuttle radar topography mission, *Rev. Geophys.*, **45**(2), RG2004, doi: 10.1029/2005RG000183.

Finlay, B. J., and K. J. Clarke, 1999: Ubiquitous dispersal of microbial species, *Nature*, **400**(6747), 828-828, doi: 10.1038/23616.

Food and Agriculture Organization (FAO), 1998: *Digital Soil map of the Word and Derived Soil Properties* [CD-ROM], Land Water Digital Media Ser. 1, Rome.

Frey, K. E., and L. C. Smith, 2005: Amplified carbon release from West Siberian peatlands by 2100, Geophys. Res. Lett., 32 (9), L09401, doi: 10.1029/2004GL022025.

Friborg, T., H. Soegaard, T. R. Christensen, C. R. Lloyd, and N. S. Panikov, 2003: Siberian wetlands: where a sink is a source, *Geophys. Res. Lett.*, **30** (21), doi: 10.1029/2003GL017797.

Frolking, S., N. T. Roulet, T. R. Moore, P. M. Lafleur, J. L. Bubier, and P. M. Crill, 2002: Modeling seasonal to annual carbon balance of Mer Bleue Bog, Ontario, Canada, *Global Biogeochem. Cy.*, **16**(3), 1030, doi: 10.1029/2001GB001457.

Fung, I., J. John, J. Lerner, E. Matthews, M. Prather, L. P. Steele, and P. J. Fraser, 1991: Three-dimensional model synthesis of the global methane cycle, *J. Geophys. Res.-Atmos.*, **96**(D7), 13,033-13,065, doi:10.1029/91JD01247.

Gedney, N., P. M. Cox, and C. Huntingford, 2004: Climate feedback from wetland methane emissions, *Geophys. Res. Lett.*, **31**, L20503, doi: 10.1029/2004GL020919.

Glagolev, M. V., 2004: Principles of quantitative theory for methane generation and methane consumption processes in the soil, *Mires and Biosphere: Proc. 3rd School Session (13-16 September, 2004)*. Tomsk: "Tomskij CNTI" Pub. P. 39-52.

Glagolev, M., I. Kleptsova, I. Filippov, S. Maksyutov, and T. Machida, 2011: Regional methane emission from West Siberia mire landscapes, *Environ. Res. Lett.*, **6**(4), 045214, doi: 10.1088/1748-9326/6/4/045214.

Glagolev, M. V., A. F. Sabrekov, I. E., Kleptsova, I. V. Filippov, E. D. Lapshina, T. Machida, Sh. Sh. Maksyutov, 2012: Methane Emission from Bogs in the Subtaiga of Western Siberia: The Development of Standard Model, *Eurasian Soil Sci.*+, **45**(10), 947-957, doi: 10.1134/S106422931210002x.

Gorham, E., 1991: Northern peatlands: role in the carbon cycle and probable responses to climate warming, *Ecol. Appl.*, **1,** 182–195, doi: 10.2307/1941811.

Graham, D. E., M. D. Wallenstein, T. A. Vishnivetskaya, M. P. Waldrop, T. J. Phelps, S. M. Pfiffner, T. C. Onstott, L. G. Whyte, E. M. Rivkina, D. A. Gilichinsky, D. A. Elias, R. Mackelprang, N. C. VerBerkmoes, R. L. Hettich, D. Wagner, S. D. Wullschleger,

and J. K. Jansson, 2012: Microbes in thawing permafrost: the unknown variable in the climate change equation, *ISME J.*, **6**(4), 709-712, doi: 10.1038/ismej.2011.163.

Hamlet, A. F., and D. P. Lettenmaier, 1999: Effects of climate change on hydrology and water resources in the Columbia River basin, *J. Am. Water Resour. As.*, **35**(6), 1597-1623, doi: 10.1111/j.1752-1688.1999.tb04240.x.

Hansen, M. C., R. S. Defries, J. R. G. Townshend, and R. Sohlberg, 2000: Global land cover classification at 1 km spatial resolution using a classification tree approach, *Int. J. Remote Sens.*, **21,** 1331–1364, doi: 10.1080/014311600210209.

Holmes, R. M., J. W. McClelland, B. J. Peterson, S. E. Tank, E. Bulygina, T. I. Eglinton, V. V. Gordeev, T. Y. Gurtovaya, P. A. Raymond, D. J. Repeta, R. Staples, R. G. Striegl, A. V. Zhulidov, and S. A. Zimov, 2008: Seasonal and annual fluxes of nutrients and organic matter from large rivers to the Arctic Ocean and surrounding seas, *Estuar. Coast.*, **35**, 369-382, doi: 10.1007/s12237-011-9386-6.

International Lake Environmental Committee (ILEC), 1988-1993: Survey of the State of the World Lakes, Data books of the world lake environments, vols. 1-5, ILEC/UNEP Publications, Otsu, Japan (also available online at http://wldb.ilec.or.jp).

Intergovernmental Panel on Climate Change (IPCC), 2007: *Climate Change 2007: The Physical Science Basis. Contribution of Working Group I to the Fourth Assessment Report of the Intergovernmental Panel on Climate Change*, edited by Solomon, S., Qin, D., Manning, N., Chen, Z., Marquis, M., Averyt, K. B., Tignor, M., and Miller, H. L., Cambridge University Press, Cambridge, 996pp.

Ito, A., and M. Inatomi, 2012: Use of a process-based model for assessing the methane budgets of global terrestrial ecosystems and evaluation of uncertainty, *Biogeosciences*, **9**, 759-773, doi: 10.5194/bg-9-759-2012.

Jiang, Y. Y., Q. L. Zhuang, S. Schaphoff, S. Sitch, A. Sokolov, D. Kicklighter, and J. Melillo, 2012: Uncertainty analysis of vegetation distribution in the northern high latitudes during the 21st century with a dynamic vegetation model, *Ecol. Evol.*, **2**(3), 593-614, doi: 10.1002/ece3.85.

Kaplan, J., 2002: Wetlands at the Last Glacial Maximum: Distribution and methane emissions, *Geophys. Res. Lett.*, **29**(6), 1079, doi: 10.1029/2001GL013366.

Kaplan, J. O., and M. New, 2006: Arctic climate change with a 2 degrees C global warming: Timing, climate patterns and vegetation change, *Climatic Change*, **79**(3-4), 213-241, doi: 10.1007/s10584-006-9113-7.

Kaplan, J., G. Folberth, and D. A. Hauglustaine, 2006: Role of methane and biogenic volatile organic compound sources in late glacial and Holocene fluctuations of atmospheric methane concentrations, *Global Biogeochem. Cy.*, **20**, GB2016, doi: 10.1029/2005GB002590.

Knorr, W., 2000: Annual and interannual CO2 exchanges of the terrestrial biosphere: Process-based simulations and uncertainties, *Glob. Ecol. Biogeogr.*, **9**, 225–252, doi: 10.1046/j.1365-2699.2000.00159.x.

Koven, C. D., B. Ringeval, P. Friedlingstein, P. Ciais, P. Cadule, D. Khvorostyanov, G. Krinner, and C. Tarnocai, 2011: Permafrost carbon-climate feedbacks accelerate global warming, *Proc. Nat. Acad. Sci.*, **108**(36), 14769-14774, doi: 10.1073/pnas.1103910108.

Kremenetski, K. V., A. A. Velichko, O. K. Borisova, G. M. MacDonald, L. C. Smith, K. E. Frey, and L. A. Orlova, 2003: Peatlands of the Western Siberian lowlands:

current knowledge on zonation, carbon content and late Quaternary history, *Quaternary Sci. Rev.*, **22**, 703-723.

Lehner, B., and P. Döll, 2004: Development and validation of a global database of lakes, reservoirs, and wetlands, *J. Hydrol.*, **296**(1-4), 1-22, doi: 10.1016/j.jhydrol.2004.03.028.

Letts, M. G., N. T. Roulet, N. T. Comer, M. R. Skarupa, and D. Verseghy, 2000: Parameterization of peatland hydraulic properties for the Canadian Land Surface Scheme, *Atmos. Oceans*, **38**, 141-160, doi: 10.1080/07055900.20009649643.

Levy, P. E., A. Burden, M. D. A. Cooper, K. J. Dinsmore, J. Drewer, C. Evans, D. Fowler, J. Gaiawyn, A. Gray, S. K. Jones, T. Jones, N. P. Mcnamara, R. Mills, N. Ostle, L. J. Sheppard, U. Skiba, A. Sowerby, S. E. Ward, and P. Zielinski, 2012: Methane emissions from soils: synthesis and analysis of a large UK data set, *Glob. Change Biol.*, **18**(5), 1657-1669, doi: 10.1111/j.1365-2486.2011.02616.x.

Liang, X., D. P. Lettenmaier, E. F. Wood, and S. J. Burges, 1994: A simple hydrologically based model of land-surface water and energy fluxes for general-circulation models, *J. Geophys. Res.-Atmos.*, **99**(D7), 14415-14428, doi: 10.1029/94JD00483.

Limpens, J., F. Berendse, C. Blodau, J. G. Canadell, C. Freeman, J. Holden, N. Roulet, H. Rydin, and G. Schaepman-Strub, 2008: Peatlands and the carbon cycle: from local processes to global implications – a synthesis, *Biogeosciences*, **5**(5), 1475-1491.

Lloyd, J., and J. A. Taylor, 1994: On the temperature dependence of soil respiration, *Funct. Ecol.*, **8**(3), p 315-323, doi: 10.2307/2389824.

Mann, P. J., A. Davydova, N. Zimov, R. G. M. Spencer, S. Davydov, E. Bulygina, S. Zimov, and R. M. Homes, 2012: Controls on the composition and lability of dissolved organic matter in Siberia's Kolyma River basin, *J. Geophys. Res.-Biogeo.*, **117**, G01028, doi: 10.1029/2011JG001798.

Matthews, E., and I. Fung, 1987: Methane emission from natural wetlands: global distribution, area, and environmental characteristics of sources, *Global Biogeochem. Cy.*, **1,** 61–86, doi: 10.1029/GB001i001p00061.

McEnroe, N. A., N. T. Roulet, T. R. Moore, and M. Garneau, 2009: Do pool surface area and depth control CO_2 and CH_4 fluxes from an ombotrophic raised bog, James Bay, Canada?, *J. Geophys. Res.-Biogeo.*, **114**, G01001, doi: 10.1029/2007JG000639.

Melton, J. R., R. Wania, E. Hodson, B. Poulter, B. Ringeval, R. Spahni, T. Bohn, C. A. Avis, D. J. Beerling, G. Chen, A. V. Eliseev, S. N. Denisov, P. O. Hopcroft, D. P. Lettenmaier, W. J. Riley, J. S. Singarayer, Z. M. Subin, H. Tian, S. Zurcher, V. Brovkin, P. M. van Bodegom, T. Kleinen, Z. C. Yu, and J. O. Kaplan, 2013: Present state of global wetland extent and wetland methane modelling: Conclusions from a model intercomparison project (WETCHIMP), *Biogeosciences*, **10**(2), 753-788, doi:10.5194/bg-10-753-2013.

Meng, L., P. G. M. Hess, N. M. Mahowald, J. B. Yavitt, W. J. Riley, Z. M. Subin, D. M. Lawrence, S. C. Swensen, J. Jauhiainen, and D. R. Fuka, 2012: Sensitivity of wetland methane emissions to model assumptions: application and model testing against site observations, *Biogeosciences*, **9**(7), 2793-2819, doi: 10.5194/bg-9-2793-2012.

Mitchell, T. D., and P. D. Jones, 2005: An improved method of constructing a database of monthly climate observations and associated high-resolution grids, *Int. J. Climatol.*, **25**(6), 693-712, doi: 10.1002/joc.1181.

Moss et al., and Coauthors, 2010: The next generation of scenarios for climate change research and assessment. *Nature,* **463,** 747–756, doi:10.1038/nature08823.

Myneni, R. B., S. Hoffman, Y. Knyazikhin, J. L. Privette, J. Glassy, Y. Tian, Y. Wang, X. Song, Y. Zhang, G. R. Smith, A. Lotsch, M. Friedl, J. T. Morisette, P. Votava, R. R. Nemani, and S. W. Running, 2002: Global products of vegetation leaf area and fraction absorbed PAR from year one of MODIS data, *Remote Sens. Environ.,* **83**, 214-231, doi: 10.1016/S0034-4257(02)00074-3.

Nakano, T., G. Inoue, and M. Fukuda, 2004: Methane consumption and soil respiration by a birch forest soil in West Siberia, *Tellus B,* **56,** 223–229, doi: 10.1111/j.1600-0889.2004.00102.x.

NASA Land Processes Distributed Active Archive Center (LP DAAC), 2001: ASTER L1B. USGS/Earth Resources Observation and Science (EROS) Center, Sioux Falls, South Dakota.

Olefeldt, D., and N. T. Roulet, 2012: Effects of permafrost and hydrology on the composition and transport of dissolved organic carbon in a subarctic peatland complex, *J. Geophys. Res.-Biogeo.,* 117, G01005, doi: 10.1029/2011JG001819.

Olefeldt, D., M. R. Turetsky, P. M. Crill, and A. D. McGuire, 2013: Environmental and physical controls on northern terrestrial methane emissions across permafrost zones, *Global Change Biol*., **19**(2), 589-603, doi: 10.1111/gcb.12071.

Olsrud, M., J. M. Melillo, T. R. Christensen, A. Michelsen, H. Wallander, and P. A. Olsson, 2004: Response of ericoid mycorrhizal colonization and functioning to global change factors, *New Phytol.,* **162**(2), 459-469, doi: 10.1111/j.1469-8137.2004.01049.x.

Panikov, N. S., and S. N. Dedysh, 2000: Cold season CH4 and CO2 emission from boreal peat bogs (West Siberia): winter fluxes and thaw activation dynamics, *Global Biogeochem. Cy.,* **14,** 1071–1080, doi: 10.1029/1999GB900097.

Panikov, N. S., S. N. Dedysh, O. M. Kolesnikov, A. I. Mardini, and M. V. Sizova, 2001: Metabolic and environmental control on methane emission from soils: mechanistic studies of mesotrophic fen in West Siberia, *Water Air Soil Pollut. Focus,* **1,** 415–428, doi: 10.1023/A:1013153927194.

Panofsky, H. A., and G. W. Brier, 1968: Some applications of statistics to meteorology, The Pennsylvania State University, University Park, 224 pp.

Papa, F., C. Prigent, F. Aires, C. Jimenez, W. B. Rossow, and E. Matthews, 2010: Interannual variability of surface water extent at the global scale, 1993-2004, *J. Geophys. Res.-Atmos.*, **115**, D12111, doi: 10.1029/2009JD012674.

Peregon, A., S. Maksyutov, and Y. Yamagata, 2009: An image-based inventory of the spatial structure of West Siberian wetlands, *Environ. Res. Lett.*, **4**, 045014, doi: 10.1088/1748-9326/4/4/045014.

Petrescu, A. M. R., L. P. H. van Beek, J. van Huissteden, C. Prigent, T. Sachs, C. A. R. Corradi, F. J. W. Parmentier, and A. J. Dolman, 2010: Modeling regional to global CH_4 emissions of boreal and arctic wetlands, *Global Biogeochem. Cy.*, **24**, GB4009, doi: 10.1029/2009GB003610.

Pickles, B. J., K. N. Egger, H. B. Massicotte, and D. S. Green, 2012: Ectomycorrhizas and climate change, *Fungal Ecol.*, **5**(1), 73-84, doi: 10.1016/j.funeco.2011.08.009.

Raymond, P. A., J. W. McClelland, R. M. Holmes, A. V. Zhulidov, K. Mull, B. J. Peterson, R. G. Striegl, G. R. Aiken, and T. Y. Gurtovaya, 2007: Flux and age of dissolved

organic carbon exported to the Arctic Ocean: A carbon isotopic study of the five largest arctic rivers, *Global Biogeochem. Cy.*, **21**, GB4011, doi: 10.1029/2007GB002934.

Repo, M. E., J. T. Huttunen, A. V. Naumov, A. V. Chichulin, E. D. Lapshina, W. Bleuten, and P. J. Martikainen, 2007: Release of CO(2) and CH(4) from small wetland lakes in western Siberia, *Tellus B*, **59**(5), 788-796, doi: 10.1111/j.1600-0889.2007.00301.x.

Richey, J. E., J. M. Melack, A. K. Aufdenkampe, V. M. Ballester, and L. L. Hess, 2002: Outgassing from Amazonian rivers and wetlands as a large tropical source of atmospheric CO2, Nature, 416, 6881, 617-620, doi: 10.1038/416617a.

Riley, W. J., Z. M. Subin, D. M. Lawrence, S. C. Swenson, M. S. Torn, L. Meng, N. M. Mahowald, and P. Hess, 2011: Barriers to predicting changes in global terrestrial methane fluxes: analyses using CLM4Me, and methane biogeochemistry model integrated in CESM, *Biogeosciences*, **8**, 1925-1953, doi: 10.5194/gb-8-1925-2011.

Ringeval, B., N. de Noblet-Ducoudré, P. Ciais, P. Bousquet, C. Prigent, F. Papa, and W. B. Rossow, 2010: An attempt to quantify the impact of changes in wetland extent on methane emissions on the seasonal and interannual time scales, *Global Biogeochem. Cy.*, **24**, GB2003, doi: 10.1029/2008GB003354.

Ringeval, B., P. Friedlingstein, C. Koven, P. Ciais, N. de Noblet-Ducoudré, B. Decharme, and P. Cadule, 2011: Climate-CH_4 feedback from wetlands and its interaction with the climate-CO2 feedback, *Biogeosciences*, **8**, 2137-2157, doi: 10.5194/bg-8-2137-2011.

Saarnio, S., J. Alm, J. Silvola, A. Lohila, H. Nykänen, and P. J. Martikainen, 1997: Seasonal variation in CH_4 emissions and production and oxidation potentials at microsites of an oligotrophic pine fen, *Oecologia*, **110**, 414-422.

Sabrekov, A. F., M. V. Glagolev, I. V. Filippov, V. S. Kazantsev, E. D. Lapshina, T. Machida, S. S. Maksyutov, 2012: Methane Emissions from North and Middle Taiga Mires of Western Siberia: Bc8 Standard Model, *Moscow University Soil Science Bulletin*, **67**(1), 45-53, doi: 10.3103/S0147687412010061.

Saulnier, G.-M., and R. Datin, 2004: Analytical solution to a bias in the TOPMODEL framework balance, *Hydrol. Process.*, **18,** 1195–1218, doi: 10.1002/hyp.1346.

Schaefer, K., T. Zhang, L. Bruhwiler, and A. P. Barrett, 2011: Amount and timing of permafrost carbon release in response to climate warming, *Tellus B*, **63**, 165-180, doi: 10.1111/j.1600-0889.2011.00527.x.

Schroeder, R., M. A. Rawlins, K. C. McDonald, E. Podest, R. Zimmermann, and M. Kueppers, 2010: Satellite microwave remote sensing of North Eurasian inundation dynamics: development of coarse-resolution products and comparison with high-resolution synthetic aperture radar data, *Environ. Res. Lett.*, **5**(1), 015003, doi: 10.1088/1748-9326/5/1/015003.

Schuldt, R. J., V. Brovkin, T. Kleinen, and J. Winderlich, 2012: Modelling Holocene carbon accumulation and methane emissions of boreal wetlands – an earth system model approach, *Biogeosciences Discuss.*, **9**, 12667-12710, doi: 10.5194/bgd-9-12667-2012.

Serreze, M. C., J. E. Walsh, F. S. Chapin, T. Osterkamp, M. Dyurgerov, V. Romanovsky, W. C. Oechel, J. Morison, T. Zhang, and R. G. Barry, 2000: Observational evidence of recent change in the northern high-latitude environment, *Climatic Change*, **46**(1-2), 159-207, doi: 10.1023/A:1005504031923.

Shannon, R. D., and J. R. White, 1994: A three-year study of controls on methane emissions from two Michigan peatlands, *J. Ecol.*, **84,** 239–246, doi: 10.1007/BF00002570.

Sheffield, J., G. Goteti, and E. F. Wood, 2006: Development of a 50-yr high-resolution global dataset of meteorological forcings for land surface modeling, *J. Climate*, **19**, 3088-3111, doi: 10.1175/JCLI3790.1.

Sheng, Y. W., L. C. Smith, G. M. MacDonald, K. V. Kremenetski, K. E. Frey, A. A. Velichko, M. Lee, D. W. Beilman, and P. Dubinin, 2004: A high-resolution GIS-based inventory of the west Siberian peat carbon pool, *Global Biogeochem. Cy.*, **18**(3), GB3004, doi: 10.1029/2003GB002190.

Shimoyama, K., T. Hiyama, Y. Fukushima, and G. Inoue, 2003: Seasonal and interannual variation in water vapor and heat fluxes in a West Siberian continental bog, *J. Geophys. Res.-Atmos.*, **108**(D20)**,** 4648, doi: 10.1029/2003JD003485.

Shindell, D. T., B. P. Walter, and G. Faluvegi, 2004: Impacts of climate change on methane emissions from wetlands, *Geophys. Res. Lett.*, **31**, L21202, doi: 10.1029/2004GL021009.

Sitch, S., C. Huntingford, N. Gedney, P. E. Levy, M. Lomas, S. L. Piao, R. Betts, P. Ciais, P. Cox, P. Friedlingstein, C. D. Jones, I. C. Prentice, and F. I. Woodward, 2008: Evaluation of the terrestrial carbon cycle, future plant geography and climate-carbon cycle feedbacks using five Dynamic Global Vegetation Models (DGVMs), *Glob. Change Biol.*, **14**(9), 2015-2039, doi: 10.1111/j.1365-2486.2008.01626.x.

Smith, L. C., G. M. MacDonald, A. A. Velichko, D. W. Beilman, O. K. Borisova, K. E. Frey, K. V. Kremenetski, and Y. Sheng, 2004: Siberian peatlands a net carbon sink and global methane source since the early Holocene, *Science*, **303**(5656), 353-356, doi: 10.1126/science.1090553.

Smith, L. C., Y. Sheng, G. M. MacDonald, and L. D. Hinzman, 2005: Disappearing Arctic lakes, *Science*, **308**(5727), 1429-1429, doi: 10.1126/science.1108142.

Spahni, R., R. Wania, L. Neef, M. van Weele, I. Pison, P. Bousquet, C. Frankenberg, P. N. Foster, F. Joos, I. C. Prentice, and P. van Velthoven, 2011: Constraining global methane emissions and uptake by ecosystems, *Biogeosciences*, **8**, 1643-1665, doi: 10.5194/bg-8-1643-2011.

Tang, J., and Q. Zhuang, 2008: Equifinality in parameterization of process-based biogeochemistry models: A significant uncertainty source to the estimation of regional carbon dynamics, *J. Geophys. Res.-Biogeo.*, **113**(G4), G04010, doi: 10.1029/2008JG000757.

Takeuchi, W., M. Tamura, and Y. Yasuoka, 2003: Estimation of methane emission from West Siberian wetlands by scaling technique between NOAA AVHRR and SPOT HRV, *Remote Sens. Environ.*, **85,** 21–29, doi: 10.1016/S0034-4257(02)00183-9.

Taylor, K. E., R. J. Stouffer, and G. A. Meehl, 2012: An overview of CMIP5 and the experiment design, *B. Am. Meteorol. Soc.*, **93**(4), 485-498, doi: 10.1175/BAMS-D-11-00094.1.

Tohjima, Y., S. Maksyutov, T. Machida, and G. Inoue, 1994: Airborne measurement of atmospheric CH4 over the West Siberian Lowland during the 1994 Siberian Terrestrial Ecosystem-Atmosphere-Cryosphere Experiment (STEACE), *Proc. 3rd Symp. on the Joint Siberian Permafrost Studies between Japan and Russia*, pp 50–57.

Troy, T. J., J. Sheffield, and E. F. Wood, 2011: Estimation of the Terrestrial Water Budget over Northern Eurasia through the Use of Multiple Data Sources, *J. Climate*, **24**(13), 3272-3293, doi: 10.1175/2011JCLI3936.1.

Valdes, P. J., D. J. Beerling, and C. E. Johnson, 2005: The ice age methane budget, *Geophys. Res. Lett.*, **32**, L02704, doi: 10.1029/2004GL021004.

Valentine, D. W., E. A. Holland, and D. S. Schimel, 1994: Ecosystem and physiological controls over methane production in northern wetlands, *J. Geophys. Res.-Atmos.*, **99**(D1), 1563–1571, doi: 10.1029/93JD00391.

Wallin, M. B., T. Grabs, I. Buffam, H. Laudon, A. Ågren, M. G. Öquist, and K. Bishop, 2013: Evasion of CO2 from streams – The dominant component of the carbon export through the aquatic conduit in a boreal landscape, *Glob. Change Biol.*, **19**, 785-797, doi: 10.1111/gcb.12083.

Walter, B. P., and M. Heimann, 2000: A process-based, climate-sensitive model to derive methane emissions from natural wetlands: Application to five wetland sites, sensitivity to model parameters, and climate, *Global Biogeochem. Cy.*, **14**(3), 745-765, doi: 10.1029/1999GB001204.

Walter, B. P., M. Heimann, and E. Matthews, 2001a: Modeling modern methane emissions from natural wetlands: 1. Model description and results, *J. Geophys. Res.-Atmos.*, **106**(D24), 34189-34206, doi: 10.1021/2001JD900165.

Walter, B. P., M. Heimann, and E. Matthews, 2001b: Modeling modern methane emissions from natural wetlands: 2. Interannual variations 1982–1993, *J. Geophys. Res.-Atmos.*, **106**(D24), 34207–34219, doi:10.1029/2001JD900164.

Walter, K. M., S. A. Zimov, J. P. Chanton, D. Verbyla, and F. S. Chapin III, 2006: Methane bubbling from Siberian thaw lakes as a positive feedback to climate warming, *Nature*, **443**, 71-75, doi: 10.1038/nature05040.

Wania, R., I. Ross, and I. C. Prentice, 2009: Integrating peatlands and permafrost into a dynamic global vegetation model: 2. Evaluation and sensitivity of vegetation and carbon cycle processes, *Global Biogeochem. Cy.*, **23**, GB3015, doi:10.1029/2008GB003413.

Wania, R., I. Ross, and I. C. Prentice, 2010: Implementation and evaluation of a new methane model within a dynamic global vegetation model: LPJ-WHyMe v1.3.1, *Geosci. Model. Dev.*, **3**, 565-584, doi:10.5194/gmd-3-565-2010.

Whitcomb, J., M. Moghaddam, K. McDonald, J. Kellndorfer, and E. Podest, 2009: Mapping vegetated wetlands of Alaska using L-band radar satellite imagery, *Can. J. Remote Sens.*, **35**(1), 54-72, doi: 10.5589/m08-080.

Willmott, C. J., and K. Matsuura, 2001: Terrestrial air temperature and precipitation: monthly and annual time series (1950-1999) (version 1.02), Center for Climate Research, University of Delaware, Newark, DE. [Available online at http://climate.geog.udel.edu/~climate/html_pages/archive.html.].

Yavitt, J. B., E. Yashiro, H. Cadillo-Quiroz, and S. H. Zinder, 2012: Methanogen diversity and community composition in peatlands of the central to northern Appalachian Mountain region, North America, *Biogeochemistry*, **109**(1-3), 117-131, doi: 10.1007/s10533-011-9644-5.

Yi, S., A. D. McGuire, E. Kasischke, J. Harden, K. Manies, M. Mack, and M. Turetsky, 2010: A dynamic organic soil biogeochemical model for simulating the effects of

wildfire on soil environmental conditions and carbon dynamics of black spruce forests, *J. Geophys. Res.-Biogeo.*, **115**, G04015, doi: 10.1029/2010JG001302.

Zhu, X., Q. Zhuang, M. Chen, A. Sirin, J. Melillo, D. Kicklighter, A. Sokolov, and L. Song, 2012: Rising methane emissions in response to climate change in Northern Eurasia during the 21st century, *Environ. Res. Lett.*, **6**, doi: 10.1088/1748-9326/6/4/045211.

Zhuang, Q., J. M. Melillo, D. W. Kicklighter, R. G. Prinn, A. D. McGuire, P. A. Steudler, B. S. Felzer, and S. Hu, 2004: Methane fluxes between terrestrial ecosystems and the atmosphere at northern high latitudes during the past century: a retrospective analysis with a process-based biogeochemistry model, *Global Biogeochem. Cy.*, **18**, GB3010, doi: 10.1029/2004GB002239.

Zhuang, Q., J. M. Melillo, M. C. Sarofim, D. W. Kicklighter, A. D. McGuire, B. S. Felzer, A. Sokolov, R. G. Prinn, P. A. Steudler, and S. Hu, 2006: CO2 and CH4 exchanges between land ecosystems and the atmosphere in northern high latitudes over the 21st century, *Geophys. Res. Lett.*, **33**, L17403, doi: 10.1029/2006GL026972.

Zimov, S. A., S. P. Davydov, G. M. Zimova, A. I. Davydova, E. A. G. Schuur, K. Dutta, and F. S. Chapin, 2006: Permafrost carbon: Stock and decomposability of a globally significant carbon pool, *Geophys. Res. Lett.*, **33**(20), L20502, doi: 10.1029/2006GL027484.

CURRICULUM VITAE

EDUCATION:

B.Sc.	Engineering Physics, University of California at Berkeley, 1991
M.A.	Geophysics, University of California at Berkeley, 1994 *Emphasis: Seismology*
Ph.D.	Civil and Environmental Engineering, University of Washington, 2013 *Emphasis: Hydrology*

POSITIONS HELD:

2012-	Tutor, Wyzant Corporation, Seattle, WA.
2005-	Research Assistant, Civil and Environmental Engineering, University of Washington.
2003-2004	Research Scientist, Civil and Environmental Engineering, University of Washington.
2002-2003	Fisheries Scientist, National Oceanic and Atmospheric Administration, Seattle, WA
1999-2001	Software Test Engineer, Microsoft, Redmond, WA.
1997-1999	Software Systems Analyst, Baker Hughes, Houston, TX.
1995-1997	Geophysicist, Schlumberger/Geco-Prakla, Houston, TX.

TEACHING

Graduate Teaching Assistant: Introductory Geology – undergraduate course at the University of California at Berkeley.
Tutor: Statistics, Algebra I and II, Geometry, Trigonometry, Calculus, Physics, Chemistry, Computer Programming (*mean rating > 4.9/5.0*) – Through Wyzant.

PROFESSIONAL MEMBERSHIPS

American Geophysical Union (AGU)
American Water Resources Association (AWRA)

SERVICE AND ACHIEVEMENTS

2011	Ronald E. Nece Fellowship for Outstanding PhD Student in Hydrology, Water Resources, and Environmental Fluid Mechanics; Department of Civil and Environmental Engineering, University of Washington
2010	Outstanding Student Oral Presentation, Global Environmental Change section of American Geophysical Union Fall Meeting, San Francisco, CA, Dec. 2010; Title: Reconstruction of Inundation and Greenhouse Gas Emissions from Siberian Wetlands of the Last Half-Century
2008	Competent Communicator Certification, Toastmasters International
2007-2008	Publicity Officer, Toastmasters International, University of Washington Chapter.
2005-2007	Webmaster, American Water Resources Association, University of Washington Chapter.
2007-	Reviewer: *Journal of Geophysical Research, Environmental Research Letters, Journal of Climate*.

1991-1992 Dan Tocher Memorial Fellowship, Department of Geology and Geophysics, University of California at Berkeley
1987-1991 Regent's Fellowship, University of California at Berkeley

PUBLICATIONS

Wania, R., J. R. Melton, E. Hodson, B. Poulter, B. Ringeval, R. Spahni, **T. Bohn**, C. A. Avis, G. Chen, A. V. Eliseev, P. O. Hopcroft, W. J. Riley, Z. M. Subin, H. Tian, V. Brovkin, P. M. van Bodegom, T. Kleinen, Z. C. Yu, J. S. Singarayer, S. Zurcher, D. P. Lettenmaier, D. J. Beerling, S. N. Denisov, and J. O. Kaplan, 2013: Present state of global wetland extent and wetland methane modelling: Methodology of a model intercomparison project (WETCHIMP), *Geosci. Model Dev.*, **6**, 617-641, doi: 10.5194/gmd-6-617-2013.

Bohn, T. J., B. Livneh, J. W. Oyler, S. W. Running, B. Nijssen, and D. P. Lettenmaier, 2013: Global evaluation of MTCLIM and related algorithms for forcing of ecological and hydrological models, *Agr. Forest Meteorol.*, **176**, 38-49, doi:10.1016/j.agrformet.2013.03.003.

Melton, J. R., R. Wania, E. L. Hodson, B. Poulter, B. Ringeval, R. Spahni, **T. Bohn**, C. A. Avis, D. J. Beerling, G. Chen, A. V. Eliseev, S. N. Denisov, P. O. Hopcroft, D. P. Lettenmaier, W. J. Riley, J. S. Singarayer, Z. M. Subin, H. Tian, S. Zurcher, V. Brovkin, P. M. van Bodegom, T. Kleinen, Z. C. Yu, and J. O. Kaplan, 2013: Present state of global wetland extent and wetland methane modelling: Conclusions from a model intercomparison project (WETCHIMP), *Biogeosciences*, **10**(2), 753-788, doi:10.5194/bg-10-753-2013.

Mo, K. C., L-C. Chen, S. Shukla, **T. J. Bohn,**, and D. P. Lettenmaier, 2012: Uncertainties in North American Land Data Assimilation Systems over the Contiguous United States, *J. Hydromet.*, **13**(3), doi: 10.1175/JHM-D-11-0132.1.

Gao, H., **T. J. Bohn,**, E. Podest, K. C. McDonald, and D. P. Lettenmaier, 2011: On the causes of the shrinking of Lake Chad, *Env. Res. Lett.*, **6**, 034021, doi: 10.1088/1748-9326/6/3/034021.

Shiklomanov A., **T. J. Bohn**, D. P. Lettenmaier, R. Lammers, J. C. Adam, P. Romanov, and M. Rawlins, 2011: "Interactions between Land Cover/Use Change and Hydrology" in *Eurasian Arctic Land Cover and Land Use in a Changing Climate*, G. Gutman and A. Reissell, eds., Springer-Verlag, 137-175, doi: 10.1007/978-90-481-9118-5_7.

Bohn, T. J., M. Y. Sonessa, and D. P. Lettenmaier, 2010: Seasonal hydrologic forecasting: Do multi-model ensemble averages always yield improvements in forecast skill?, *J. Hydromet.*, **11**(6), 1357-1371, doi: 10.1175/2010JHM1267.1.

Bohn, T. J., and D. P. Lettenmaier, 2010: Systematic biases in large-scale estimates of wetland methane emissions arising from water table formulations, *Geophys. Res. Lett.*, **37**, L22401, doi: 10.1029/2010GL045450.

Lettenmaier, D. P., V. Aizen, A. Amani, **T. J. Bohn**, F. Giorgi, S. Harrison, T. Huntington, R. Lawford, P. Letitre, H. Lins, J. Magome, G.-K. Park, I. Severskiy, W. J. Shuttleworth, P. Singh, S. Sorooshian, W. Struckmeier, K. Takeuchi, L. Tallaksen, C. Vorosmarty, T. Yan, and T. Zhang, 2009: "Changes in the Global Water Cycle" in *The United Nations World Water Development Report 3: Water in a Changing World*, World Water Assessment Programme, eds., Paris: UNESCO Publishing, and London: Earthscan.

Munoz-Arriola, F., S. Shukla, **T. Bohn**, C. Zhu, B. Livneh, D.P. Lettenmaier, R. Lobato-Sanchez, and A. Wagner-Gomez, 2009: Prediccion de la Hidrologia Superficial en Norte America, *Resumen del Clima de la Frontera* , Julio 13: 1-5.

Wang A., **T. J. Bohn**, S. P. Mahanama, R. D. Koster, and D. P. Lettenmaier, 2009: Multimodel ensemble reconstruction of drought over the continental United States, *J. Climate*, **22**, 2694–2712, doi: 10.1175/2008JCLI2586.1.

Slater, A. G., **T. J. Bohn**, J. L. McCreight, M. C. Serreze, and D. P. Lettenmaier, 2007: A Multi-Model Simulation of Pan-Arctic Hydrology, *J. Geophys. Res.*, **112**(G4), G04S45, doi: 10.1029/2006JG000303.

Bohn, T. J., D. P. Lettenmaier, K. Sathulur, L. C. Bowling, E. Podest, K. C. McDonald, and T. Friborg, 2007: Methane emissions from western Siberian wetlands: heterogeneity and sensitivity to climate change, *Env. Res. Lett.*, **2**, 045015, doi: 10.1088/1748-9326/2/4/045015.

Bohn, T. J., D. P. Lettenmaier, K. Sathulur, and L. C. Bowling, 2007: Large-scale modeling of wetland methane emissions, *iLEAPS Newsletter* 4, 40-42.

Burke, B., K. Frick, M. L. Moser, **T. J. Bohn**, and T. C. Bjornn, 2005. Adult fall chinook salmon passage through fishways at lower Columbia River dams in 1998, 2000, and 2001. *Report by Fish Ecology Division, Northwest Fisheries Science Center, National Marine Fisheries Service, National Oceanic and Atmospheric Administration to the U.S. Army Corps of Engineers, Project No. ADS-00-1 through 5 and ADS-00-12, vi*, 82 p.

In Press:

Bohn, T. J., E. Podest, R. Schroeder, N. Pinto, K. C. McDonald, M. Glagolev, I. Filippov, S. Maksyutov, M. Heimann, and D. P. Lettenmaier, 2013: The effects of surface moisture heterogeneity on wetland carbon fluxes in the West Siberian Lowland, *Biogeosciences Discussions*, 10, 6517-6562, doi:10.5194/bgd-10-6517-2013 (in review).

Gao, H., Q. Tang, X. Shi, C. Zhu, **T. J. Bohn**, F. Su, J. Sheffield, M. Pan, D. P. Lettenmaier, and E. F. Wood, 2010: Water Budget Record from Variable Infiltration Capacity (VIC) Model. In *Algorithm Theoretical Basis Document for Terrestrial Water Cycle Data Records* (in review).

Working Papers:

Bohn, T. J., and D. P. Lettenmaier, 2013: Exploring the response of West Siberian wetland methane emissions to future changes in climate, vegetation, and soil microbial communities (in preparation).

SELECTED PRESENTATIONS

Bohn, T. J., and D.P. Lettenmaier, AGU Fall Meeting, San Fransisco, CA, Dec. **2012**, The Role of Fractional Inundation and Saturation in the Carbon Cycle of West Siberian Wetlands.

Bohn, T. J., and D.P. Lettenmaier, AGU Fall Meeting, San Fransisco, CA, Dec. **2010**, Reconstruction of Inundation and Greenhouse Gas Emissions from Siberian Wetlands of the Last Half-Century.